

Characterization of Anomalous Fe-Ni Alloy Coating by Electrodeposition and its Properties

by

Md. Aminul Islam

MASTER OF PHILOSOPHY IN MATERIALS SCIENCE




Department of Materials and Metallurgical Engineering

BANGLADESH UNIVERSITY OF ENGINEERING AND TECHNOLOGY

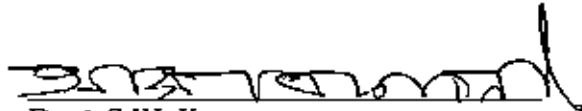
2008

The thesis titled "Characterization of Anomalous Fe-Ni Alloy Coating by Electrodeposition and its Properties" Submitted by Md. Aminul Islam, Roll No: 040511101F, Session: April 2005, has been accepted as satisfactory in partial fulfilment of the requirement for the degree of Master of Philosophy in Materials Science on 01 June, 2008.


BOARD OF EXAMINERS

1. 

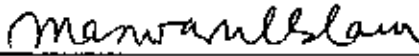
Dr. Md. Moniruzzaman
Associate Professor
Department of MME, BUET, Dhaka. **Chairman**

2. 

Dr. A.S.W. Kurny
Professor
Department of MME, BUET, Dhaka **Member**

3. 

Dr. Md. Fakhrul Islam
Professor and Head
Department of MME, BUET, Dhaka **Member
(Ex-Officio)**

4. 

Dr. Md. Manwarul Islam
Professor
Department of Chemistry, BUET, Dhaka **Member
(External)**

DECLARATION

It is hereby declared that this thesis or any part of it has not been submitted elsewhere for the award of any degree or diploma.

Md. Aminul Islam
Md. Aminul Islam

DEDICATION

**To my Father,
who helps me to grow up and to realize the philosophy of life
and
To my Mother,
who furnished incentive and encouragement.**

CONTENTS

List of Tables	1
List of Figures	2
ACKNOWLEDGEMENT	6
ABSTRACT	7
CHAPTER 1 INTRODUCTION	9
1.1 A General Overview of Fe-Ni Alloy Coating	9
1.2 Present State and Goal of the Work	10
CHAPTER 2 LITERATURE REVIEW	12
2.1 Electrodeposition	15
2.1.1 Basic Concept of Electrodeposition	15
2.1.2 Alloy Electrodeposition	17
2.1.3 Kinetics of Electrodeposition Reactions	20
2.1.4 Role of Static Potentials in the Electrodeposition of Alloys	21
2.1.5 The Nernst Equation	24
2.2 Principles of Alloy Deposition	25
2.2.1 Plating Variables	26
2.2.2 Variation in the Composition of Electrodeposited Alloys with the Composition of the Bath and the Plating	27
2.2.2.1 Effect of Metal Ratio of the Bath on the Composition of the Deposit	27
2.2.2.2 Effect of Total Metal Content of the Bath on the Composition of the Deposit	30

2.2.2.3	Effect of pH of the Plating Bath on the Composition of the Deposit	32
2.2.2.4	Relation between Current Density and Composition of Electrodeposited Alloys	33
2.2.2.5	Effect of Bath Temperature on Composition of Electrodeposited Alloys	36
2.2.2.6	Effect of Bath Temperature on Composition of Alloys in Anomalous Codeposition	37
2.2.2.7	Effect of Agitation of Bath or Rotation of Cathode on the Composition of Electrodeposited Alloys	39
2.3	Types of Alloy Plating Systems	40
2.4	Purposes of Electrodeposition	42
2.4.1	Decorative Plating	42
2.4.2	Protective Plating	43
2.4.3	Special Surface Properties	44
2.5	The Plating Bath	44
2.5.1	Ingredients of Plating Bath	44
2.6	Bulk Behavior of Nanostructured Materials	46
2.6.1	Mechanical Behavior	47
2.6.1.1	Structural Nanostructured Materials	47
2.6.1.2	Elastic Properties	48
2.6.1.3	Hardness and Strength	49
2.6.1.4	Ductility and Toughness	51
2.6.1.5	Superplastic Behavior	54
2.7	Unique Mechanical Properties of Nanocrystalline Materials	55
2.8	Ferromagnetic Nanostructured Materials	56
2.8.1	Soft Magnetic Nanocrystalline Alloys	56

2.8.2	Magnetic Properties Derived from Hysteresis Loops	58
2.8.3	Hard and Soft Magnetic Materials	62
2.8.4	Permanent Magnet Materials	64
2.8.5	Giant Magnetoresistance (GMR)	65
2.9	Other Ferromagnetic Nanocrystalline Materials	66
2.10	Other Bulk Applications of Nanostructured Materials	67
2.10.1	Nanocrystalline Hydrogen Storage Materials	67
2.10.2	Nanocrystalline Corrosion-Resistant Materials	67
2.10.2.1	Corrosion of Metals and Their Alloys	67
2.10.2.2	Forms of Corrosion	68
2.11	Applications of the Thin Films of Electrodeposited Iron-Nickel Alloy	70
2.11.1	Low Thermal Expansion Applications	70
2.11.2	Microelectromechanical Systems	71
2.11.3	Magnetic Applications	71
2.11.4	Other Applications	71

CHAPTER 3	EXPERIMENTAL	73
3.1	Materials	73
3.2	Preparation of Specimen for Electrodeposition	73
3.3	Electrodeposition Set-up	75
3.4	Electroplating Operation	77
3.5	Methods of Investigation	78
3.5.1	Chemical Analysis of the Fe-Ni Alloy Deposit	78
3.5.2	Microhardness Measurement	80
3.5.3	Corrosion Test	80

3.5.4	Investigation of Surface Morphology of Fe-Ni Alloy Coating	82
3.5.5	Investigation of Magnetic Properties of Fe-Ni Alloy Coating	82
CHAPTER 4 RESULTS AND DISCUSSION		84
4.1	Electrodeposition of Fe-Ni Alloy Coating	84
4.2	Chemical Analysis	86
4.3	Microhardness (VHN)	93
4.4	Corrosion Properties	97
4.5	Morphology	103
4.6	Magnetic Properties	111
CHAPTER 5 CONCLUSIONS		116
5.1	Conclusions Drawn from the Present Work	116
5.2	Suggestions for Future Work	117
REFERENCES		118
List of Publications/Presentations		125

List of Tables

- 3.1 Particulars of pickling and acid dipping operations.
- 3.2a Composition of simple baths used in the study.
- 3.2b Composition of complex baths used in the study.
- 3.3 Operating conditions of Scanning Electron Microscope (SEM).
- 4.1 Current density (cd) and bath pH for uniform and bright coating deposited from complex bath.
- 4.2 % Ni in coatings deposited from simple baths at different current density.
- 4.3 % Ni in coatings deposited from complex baths at different current density.
- 4.4 % Fe in coatings deposited from simple baths at different current density.
- 4.5 % Fe in coatings deposited from complex baths at different current density.
- 4.6 Microhardness and % Ni of Fe-Ni coatings deposited from simple baths at different current density.
- 4.7 Microhardness and % Ni of Fe-Ni coatings deposited from complex baths at different current density.
- 4.8 Corrosion rate (mdd) and %Ni of coatings deposited at various current density from simple baths.
- 4.9 Corrosion rate (mdd) and %Ni of coatings deposited at various current density from complex baths.
- 4.10 The saturation magnetization (emu/g) and %Ni obtained from simple baths.

List of Figures

- 2.1 Schematics of an electrolytic cell for plating metal.
- 2.2 Schematic illustrations of kinetic and mass transport control.
- 2.3 An ideal polarization curve for the electrodeposition of the binary alloy AB results from the sum of pure metal (A and B) polarization curves.
- 2.4 Typical curves illustrating the relation between the composition of electrodeposited alloys and the composition of the bath in normal co-deposition
- 2.5 Relation between the composition of the deposit and the composition of the bath in anomalous co-deposition.
- 2.6 Relation between the composition of the deposit and the total metal content of the bath in anomalous co-deposition.
- 2.7 Effect of pH on the composition of deposits in anomalous co-deposition.
- 2.8 Relation between alloy composition and current density in anomalous co-deposition.
- 2.9 Relation between alloy composition and Temperature in anomalous codeposition (a: data represented by circles on curves and b: data represented by crosses on curves).
- 2.10 Ratio of the Young's (E) and shear (G) moduli of nanocrystalline materials to those of conventional grain size materials as a function of grain size. The dashed and solid curves correspond to a grain boundary thickness of 0.5 and 1 nm, respectively (Shen et al. 1995).
- 2.11 Elongation to failure in tension vs. grain size for some nanocrystalline metals and alloys
- 2.12 Effective permeability, μ_e , vs. saturation magnetic flux density, B_s , for soft ferromagnetic materials (after A. Inoue 1997).

- 2.13 Schematic diagram of M vs. H or hysteresis loop showing magnetic properties and domain structures during different stages of magnetization.
- 2.14 Hysteresis loop behavior for soft iron and hardened steel.
- 2.14 Relative permeabilities and coercivities of ferromagnetic materials
- 3.1 Electrodeposition set-up.
- 3.2 Salt Immersion Test.
- 3.3 Section of electrodeposited film used for the corrosion test.
- 3.4 Schematic diagram of Vibrating Sample Magnetometer (VSM).
- 4.1 Relation between pH and current density for bright deposition obtained from baths (a) B-3a and (b) B-3b.
- 4.2: Effect of current density on % Ni in coating deposited from simple baths
- 4.3 Effect of current density on % Ni in coating deposited from complex baths B-3a, B-3b and B-3c.
- 4.4 % Ni deposited from simple bath B-1 and complex baths B-3a, B-3b and B-3c. All depositions were carried on at 50 mA/cm^2 .
- 4.5 Effect of complexing agent on % Ni in coating deposited from complex baths B-4a, B-4b and B-4c. All depositions were carried on at 30 mA/cm^2 .
- 4.6 Effect of current density on microhardness of coating deposited from simple baths.
- 4.7 Effect of current density on microhardness of coating deposited from complex baths.
- 4.8 Effect of % Ni in coating on its microhardness deposited from simple baths.
- 4.9 Effect of % Ni in coating on its microhardness deposited from complex baths.
- 4.10 Effect of complexing agent on microhardness of coating deposited from complex baths.

- 4.11 Effect of % Ni in coating on its corrosion rate deposited from simple baths B-1 and B-2.
- 4.12 Effect of % Ni in coating on its corrosion rate deposited from Complex baths B-3a, B-3b and B-3c.
- 4.13 Effect of % Ni in coating on its corrosion rate. Coatings were deposited from complex baths B-4a, B-4b and B-4c at the same current density of 30 mA/cm^2
- 4.14 % Ni deposited from simple bath B-1 and complex baths B-3a, B-3b and B-3c All depositions were carried on at 50 mA/cm^2 .
- 4.15 Photograph of corroded samples obtained from baths and at current densities of (a) B-1 and 50 mA/cm^2 (b) B-1 and 120 mA/cm^2 (c) B-2 and 50 mA/cm^2 (d) B-2 and 120 mA/cm^2 respectively.
- 4.16 Photograph of corroded samples obtained from baths and at current densities of (a) B-3a and 50 mA/cm^2 (b) B-3b and 50 mA/cm^2 (c) B-3c and 50 mA/cm^2 (d) B-4b and 30 mA/cm^2 respectively.
- 4.17 SEM images of the deposit obtained from bath B-1 at current density of (a) 50 mA/cm^2 (b) 70 mA/cm^2 (c) 100 mA/cm^2 (d) 120 mA/cm^2 .
- 4.18 SEM images of the deposit obtained from bath B-2 at current density of (a) 50 mA/cm^2 (b) 70 mA/cm^2 (c) 100 mA/cm^2 (d) 120 mA/cm^2 .
- 4.19 SEM images of the deposit obtained from bath B-3a at current density and pH value of (a) 30 mA/cm^2 and 1.85 (b) 40 mA/cm^2 and 1.78 (c) 50 mA/cm^2 and 1.31 (d) 100 mA/cm^2 and 1.40 respectively.
- 4.20 SEM images of the deposit obtained from bath B-3b at current density and pH value of (a) 50 mA/cm^2 and 1.31 (b) 40 mA/cm^2 and 1.78 (c) 100 mA/cm^2 and 1.31 (d) 140 mA/cm^2 and 1.00 respectively.
- 4.21 SEM images of the deposit obtained from bath B-3c at current density and pH value of (a) 50 mA/cm^2 and 1.80 (b) 60 mA/cm^2 and 1.78 (c) 100 mA/cm^2 and 1.31 (d) 140 mA/cm^2 and 1.00 respectively.
- 4.22 SEM images of the deposit obtained at a current density of 30 mA/cm^2 from baths (a) B-4a (b) B-4b and (c) B-4c.

- 4.23 Magnetic hysteresis loops of Fe-Ni coatings obtained from simple bath B-1.
- 4.24 Magnetic hysteresis loops of the Fe-Ni coatings deposited from simple bath B-2.
- 4.25 Variation of magnetization saturation with Ni content for simple baths.
- 4.26 Magnetic hysteresis loop of the Fe-Ni coating (44.13 %Ni) deposited from complex bath B-3a.

ACKNOWLEDGEMENT

First and foremost, I would like to express my utmost gratitude, profound regard and indebtedness towards my supervisor, Dr. Md. Moniruzzaman, Associate Professor, Department of Materials and Metallurgical Engineering, Bangladesh University of Engineering and Technology (BUET), Dhaka, for his kindness and patience throughout the whole study. His thoughtful suggestion not only motivated me, but also encouraged at all stages of my research work and finally made the successful completion of the thesis possible.

I am thankful to Dr. Md. Fakhru Islam, Professor and Head, Department of MME, BUET, for his kind help and co-operation during my research work. I would also like to thank all the teachers of MME Department, BUET, for their encouragement and guidance. I remember with gratefulness the kind help and inspiration of Dr. Kazi Mohammad Shorowordi, Assistant Professor, IAT, BUET.

I am grateful to Dr. Sheikh Manjura Hoque and Dr. A.K.M. Abdul Hakim of Materials Science Division, Atomic Energy Center, Dhaka, Bangladesh for their advice, assistance and permission to use the VSM for magnetization test of my samples.

I acknowledge with appreciation the co-operation of Mr. Md. Yusuf Khan, Mr. Md. Ashiqur Rahman, Mr. Ahmed Ulah of MME Department. Thanks are also to other officers and staffs of the department for their help in various stages of my research. I would like to offer thanks to my friends Manish Kumar Debnath and others who shared with me to solve the problems confronted in the whole research period.

I am grateful to BUET for providing me financial support for conducting the research.

Last but not least, I would like to express my deep gratitude to my beloved parents for their sacrifice, continuous encouragement and support throughout the research.

MME Department, BUET

The Author

ABSTRACT

Iron-nickel (Fe-Ni) alloys are of great commercial interest as they possess low thermal expansion, soft magnetic and wide spectrum of physical properties. Attempts have been made to explain the anomalous mechanism of Fe-Ni alloy codeposition and researchers have proposed several models. Main focus of this work is to investigate the effect and the interaction of complexing agents on the properties of electrodeposited Fe-Ni alloy coating as well as the special characteristic of anomalous nature.

The Fe-Ni films were deposited from eight different baths; two of them were simple, containing NiSO_4 , FeSO_4 , Na_2SO_4 , H_3BO_3 as main ingredients and another six were complex, containing ascorbic acid, saccharin and citric acid as complexing agent along with the main ingredients in varying composition. Fe-Ni alloy coatings were electrodeposited on Cu substrate at room temperature in the current density range of 20-140 mA/cm^2 . The effects of current density, pH and bath composition on the coating appearance, composition, hardness, corrosion resistance, morphologies and magnetization were studied. Chemical analysis, Microhardness, Corrosion resistance, Morphologies and Magnetization of the coatings were studied by means of Conventional Wet Method, Microhardness Tester, Salt Immersion Test, Scanning Electron Microscope (SEM) and Vibrating Sample Magnetometer (VSM) respectively.

It was observed that coating obtained at higher current density with higher bath pH was blackish (examined with naked eye) while lower current density with higher pH or higher current density with lower pH resulted in uniform and bright coatings. The Ni percentage of the coating as well as its VHN increased with increasing current density for simple baths but the reverse situations occurred for complex baths. Addition of complexing agents suppressed the anomalous characteristics of the Fe-Ni alloy electrodeposition. The corrosion rate decreased with increasing Ni content of the films. Formation of protective NiO layer is supposed to increase the corrosion resistance of high Ni content thin film. Thus, the properties of electrodeposited Fe-Ni alloy are strongly influenced by the electrolytic composition and deposition parameters. The film

obtained from simple baths did not exhibit smooth surface and the coating developed sharp line microcracks due to the internal stress developed during deposition in it. No cracks were observed and the coating grain size became finer for the coatings from complex baths compared to the simple baths. A clear morphological modification was observed due to the addition of complexing agent. The saturation magnetization of the electrodeposited Fe-Ni coating was found to decrease with increasing Ni content which is in good agreement with suppression of ferromagnetic character of the films. The highest saturation magnetization was seen 131.13 emu/g among the coatings studied which is very close to the acceptable limit (135 emu/g). Characterization of Fe-Ni alloy plating parameters with its properties was attempted.



1 INTRODUCTION

CHAPTER 1

1.1 A General Overview of Fe-Ni Alloy Coating

There has been a great research interest in the development and characterization of iron-nickel (Fe-Ni) thin films due to their operational capacity, economic interest, magnetic and other properties [1]. Due to the unique properties of low coefficient of thermal expansion (CTE) and soft magnetic nature, Fe-Ni alloys have been used in industrial applications for over 100 years. Typical examples of applications that are based on the low CTE of Fe-Ni alloys include: thermostatic bimetals, glass sealing, integrated circuit packaging, cathode ray tube, shadow masks and membranes for liquid natural gas tankers [2]; applications based on the soft magnetic properties include: read-write heads for magnetic storage, magnetic actuators, magnetic shielding and high performance transformer cores. In the field of magnetic data storage devices, thin film magnetic heads have played an important role in enhancement of the magnetic recording density. Commercial alloys such as permalloy ($\text{Ni}_{81}\text{Fe}_{19}$) and invaralloy ($\text{Ni}_{36}\text{Fe}_{64}$) are the important component of bimetallic sensors and magnetic storage devices respectively [3].

A simple and inexpensive technique for the production of thin film is electrodeposition. It has been used in the case of Fe-Ni alloys for a wide range of concentrations of both elements. The properties, the composition and the grain size of electrodeposited Fe-Ni alloys are strongly dependent on the electrolyte composition and the deposition parameters [1]. The potential for performance enhancement for various applications of Fe-Ni alloys arising from the enhanced properties due to the finer grain size of the alloys. Structure-property relationships for microcrystalline/ nanocrystalline materials produced by electroplating have been extensively investigated over the past decade. An important feature of the Fe-Ni alloy system is its structural evolution, with a change from bcc for the Fe-rich alloy to fcc for the alloy with higher Ni content. Much attention has been focused on the low thermal expansion behavior of invaralloy ($\text{Ni}_{36}\text{Fe}_{64}$) [4].

Properties that strongly depend on the interactions of grain boundaries with other defects are greatly influenced by grain size reduction. Examples include creep behavior, ductility, hardness, yield and tensile strength. From an application point of view, it is the onset of grain growth that ultimately limits service temperature of the material. In turn, these factors are dependent on deposition conditions such as electrolyte composition, pH, applied current density and agitation [5]. Researchers are now focusing on the improvement of corrosion resistance of the coatings together with better adhesion of the coatings with substrate, accounted for the formability of Ni content of the coatings. The corrosion resistance of Fe-Ni coated substrate increases when the average Ni content increases. They have shown that mechanical interlocking of electrodeposited coating is determined by its hardness, ductility, microcracks, grain size distribution, defects, and preferred crystallographic orientation. Many efforts have been made to keep its density maximum and to correlate the plating parameters, such as bath composition, temperature, pH value, current density, flow velocity and Ni content, which, in turn, determines the performance of the coatings. One serious drawback of the electrodeposition process is the generation of internal stresses resulting in the formation of microcracks. However, the internal stress level can be reduced by heat treatment or the addition of inhibitors [6].

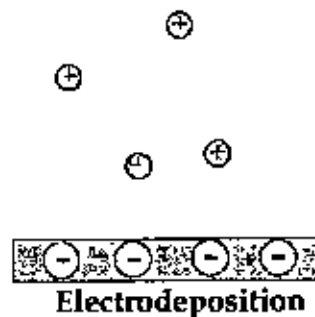
In addition, Fe-Ni electrodeposition exhibits the phenomenon of “anomalous codeposition”. According to Brenner’s definition [7], the codeposition of iron group metals (e.g., Fe, Co, and Ni) is widely recognized as an electroplating of the anomalous type since the less noble metal is deposited preferentially and its percentage in the deposit is obviously higher than that in electrolytes. Thus electrodeposition of Fe-Ni alloys has attracted considerable attention because of its special characteristic nature and wide range of unique properties.

1.2 Present State and Goal of the Work

Previous studies have reported the effects, such as pH, Ni/Fe ratio in the bath, deposition rate and structure of the electrodeposited Fe-Ni alloys on their properties. However, no information regarding the addition of complexing agents into the baths and its interaction with the plating parameters on the properties of electrodeposited Fe-Ni alloy

coating is available in the literature. Several attempts have been made to explain the anomalous codeposition of Fe-Ni alloys. Grande and Talbot established a mathematical model for the formation of Fe-Ni electrodeposited film [8]. The focus of this study, however, is not the mechanism of anomalous codeposition but the major aim is to investigate the influence of complexing agents on anomalous characteristics as well as on the generation of internal stresses resulting in the formation of microcracks, the smoothness and other properties of Fe-Ni thin films. The properties include coating composition, microhardness, corrosion resistance and magnetization. In the present Fe-Ni electroplating system, the electrolytic composition, current density, pH and relationship between current density and pH for bright deposition are investigated systemically, what, to our knowledge, has not yet been studied. Characterization of Fe-Ni alloy plating parameters with its properties is also attempted.

Electrochemical deposition, or electrodeposition for short, has been around for a very long time now. To begin, electrodeposition is a fascinating phenomenon. Electrodeposition should be defined as the process in which the deposit of a (usually) thin layer (of metal) is formed "electrolytically" upon a substrate (that is often, but not always, also a metal) simply by donating electrons to ions in a solution.



Meanwhile, electrolytic deposition really took off with the development of effective electrolytes for silver and gold deposition around 1840. These became the basis of an extraordinarily successful decorative plating industry with the spreading of technology. However, the electrolytes were extremely toxic, as they incorporated cyanide, and the search for better, safer substitutes continues. Finding environmentally friendly alternatives to established electrodeposition processes is still an important general challenge. Electrodeposition has three main attributes that make it so well suited for nano-, bio- and microtechnologies [9].

- a. It can be performed near room temperature from water-based electrolytes.
- b. It can be scaled down to the deposition of a few atoms or up to large dimensions.
- c. It can be used to grow functional material through complex 3D masks.

Moreover, thin film coatings, with the exception of certain materials which are not commonly used, are virtually nonpolluting. Because thin films are applied directly onto a substrate, there are no lacquers, thinners, or strippers, as we would normally find with decorative plating and nearly any substrate can be plated [10].

Alloy electrodeposition is widely employed in the production of new materials for applications requiring specific mechanical, chemical and physical properties. The process has numerous applications in depositing thin films for protective coatings, magnetic sensor and storage devices and as structures for micro-electro-mechanical systems (MEMS). Investigations of the electrodeposition of Fe-Ni alloys have been carried out mainly to identify the ability of these alloys to display stable, beneficial magnetic properties at room temperature [11]. The electrodeposition technique has major advantages over other methods of thin film production, namely, the possibility of performing deposition at normal conditions of pressure and temperature, requiring relatively inexpensive equipment.

Bulk nanostructured materials are defined as bulk solids with nanoscale or partly nanoscale microstructures. This category of nanostructured materials has historical roots going back many decades but has a relatively recent focus due to new discoveries of unique properties of some nanoscale materials. Early in the century, when "microstructures" were revealed primarily with the optical microscope, it was recognized that refined microstructures, for example, small grain sizes, often provided attractive properties such as increased strength and toughness in structural materials. The field of nanocrystalline materials as a major identifiable activity in modern materials science results to a large degree from the work of Gleiter and coworkers who synthesized ultrafine-grained materials by the in situ consolidation of nanoscale atomic clusters. The ultrasmall size (< 100 nm) of the grains in these nanocrystalline materials can result in dramatically improved of different properties from conventional grain size (>1 μm) polycrystalline or single crystal materials of the same chemical composition. This is the stimulus for the tremendous appeal of these materials. A number of bulk properties that may be dramatically changed when the microstructure is nanoscale are [12]:

- a. The mechanical properties of nanostructured materials for a variety of potential structural applications.
- b. Ferromagnetic materials with nanoscale microstructures for potential applications as soft magnetic materials and permanent magnet materials.
- c. Other special applications such as information storage, magnetoresistance spin valves and magnetic nanocomposite refrigerants.

Metallic alloy films, which are composed of magnetic elements, have regained attention over the past decade due to their magnetic and magnetoresistive properties. The properties of magnetoresistive systems are closely related to their constituent elements and their structures. Fe-Ni systems generally show anisotropic magnetoresistance properties [13]. Investigations on the magnetic and magnetoresistance properties of Fe-Ni alloy films are mostly focused on the properties of $\text{Ni}_{81}\text{Fe}_{19}$ permalloy systems. Different techniques may cause the films to have different structural and therefore different physical properties. Electrodeposition, which is a relatively cheap technique, does not need any sophisticated equipment and may easily be employed to grow Fe-Ni alloy films with different properties by controlling electrodeposition variables. At this time, a number of studies utilizing a more fundamental approach to the study of these binary alloys of varying composition produced using electrodeposition methodology began to emerge. This advancement in magnetic storage technology and the realization of the significance of permalloy in the magnetic recording industry at approximately the same time probably led to the considerable increase in the scientific interest in this alloy system.

Recently, electrochemical processes (electrodeposition and electroless deposition) have been widely used in electronic industries including [14]; computer read/write heads, microelectromechanical systems (MEMS), ultralarge scale integration (ULSI) devices, and electronic circuit packaging. Magnetic materials have recently been incorporated into MEMS devices such as sensors, microactuators, micromotors, and frictionless microgears because magnetically actuated MEMS are more durable for force applications [15]. In general, electroless deposits are less porous, more uniform and more corrosion resistant than electrodeposits. However, they are more expensive and less stable, and have slower deposition rates than that of the electrodeposition process [16]. Therefore, electrodeposition process may be more suitable for integration of magnetic materials into computer read/write heads and MEMS devices. In order to incorporate magnetic materials using electrodeposition process into devices, magnetic materials must have good adhesion, low-stress, high corrosion resistance and be thermally stable with excellent magnetic properties.

2.1 Electrodeposition

2.1.1 Basic Concepts of Electrodeposition

Electroplating is the deposition of a metallic coating by applying a negative charge onto a substrate in an electrochemical cell. An electrochemical cell is schematically depicted in Fig. 2.1. It consists of at least two electrodes (cathode and anode) where the electrochemical reactions occur, an electrolyte for conduction of ions, and an external conductor to provide for continuity of the circuit.

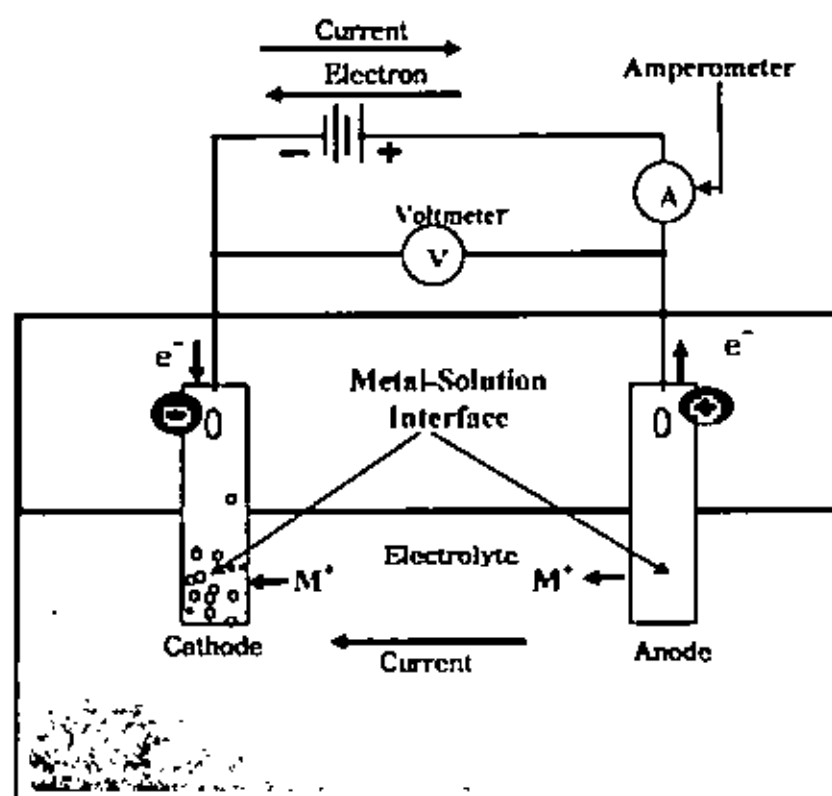


Fig. 2.1 Schematics of an electrolytic cell for plating metal

The anodic reactions are dependent on the anode materials chosen. Faraday's law, shown in Equation 2.1, relates the amount of charge passed to the amount of substance oxidized or reduced, which can be used to calculate the thickness of deposited metal films in electrodeposition [17].

$$It\eta = nF \left[\frac{m}{sM} \right] \text{-----} (2.1)$$

Where I is the applied current, t is the charging time, η is the current efficiency, n is the number of electrons transferred, F is the Faraday's constant (96485 C/equiv), m is the mass reacted, s is the stoichiometric coefficient and M is the molecular weight. At large applied current or potentials the mass transport mechanism dominates and causes the current to reach a limiting value.

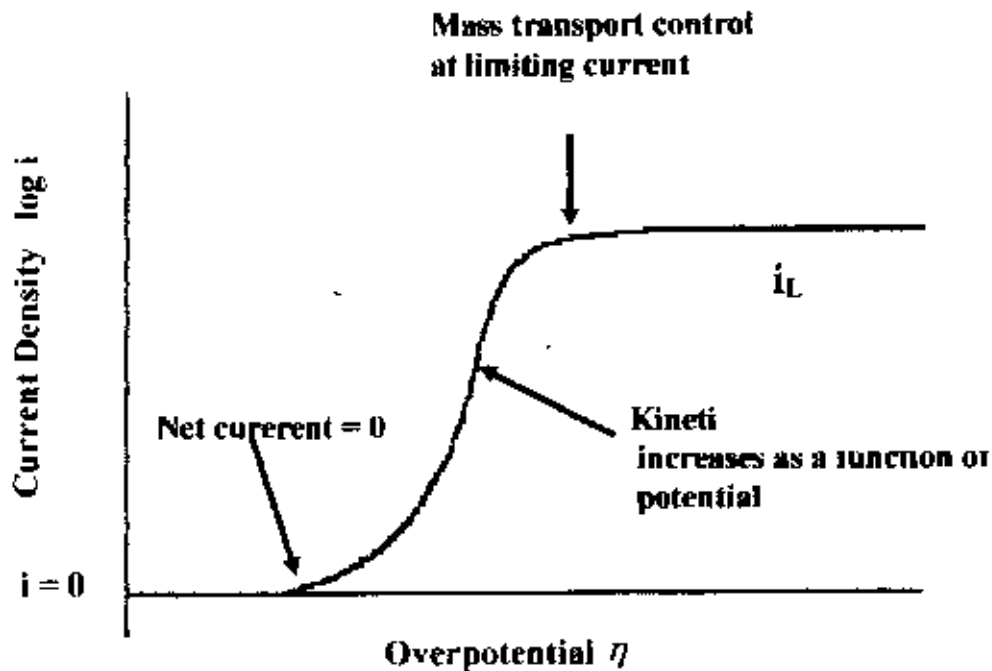


Fig. 2.2 Schematic illustrations of kinetic and mass transport control

Figure 2.2 shows the current response applied potential at steady state for a single reactant. At a low applied potential, the reduction reaction is under kinetic control. The surface concentration is approximately equal to the bulk concentration, and the reduction rate is dependent on the applied potential in an exponential way. The system is under a mixed control of kinetic and mass transport when the overpotential becomes larger. With further increase of overpotential, the surface concentration becomes less than the bulk concentration, and a concentration gradient of metal ions appears on the electrode surface. Finally when the surface concentration drops to zero, the mass transport control becomes completely dominant and the concentration gradient reaches a maximum value.

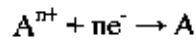
At this moment, a maximum current, referred to as the limiting current, is reached and the reaction rate reaches a maximum.

2.1.2 Alloy Electrodeposition

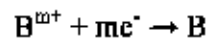
Alloy electrodeposition was first developed in the 1840s at nearly the same time as metal deposition, with brass coatings being an early commercial application. Despite this long history, alloy electrodeposition continues to attract attention; the majority of the electrodeposition related articles published by The Electrochemical Society are on alloys. The enduring interest in alloy electrodeposition is tied to the wide range and tunability of physical properties one can achieve by varying alloy composition. As a result, most high-value-added applications of electrodeposition involve alloys, with the notable exception of copper interconnects for integrated circuits. For example, in the emerging field of nano- and microelectromechanical systems (NEMS/MEMS), alloying is key for achieving materials that are sufficiently strong to withstand severe mechanical and environmental demands [17]. Other recent examples of alloy electrodeposition from the Journal and Letters include lithium-ion secondary battery anodes, magnetic recording materials; solder bumps, and catalysts for direct methanol fuel cells. The purpose of this tutorial is to provide non-expert practitioners of the art a flavor for the science, engineering, and issues that underpin and rationalize alloy electrodeposition.

Electrodeposition involves the reduction of precursor metal ions and/or metal ion complexes from solution at a conductive substrate (Chemical rednctants are used as the source of electrons in electroless deposition). At a minimum, an alloy electrodeposition process requires an electrolyte with two or more reducible metal ions, a conductive substrate, a counter electrode, a power supply, and a container to hold the electrolyte and electrodes. This simplicity accounts for the appeal of electrodeposition, but may also lead one to neglect some basic controls needed to ensure reproducibility. As we describe below, good alloy electrodeposition also requires a means for reproducibly mixing the electrolyte, some consideration of cell geometry, and, like all electrodeposition processes, careful substrate preparation.

Fig. 2.3 shows the polarization behavior for an ideal alloy codeposition system. In this ideal system, the deposition current for alloy AB is the sum of the pure metal partial currents from the independent reactions-



And



Where the constants n and m are the number of electrons transferred.

Deposition begins when the substrate potential is brought negative of the Nernst equilibrium potential for A, denoted E^{eq}_A . At this point, however, only A deposits since the substrate remains positive of the equilibrium potential for B, E^{eq}_B .

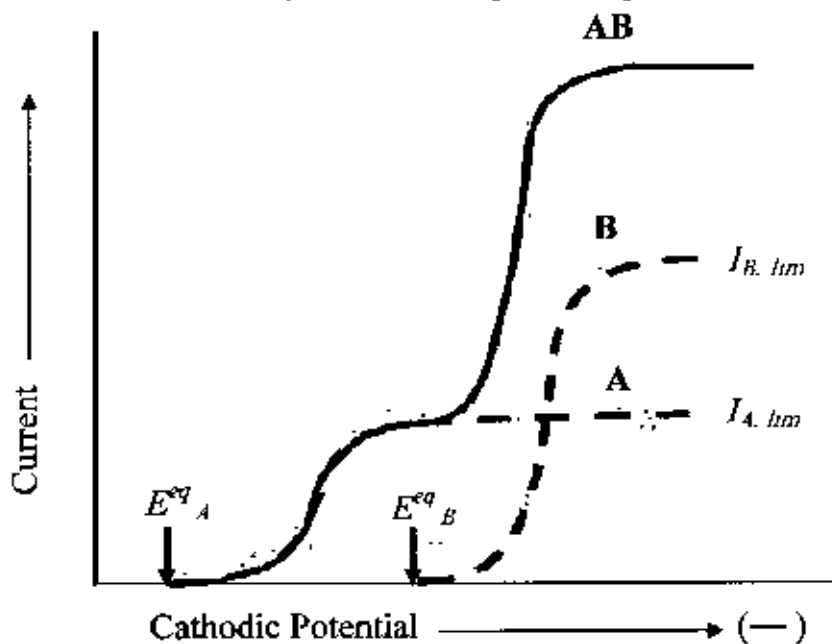


Fig. 2.3 An ideal polarization curve for the electrodeposition of the binary alloy AB results from the sum of pure metal (A and B) polarization curves.

Codeposition (i.e., alloy formation) begins when the potential is negative of the equilibrium potential for B [17]. The instantaneous composition of the resulting alloy is determined from Faraday's Law

$$X_A = \frac{I_A}{n} / \left(\frac{I_A}{n} + \frac{I_B}{m} \right) \dots \dots \dots (2.2)$$

Where X_A is the mole fraction of A in the AB alloy, and I_A and I_B are the partial currents for each alloy species.

Certain details of the polarization curves may explain why surface preparation and electrolyte agitation are important. The partial current for a species normally rises exponentially as the electrode potential moves negative of the equilibrium potential (called Tafel behavior). In this exponential region, the species partial current is limited by charge transfer between the conductive substrate and the precursor ion in solution. Charge transfer processes are highly dependent on the nature of the surface; reproducible cleaning and preparation of the substrate is essential if either species is charge transfer limited. Moreover, surface preparation also impacts nucleation and growth on the substrate, which can affect the deposit grain size and roughness. As the potential of the substrate becomes even more negative compared to the species equilibrium potential, one normally reaches the mass transfer limiting current for that species, denoted $I_{A \text{ lim}}$ and $I_{B \text{ lim}}$ for A and B, respectively, in Fig. 2.3. The mass transfer limiting current is the maximum current achievable, and is proportional to the precursor ion concentration and diffusivity (the ease with which the precursor ion moves through the solvent), as well as how strongly the electrolyte is agitated. Thus, if one or more species are mass transfer limited, how the electrolyte is mixed impacts the alloy composition.

In most real alloy electrodeposition systems, both mass transfer and charge transfer effects are important, meaning the surface preparation and mixing conditions must be controlled for reproducible results. Further, the influence of electrolyte resistance between the substrate and counter electrode must be recognized. How one arranges the two electrodes, therefore, may change the cell potential and affects how current is distributed to the substrate (current follows the path of least resistance through the electrolyte). Alloy electrodeposition systems may have many further complexities, none of which undermines the lessons learned from an idealized system. Water electrolysis often obscures the alloy deposition behavior shown in Fig. 2.3 and also reduces the

electrodeposition current efficiency. In anomalous codeposition systems, interactions between the depositing species cause the less easily reduced metal to inhibit deposition of the more easily reduced metal.

In induced codeposition systems, one species catalyzes the deposition of the other. For example, molybdenum and tungsten cannot be electrodeposited from aqueous electrolytes unless they are codeposited with iron-group elements [18]. We have also not discussed the nature of electrolytes and the use of various metal ion complexants like cyanide, citrate, sulfamate, fluoroborate, pyrophosphate, etc. to control the solubility, charge transfer kinetics, and equilibrium potentials of reducible metals.

2.1.3 Kinetics of Electrodeposition Reactions

From the moment that a current flows through an electrode, the electrode acquires a potential different from the reversible equilibrium potential. It is well to note here that equilibrium means dynamic equilibrium and that although no net current flows through the electrode, oxidation and reduction reactions will take place simultaneously, such that the oxidation current density i_{ox} is equal in magnitude to the reduction current density i_{red} . Both are, at equilibrium, equal to the so-called exchange current density and the equilibrium potential across the electrode is $\Delta\phi_e$.

In order to realize electrodeposition at a cathode, a net current $i = (i_{ox} - i_{red}) < 0$ has to flow through the cathode. Therefore the potential $\Delta\phi$ over the electrode interface has to deviate from $\Delta\phi_e$. This deviation is called the activation overpotential (η).

$$\text{Hence } \Delta\phi = \Delta\phi_e + \eta \dots\dots\dots (2.3)$$

The term “activation” refers to the fact that the electrode reaction is a kinetic process, in which substances must acquire certain activation energy before they can jump through the electrode interface. Deviation from the equilibrium potential is called polarization. As a result of the electrode reaction, the ionic concentration tends to change in the vicinity of the electrode, resulting in concentration overpotential η_{con} . For a reduction reaction at the cathode, for example, the concentration of positive ions is lowered, and

the equilibrium potential shifts according to the Nernst equation. If, as a result of an increasing cathodic polarization, the reduction current density is increased, positive ions have to be brought to the cathode surface faster and faster. This can occur by

- i) Migration under influence of the electrical field,
- ii) Diffusion due to the created concentration differences,
- iii) Natural or forced convection.

Another component is the crystallization overpotential (η_{cr}) originating from difficulties encountered with nucleation and growth. Minute concentrations of foreign substances can drastically increase the crystallization overpotential, and thus effectively slow down the electrodeposition process. The global electrode over potential is, now

$$\eta_{tot} = \eta + \eta_{con} + \eta_{cr} \dots\dots\dots (2.4)$$

An electrodeposition cell contains two electrodes: a cathode and an anode. Both contribute to the total cell potential according to equation (2.4). In addition there is the resistance of the electrolyte leading to a potential IR , and various other resistances in the cell circuit creating a potential E_R . The total cell potential is then,

$$E_{tot} = E_{rev} + \eta_{tot}^{an} + \eta_{tot}^{cat} + IR + E_R \dots\dots\dots (2.5)$$

The practical cell potential is therefore sometimes much higher than the reversible cell potential calculated from purely thermodynamic considerations.

2.1.4 Role of Static Potentials in the Electrodeposition of Alloys

In an electrochemical cell, an electric potential is created between two dissimilar metals. This potential is a measure of the energy per unit charge which is available from the oxidation/reduction reactions to drive the reaction. It is customary to visualize the cell reaction in terms of two half-reactions, an oxidation half-reaction and a reduction half-reaction.

Reduced species \rightarrow oxidized species + ne^- Oxidation at anode

Oxidized species + $ne^- \rightarrow$ reduced species Reduction at cathode

The cell potential (often called the electromotive force or emf) has a contribution from the anode which is a measure of its ability to lose electrons - it will be called its "oxidation potential". The cathode has a contribution based on its ability to gain electrons, its "reduction potential" The cell potential can then be written

$$E_{\text{cell}} = \text{oxidation potential} + \text{reduction potential}$$

If we could tabulate the oxidation and reduction potentials of all available electrodes, then we could predict the cell potentials of voltaic cells created from any pair of electrodes. Actually, tabulating one or the other is sufficient, since the oxidation potential of a half-reaction is the negative of the reduction potential for the reverse of that reaction. Two main hurdles must be overcome to establish such a tabulation

1. The electrode potential cannot be determined in isolation, but in a reaction with some other electrode.
2. The electrode potential depends upon the concentrations of the substances, the temperature, and the pressure in the case of a gas electrode.

In practice, the first of these hurdles is overcome by measuring the potentials with respect to a standard hydrogen electrode. It is the nature of electric potential that the zero of potential is arbitrary; it is the difference in potential which has practical consequence. Tabulating all electrode potentials with respect to the same standard electrode provides a practical working framework for a wide range of calculations and predictions. The standard hydrogen electrode is assigned a potential of zero volts. The second hurdle is overcome by choosing standard thermodynamic conditions for the measurement of the potentials. The standard electrode potentials are customarily determined at solute concentrations of 1 Molar, gas pressures of 1 atmosphere, and a standard temperature which is usually 25°C. The standard cell potential is denoted by a degree sign as a superscript. The example below shows values for Standard Electrode Potentials:

STANDARD ELECTRODE POTENTIALS

Cathode (Reduction) Half-Reaction	E^0 (Volts)
$\text{Li}^+ + \text{e}^- \rightleftharpoons \text{Li}$	-3.04
$\text{K}^+ + \text{e}^- \rightleftharpoons \text{K}$	-2.92
$\text{Ba}^{2+} + 2\text{e}^- \rightleftharpoons \text{Ba}$	-2.90
$\text{Ca}^{2+} + 2\text{e}^- \rightleftharpoons \text{Ca}$	-2.87
$\text{Na}^+ + \text{e}^- \rightleftharpoons \text{Na}$	-2.71
$\text{Mg}^{2+} + 2\text{e}^- \rightleftharpoons \text{Mg}$	-2.37
$\text{Al}^{3+} + 3\text{e}^- \rightleftharpoons \text{Al}$	-1.66
$\text{Mn}^{2+} + 2\text{e}^- \rightleftharpoons \text{Mn}$	-1.18
$2\text{H}_2\text{O} + 2\text{e}^- \rightleftharpoons \text{H}_2(\text{g}) + 2\text{OH}^-$	-0.83
$\text{Zn}^{2+} + 2\text{e}^- \rightleftharpoons \text{Zn}$	-0.76
$\text{Cr}^{2+} + 2\text{e}^- \rightleftharpoons \text{Cr}$	-0.74
$\text{Fe}^{2+} + 2\text{e}^- \rightleftharpoons \text{Fe}$	-0.44
$\text{Cr}^{3+} + 3\text{e}^- \rightleftharpoons \text{Cr}$	-0.41
$\text{Cd}^{2+} + 2\text{e}^- \rightleftharpoons \text{Cd}$	-0.40
$\text{Co}^{2+} + 2\text{e}^- \rightleftharpoons \text{Co}$	-0.28
$\text{Ni}^{2+} + 2\text{e}^- \rightleftharpoons \text{Ni}$	-0.25
$\text{Sn}^{2+} + 2\text{e}^- \rightleftharpoons \text{Sn}$	-0.14
$\text{Pb}^{2+} + 2\text{e}^- \rightleftharpoons \text{Pb}$	-0.13
$\text{Fe}^{3+} + 3\text{e}^- \rightleftharpoons \text{Fe}$	-0.04
$2\text{H}^+ + 2\text{e}^- \rightleftharpoons \text{H}_2(\text{g})$	0.00
$\text{Cu}^{2+} + \text{e}^- \rightleftharpoons \text{Cu}^+$	0.16
$\text{Cu}^{2+} + 2\text{e}^- \rightleftharpoons \text{Cu}$	0.34
$2\text{H}_2\text{O} + \text{O}_2 + 4\text{e}^- \rightleftharpoons 4\text{OH}^-$	0.40
$\text{Cu}^+ + \text{e}^- \rightleftharpoons \text{Cu}$	0.52
$\text{Fe}^{3+} + \text{e}^- \rightleftharpoons \text{Fe}^{2+}$	0.77
$\text{Hg}^{2+} + 2\text{e}^- \rightleftharpoons \text{Hg}(\text{l})$	0.78
$\text{Ag}^+ + \text{e}^- \rightleftharpoons \text{Ag}$	0.80
$\text{O}_2(\text{g}) + 4\text{H}^+ + 4\text{e}^- \rightleftharpoons 2\text{H}_2\text{O}$	1.23
$\text{Cr}_2\text{O}_7^{2-} + 14\text{H}^+ + 6\text{e}^- \rightleftharpoons 2\text{Cr}^{3+} + 7\text{H}_2\text{O}$	1.33
$\text{Cl}_2 + 2\text{e}^- \rightleftharpoons 2\text{Cl}^-$	1.36
$\text{Au}^{3+} + 3\text{e}^- \rightleftharpoons \text{Au}$	1.50
$\text{F}_2 + 2\text{e}^- \rightleftharpoons 2\text{F}^-$	2.87

The values for the table entries are reduction potentials, so lithium at the top of the list has the most negative number, indicating that it is the strongest reducing agent. The strongest oxidizing agent is fluorine with the largest positive number for standard electrode potential.

Useful applications of the standard electrode potentials include the following.

- Strengths of oxidizing and reducing agents
- Electrode potentials under non-standard conditions
- Potentials for voltaic cells
- Relationship to Gibbs free energy
- Relationship to equilibrium constants

2.1.5 The Nernst Equation

The cell potential for a voltaic cell under standard conditions can be calculated from the standard electrode potentials. But real voltaic cells will typically differ from the standard conditions. The Nernst equation relates the cell potential to its standard cell potential. The Nernst equation allows us to predict the cell potential for voltaic cells under conditions other than standard conditions of 1M, 1 atmosphere, 25°C.

The effects of different temperatures and concentrations may be tracked in terms of the Gibbs free energy change ΔG . This free energy change depends upon the temperature and concentrations according to

$$\Delta G = \Delta G^{\circ} + RT \ln Q \dots\dots\dots (2.6)$$

Where ΔG° is the free energy change under standard conditions and Q is the thermodynamic reaction quotient, R is the gas constant and T is the temperature in Kelvin. The free energy change is related to the cell potential E_{cell} by

$$\Delta G = -nFE_{cell} \dots\dots\dots (2.7)$$

Where
 F = Faraday's constant
 n = number of electrons transferred

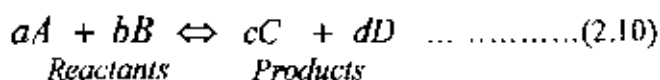
So for non-standard conditions

$$-nFE_{cell} = -nFE^{\circ}_{cell} + RT \ln Q \dots\dots\dots(2.8)$$

$$E_{cell} = E^{\circ}_{cell} - \frac{RT}{nF} \ln Q \dots\dots\dots(2.9)$$

This is called the Nernst equation.

The quantity Q, the thermodynamic reaction constant, is like a dynamic version of the equilibrium constant in which the concentrations and gas pressures are the instantaneous values in the reaction mixture. For a reaction



The reaction quotient has the form

$$Q = \frac{[C]^c [D]^d}{[A]^a [B]^b} \dots\dots\dots(2.11)$$

Where [C] is understood to be the molar concentration of product C, or the partial pressure in atmospheres if it is a gas.

2.2 Principles of Alloy Deposition

The six principles of alloy deposition are:

- i) If an alloy plating bath, which is in continuous operation, is replenished with two metals in a constant ratio M/N (for example, by adding metallic salts or by the use of soluble anodes) the ratio of the metals in the deposit will approach and ultimately take on the value M/N.
- ii) An increase in the metal-percentage (or ratio) of a parent metal in an alloy plating bath results in an increase in its percentage (or ratio) in the deposit.
- iii) In alloy deposition, the ratio of the concentration of the more readily depositable metal to the other is smaller at the cathode-solution interface than in the body of the bath.

iv) In the deposition of alloys from the normal alloy plating systems, the most fundamental mechanism is the tendency of the concentrations of the metal ions at the cathode-solution interface to approach mutual equilibrium with respect to the two parent metals. Both principles iii) and iv) lead to the relation

$$C_m / C_n < C_m^0 / C_n^0$$

Where,

C_m = Concentration of more readily depositable metal at the cathode-solution interface.

C_n = Concentration of less readily depositable metal at the cathode-solution interface.

C_m^0 = Concentration of more readily depositable metal in the body of the bath

C_n^0 = Concentration of less readily depositable metal in the body of the bath.

v) A variation in a plating condition that brings closer together the potentials for the deposition of the parent metals separately, i.e., decreases the interval of potential between them increases the percentage of the less noble metal in the electrodeposited alloy and vice-versa.

vi) In depositing alloys in which the content of the less noble metal increases with current density, the operating conditions for obtaining the more constant composition of deposit are: (a) constant potential if the uncontrollable variable affect the potentials of the more noble metal and (b) constant current density if the uncontrollable variables affect the potential of the less noble metal. Conditions (a) and (b) are interchanged if the content of the less noble metal decreases with current density.

2.2.1 Plating Variables

The composition of an electrodeposited alloy is a function of a large number of variables, the main ones of which are as follows:

A. Variables of bath content

1. Concentrations of depositable metals

- a) Ratio of the concentrations of depositable metals to each other
 - b) Total concentration of the depositable metals
2. Concentration of complexing agents
 3. pH of plating bath
 4. Presence of addition agents
 5. Presence of indifferent electrolytes or conducting salts.

B Variables of bath operation

1. Current density
2. Temperature
3. Agitation of bath or movement of cathode

C. Miscellaneous variables

1. Cathode current efficiency (CCE.)
2. Shape and surface of cathode
3. Basis metal
4. Anode-cathode distance
5. Thickness of deposit
6. Type and distribution of current.

2.2.2 Variation in the Composition of Electrodeposited Alloy with the Composition of the Bath and the Plating

2.2.2.1 Effect of Metal Ratio of the Bath on the Composition of the Deposit

The relation between the compositions of an electrodeposited alloy and the ratio of the parent metals in the bath is the most important relation in alloy plating system showing in Fig. 2.4.

Curve 1- Bismuth -copper alloys deposited from perchlorate bath

Curve 2- Copper-zinc alloys deposited from cyanide bath

One feature of Fig. 2.4 and 2.5 is that they contain an auxiliary line, AB which is referred to as the composition reference line. It is used as an aid visualizing the relation between the percentage composition of the alloy and the metal-percentage of the bath.

Points falling upon the composition reference line would represent alloys having the same percentage composition as the metal percentage of the bath.

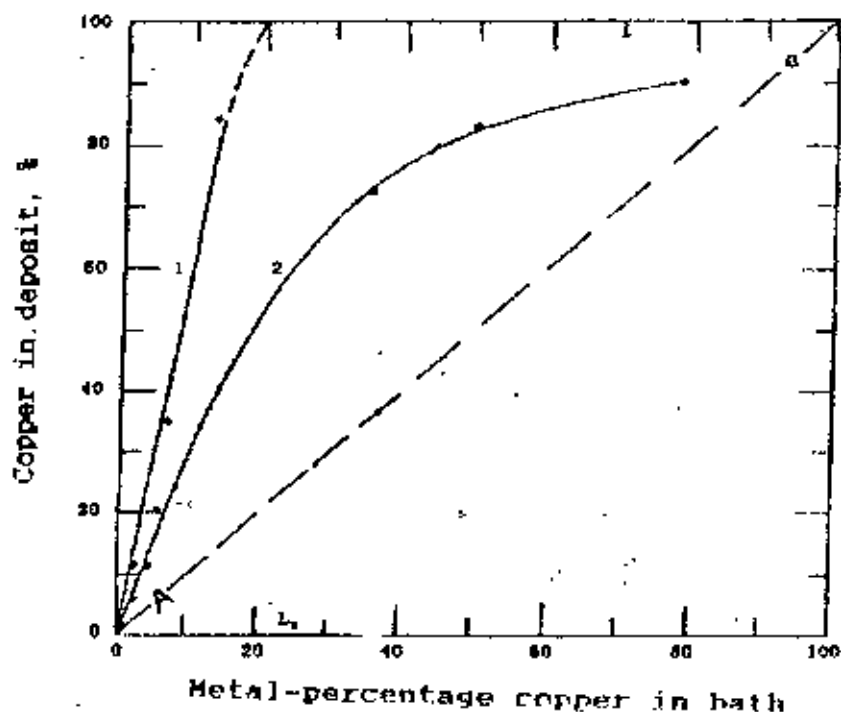


Fig. 2.4 Typical curves illustrating the relation between the composition of electrodeposited alloys and the composition of the bath in normal co deposition

A composition curve that rises above the composition reference line indicates that the metal in question is preferentially deposited because its percentage in the deposit is larger than its metal percentage in the bath. In normal codeposition, the more noble metal deposits preferentially, hence the curve for the percentage of the more noble metal in a deposit always lies above the composition reference line.

Similarly, Fig. 2.5 representing the percentage of the less noble metal plotted against its metal percentage in the bath lies below the composition reference line.

Curve 1: Iron-nickel alloys from the data of Iwase and Nasu deposited from sulfate bath [18].

Curve 2, 3, 7: Iron-nickel alloys from the data of Glasstone and Symes deposited from sulfate bath [21,22].

Curve 4. Iron-nickel alloys from the data of Korovin deposited from sulfate bath [23].

Curve 5: Iron-nickel alloys from the data of Engemann deposited from sulfate bath [24].

Curve 6: Iron-nickel alloys from the data of Toepffer deposited from sulfate bath [25].

Curve 8: Iron-nickel alloys from the data of Kremann and Mass deposited from sulfate bath [26].

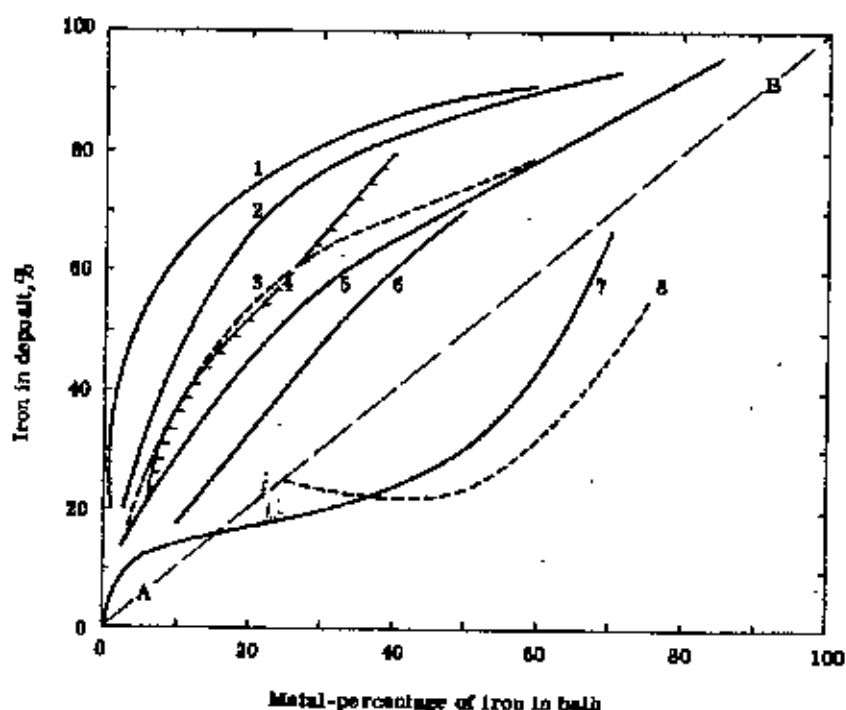


Fig. 2.5 Relation between the composition of the deposit and the composition of the bath in anomalous co-deposition

Fig. 2.5 illustrates the relation between the composition of the deposit and the composition of the bath in anomalous codeposition. The two important characteristics of the curves in Fig. 2.5 are as follows. (a) Under most conditions of deposition iron is more readily deposited than nickel, although it is the less noble metal. This is shown by the position of curves 1-6 above the composition-reference line AB. Thus, the codeposition is anomalous. This type of codeposition takes place mainly at room temperature and at current densities above 1 amp/dm^2 . (b) At elevated temperatures, represented by curve 8, or at lower current density (for example, 0.25 amp/dm^2),

represented by curve 7, the codeposition becomes normal over a limited range of bath composition. This is shown in the figure by these two curves lying at least partly below the composition-reference line AB.

Some of the alloy composition curves of the iron-nickel alloys look very similar to those of a normal alloy plating system possessing equilibrium codeposition. The characteristic of such curves is that they lie partly above and partly below the composition-reference line AB. For example, curve 7 of Fig. 2.5. At first blush, this gives the impression that where the iron-nickel composition curves cut the composition-reference line AB, equilibrium codeposition must be taking place, because here the composition of the alloy has the same composition as the deposit. However, this resemblance is only superficial.

Actually the iron-nickel composition curves are the inverse of what they should be for equilibrium codeposition; that is, the portion of the curve representing a low iron: nickel ratio in the bath should lie below AB and the portion of the curve representing the high iron: nickel ratio should lie above AB, if the deposition were of the equilibrium type.

2.2.2.2 Effect of Total Metal Content of the Bath on the Composition of the Deposit

Variation of the total metal content of a bath, at a fixed metal ratio, appreciably affects the composition of alloys in regular codeposition but has either slight effect or no uniform trend in irregular anomalous and induced codeposition

Curves 1 and 3: From the data of Glasstone and Speakman [27]

Curve 2: From the data of Fink and Lah [28]

In most instances an increase in the total metal ion concentration of the bath (at constant metal ratio) increased the iron content of the deposit. This result is very similar to the effect of total metal concentration in increasing the cobalt content of cobalt-nickel alloys. The effect of total metal content of the bath on the composition of the deposit in anomalous codeposition is illustrated in Fig. 2.6 with data on the deposition of Co-Ni

alloys taken from the work of Glasstone and Speakman [27] and Fink and Lah [28]. The alloys were deposited from simple sulfate baths. Cobalt deposited preferentially although it is less noble than Ni. The curves show that for a sevenfold increase in total metal content of the bath, the cobalt content of the deposit increased only slightly. At a given current density, the rate of deposition of the more noble metal is relatively much closer to its limiting value than that of the less noble metal. An increase of current density, therefore, must be borne mainly by an increase in the rate of deposition of the less noble metal.

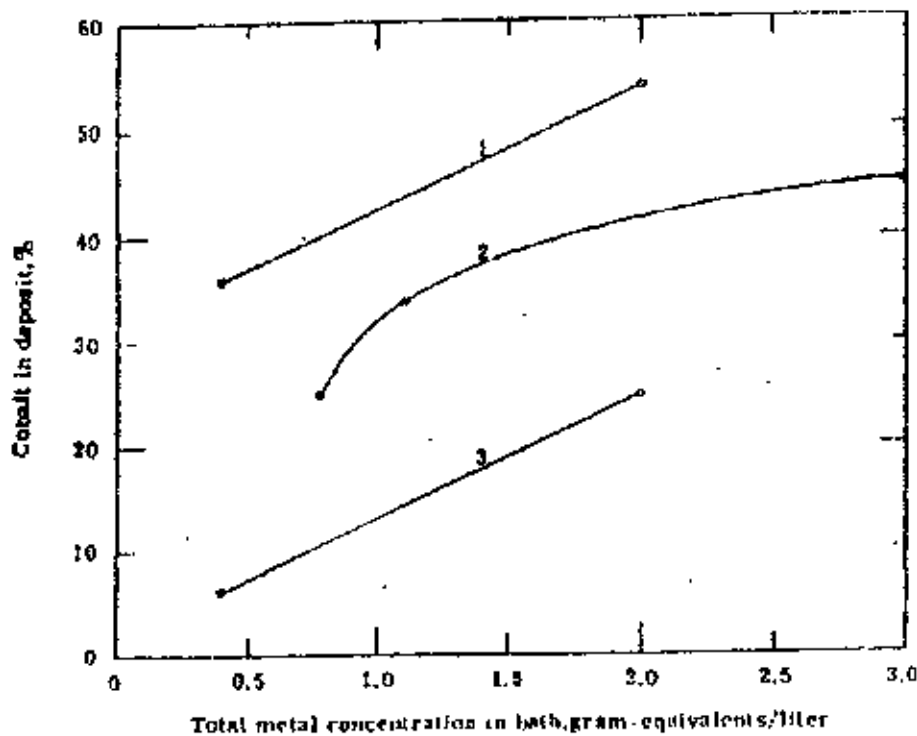


Fig. 2.6 Relation between the composition of the deposit and the total metal content of the bath in anomalous co-deposition.

Data of Marschak and co-workers [29] on solutions 0.35 and 1.0 M in total content of iron and nickel confirmed Glasstone's work. Chernilovskaya and co-workers [30] also found an increase in the iron content of the deposit with total metal concentration of the bath.

2.2.2.3 Effect of pH of the Plating Bath on the Composition of the Deposit

The effect of pH on the composition of an electrodeposited alloy is specific and usually unpredictable. In some baths, pH has a large effect and in others a small effect on the composition of the deposit. The determining factor is the chemical nature of the metallic compounds, because the pH does not exert its effect directly but by altering the state of chemical combination of the metals in solution. Simple metallic ions are only slightly sensitive to variations in the pH of the solution. On the other hand, the composition and stability of many complexes - in both alkaline and acid solution are a function of the pH. For example, complexes, such as stannate, zincate, cyanides and amines, which are stable in alkaline solution, decompose when acidified. As a general rule, variations of pH should have little effect on the composition of alloys deposited from baths containing the metals as simple ions and should have a large effect on the composition of alloy deposited from baths in which the parent metals were present as complexes with large instability constants.

Glasstone and Speakman [27] determined the most noble potentials at which the iron-group metals and their mutual alloys deposited from solutions of various pH. They did this by gradually increasing the current density and noting the potential at which codeposition was initiated. As might be expected the more acid the solution, the higher was the current density required to initiate metal deposition.

However, rather unexpected was the finding that the potential at which deposition initiated was, about the same in the solutions of various acidity. Since the potential of initial deposition was independent of the pH of the bath, one might surmise that the composition of the electrodeposited alloys might also be little influenced by variations in pH.

Curve 1-3, 5-6: Iron-nickel alloys from the data of Glasstone and Symes deposited from sulfate bath [21,22]

Curve 4: Iron-nickel alloys from the data of Aotani deposited from sulfate bath [31]

Within the range of pH about 3-5 the composition of the Fe-Ni alloys electrodeposited from the simple-salt plating bath did not show any definite trend with pH. This is shown in Fig. 2.7 with data mainly from Glasstone and Symes [21,22]. The figure also shows, that, with one or two exceptions, the variation of pH changed the composition of the deposit by a small percentage. This latter conclusion is also supported by the data of Kremann [26] and Engeman [24].

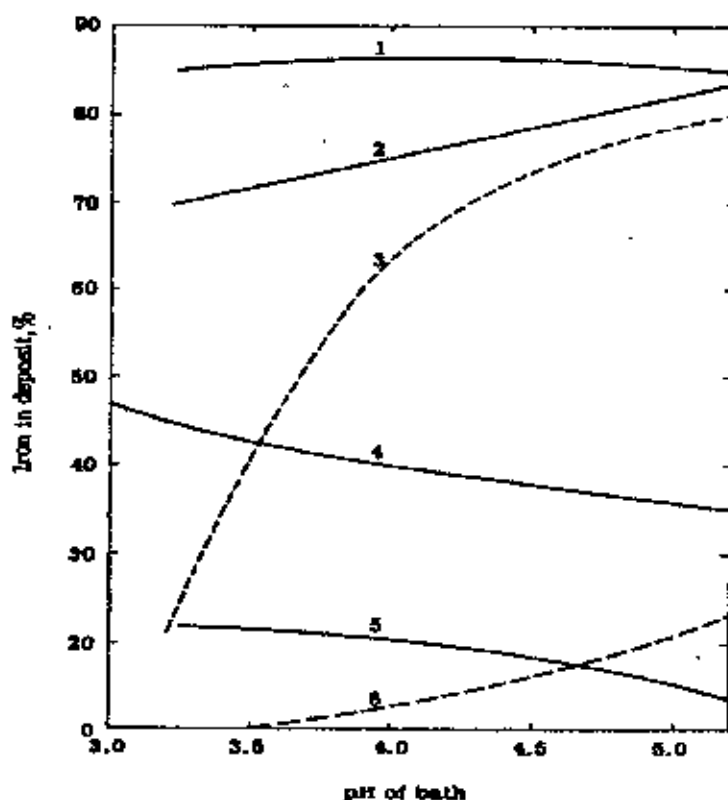


Fig. 2.7 Effect of pH on the composition of deposits in anomalous co-deposition

The reason for the lack of either a definite trend or large variations in composition of the alloy with pH is that there are no specific effects of pH on the alloy plating system.

2.2.2.4 Relation between Current Density and Composition of Electrodeposited Alloys

Current density is the most important of the operating variables. The mechanism may be examined from two view points: diffusion control and the cathode potential. diffusion

layer. At a given current density, the rate of deposition of the more noble metal is relatively much closer to its limiting value than that of the less noble metal. According to simple diffusion theory, the rate of deposition of a metal has an upper limit which is determined by the rate at which its ions can move through the cathode

An increase of current density, therefore, must be borne mainly by an increase in the rate of deposition of the less noble metal. With regard to the cathode potential, an increase of current density causes the cathode potential to become more negative (less noble) and hence this condition should increase the proportion of the less noble metal in the deposit. The situation is however different in anomalous codeposition showing the numerous curves in Fig. 2.8.

Curve 1, 3, 6: Iron-nickel alloys deposited from the data of Glasstone and Symes deposited from sulfate bath [21,22].

Curve 2, 4: Iron-nickel alloys deposited from the data of Marschak deposited from sulfate bath [29].

Curve 5: Iron-nickel alloys deposited from the data of Topffer deposited from sulfate bath [25].

Curve 7: Iron-nickel alloys deposited from the data of Engemann deposited from sulfate bath [24].

Curve 8: Iron-nickel alloys deposited from the data of Sysocva deposited from sulfate bath [32]

The numerous curves in Fig. 2.8 show that there was no uniform trend of the composition of the iron-nickel alloys with current density. In general, the variations in composition were small at the commonly used range of current density of a few amp/dm².

The reason for the vagarious nature of the relation between alloy composition and current density lies in the anomalous nature of the codeposition. The codeposition of the two metals can be of several processes, ranging from normal codeposition process at low current density to diffusion controlled process at high current density.

The effect of an elevation of current density in shifting codeposition from the normal to the anomalous type is strikingly illustrated in Fig. 2.5 by curves 3 and 7. The latter

curve represents deposition at 0.25 amp/dm^2 and lies mostly below the composition-reference line, thus indicating normal codeposition. Curve 3, representing deposition at 2 amp/dm^2 from the same bath is above the reference line, and thus indicates anomalous codeposition.

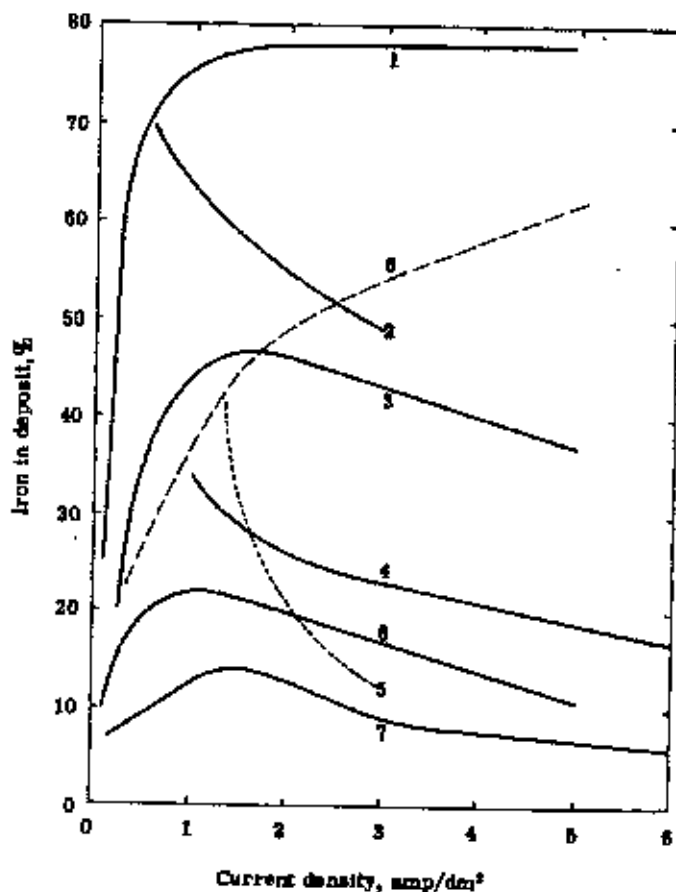


Fig. 2.8 Relation between alloy composition and current density in anomalous codeposition

In the curves presented in Fig. 2.5 and 2.8 there is evidence of the plating system coming under diffusion control as the current density was increased. The maximum of curves 3, 6, and 7 of Fig. 2.8 can be interpreted as indicating the current density at which the impoverishment of the diffusion layer in iron is causing the system to come under diffusion control. The effects of the latter are more evident in curve 5 which represents a dilute bath, only 0.065 M in total metal. With increasing current density the iron content of the deposit decreased and approached the metal-percentage of iron in the bath (1.0%) as limit.

Curve 8 taken from the data of Syssoeva [32] is of interest because it represents much higher current densities than those used by anyone else (the abscissa is to be multiplied by 10 for this curve); and despite the high current density it does not show a downward trend of iron content as might be expected.

2.2.2.5 Effect of Bath Temperature on Composition of Electrodeposited Alloys

General

Temperature is a critical variable in most practical plating baths, and for best results must usually be controlled within plus or minus about 2°C from the “optimum.” An increase in temperature increases the rate of diffusion and increases ionic mobilities, and therefore the conductivity of the bath. It also increases the rate of evaporation, rate of hydrolysis of bath constituents, and the rate of decomposition of additives. Most compounds become more soluble with increasing temperature, but there are exceptions. The effect of temperature on the composition of electrodeposited alloys may be the net result of changes in several characteristics of the plating system, such as the following:

(a) **Equilibrium potential:** The equilibrium potentials of the metals may change. This is probably not an important factor since the equilibrium potentials of metals do not change greatly with temperature and furthermore electrodeposition is far removed from equilibrium conditions.

(b) **Polarization:** The deposition potentials of metals usually become more noble with increase in temperature, because polarization is decreased. Whether the deposition of the more noble or less noble metal is favored depends on which deposition undergoes the largest decrease in polarization. These effects are specific and, therefore, the effect of temperature, via polarization, cannot be predicted without actual measurements on the deposition potentials of each of the metals.

(c) **Concentration:** An increase in temperature increases the concentration of metal in the cathode diffusion layer, because the rates of diffusion and of convection increase with

temperature. This is the most important mechanism by which temperature affects the composition of electrodeposited alloys. According to the principle of alloy deposition, an increase in metal concentration at the solution cathode interface favors increased deposition of that metal which already was depositing preferentially.

(d) Cathode current efficiency: Temperature may affect the composition of an electrodeposited alloy indirectly through its effect on the cathode current efficiency of deposition of the metals, particularly those deposited from complex ions. For example, an increase in temperature increases the cathode current efficiency of deposition of Sn from a stannate bath, and of Cu from a cyanide bath. In codepositing Sn or Cu with other metals whose efficiencies of deposition are unaffected by temperature the Sn or Cu content of the deposit will increase with temperature regardless of whether Sn or Cu happen to be the more noble or the less noble metal of the pair.

Of these four factors, (c) and (d) are the most important.

2.2.2.6 Effect of Bath Temperature on Composition of Alloys in Anomalous Codeposition

A complex relation occurs in the variations of alloy composition of anomalous type with the temperature of the bath. The effect of temperature can be qualitatively explained on the basis of two factors namely (i) Polarization and (ii) diffusion phenomenon. These two factors have opposite effects on the deposit composition. With increasing bath temperature, factor (i) favours a decrease and factor (ii) an increase in the content of the less noble metal in the deposit. These two opposing influences are responsible for the apparently inconsistent and rather indeterminate trends of alloy composition with temperature in anomalous codeposition.

The influence of polarization is especially important in anomalous codeposition, since the failure of the more noble metal to deposit preferentially may be construed as indicative of some kind of large polarization in the deposition of this metal. If this be granted then the reduction of polarization which occurs on raising the temperature of the plating bath should be, larger for the more noble metal and the deposition of the latter

should be favored to a larger extent than that of the less noble metal. Hence, in anomalous codeposition, the content of the more noble metal in the deposit may increase with temperature. An increase in temperature favours the deposition of that metal which is preferentially deposited, because it speeds up diffusion and thus relieves the depletion of metal at the cathode. Since in anomalous codeposition, the less noble metal deposits preferentially, an elevation of temperature should increase the content of the less noble metal in the deposit.

Curve 1, 2^a, 4^a: Iron-nickel alloys deposited from the data of Glasstone and Symes deposited from sulfate bath [21,22].

Curve 2^b: Iron-nickel alloys deposited from the data of Aotani deposited from sulfate bath [31].

Curve 3: Iron-nickel alloys deposited from the data of Marschak deposited from sulfate bath [29].

Curve 4^b: Iron-nickel alloys deposited from the data of Engemann deposited from sulfate bath [24].

Curve 5: Iron-nickel alloys deposited from the data of Sysoeva deposited from sulfate bath [32].

As was the case with the cobalt-nickel alloys, the composition of the electrodeposited iron-nickel alloys did not show a definite trend of composition with elevation of temperature. Typical data are given in Fig. 2.9 from several sources. The data of Aotani and Engemann coincided so closely with curves 2 and 4 of Glasstone and Symes that their data have been represented only by crosses on these curves. In some instances, an elevation of temperature tended to relieve anomalous codeposition and bring about normal codeposition. This resulted in a decrease in the iron content of the deposit as illustrated by a comparison of curve 2 with curve 8 in Fig.2.5. The latter curve represents a temperature of deposition of 75°C, and it lies below the composition-reference line AB. This indicates normal codeposition.

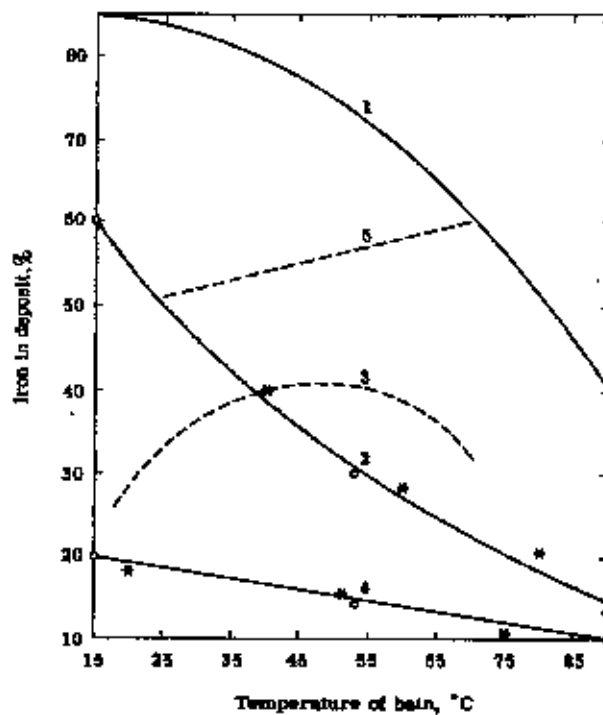


Fig. 2.9 Relation between alloy composition and Temperature in anomalous codeposition (a: data represented by circles on curves and b: data represented by crosses on curves)

2.2.2.7 Effect of Agitation of Bath or Rotation of Cathode on the Composition of Electrodeposited Alloys

Agitation of an alloy plating bath or rotation of the cathode can directly affect the composition of the alloy by reducing the thickness of the cathode diffusion layer. This is a purely mechanical action which does not change the electrochemical properties of the solution or the mechanism of the plating process. Being of this nature, agitation has a more consistent influence on the composition of the deposit than either temperature or current density.

The effect of agitation on the composition of the deposit is due to the concentration changes which it produces at the cathode-solution interface. During alloy deposition, the cathode diffusion layer is depleted in metal ions and furthermore, the ratio of the concentrations of the metals in the layer differs from that in the body of the bath. Agitation of the bath or rotation of the cathode, by decreasing the thickness of the

cathode diffusion layer not only results in an increase in the concentration of metal ion in the cathode diffusion layer, but also causes the metal ratio of the diffusion layer to approach more closely to that of the solution in the body of the bath. This favors an increased rate of deposition of that metal which is already depositing preferentially. The effect of agitation, thus, is similar to that of increasing the concentration or the temperature of a bath.

The effect of agitation of the bath on the composition of electrodeposited iron-nickel alloys appears to depend on the range of current density used. For example, Glasstone and Symes [21,22] found that at current densities of 1 or 2 amp/dm², agitation increased the iron content of the deposit. However, at current density of 0.5 amp/dm², they observed that agitation reduced the iron content of the deposit. The difference in these two effects of agitation is probably owing to the alloy plating system being of the diffusion controlled, anomalous type at the high current density and of the normal type at the low current density. The effect of agitation at the high current density is similar to that generally observed for the deposition of cobalt-nickel alloys. That is, the decrease in the content of the preferentially deposited metals, iron cobalt, in the deposit is evidence that the systems are under diffusion control.

2.3 Types of Alloy Plating Systems

The data on the effects of variables on the composition of electrodeposited alloys constitute a massive array of details. The organization, presentation and theoretical discussion of these data are, greatly simplified by dividing the entire alloy plating processes into five types. These are:

- i) Regular codeposition
- ii) Irregular codeposition
- iii) Equilibrium codeposition
- iv) Anomalous codeposition
- v) Induced codeposition

Types i) -iii) are collectively referred to as normal alloy plating systems and are characterized by the preferential deposition of the more noble metal. Types iv) and v) are referred to as abnormal codeposition because the more noble metal does not necessarily deposit preferentially.

i) Regular codeposition: Regular codeposition is characterized by the deposition being under diffusion control. The effects of plating variables on the composition of the deposit are determined by changes in the concentrations of metal ions in the cathode diffusion layer and are predictable from simple diffusion theory. The percentage of the more noble metal in the deposit is increased by those agencies that increase the metal ion content of the cathode diffusion layer. The agencies are: increase in total metal content of bath, decrease of current density, elevation of bath temperature and increased agitation of bath. Deposition of Pb-Sn, Bi-Ca etc. is the examples of regular codeposition system.

ii) Irregular codeposition: The system is characterized by being controlled by the potentials of the metals (cathode potentials) against the solution to a greater extent than by diffusion phenomena. The effects of some of the plating variables on the composition of the deposit are in accord with simple diffusion theory and the effects of others are contrary to diffusion theory. Also, the effects of plating variables on the composition of the deposit are much smaller than with the regular alloy plating systems. Irregular codeposition is most likely to occur with solutions of complex ions. It is the least well characterized of the five types. The examples of this system are the deposition of brass, bronze and Sn-Zn.

iii) Equilibrium Codeposition: Equilibrium codeposition is characterized by deposition from a solution which is in chemical equilibrium with both of the parent metals. Only a few alloy plating systems of this type have been investigated. There are the Cu-Bi and Pb-Sn alloys deposited from an acid bath and perhaps Cu-Ni alloys deposited from a thiosulfate bath.

iv) **Anomalous Codeposition.** Anomalous codeposition is characterized by the anomaly that the less noble metal deposits preferentially. With a given plating bath, anomalous codeposition occurs only under certain conditions of concentration and operating variables.

Otherwise the codeposition falls under one of the three other types. Anomalous codeposition can occur in baths containing either simple or complex ions of the metals. Anomalous codeposition is rather rare. Fe-Ni alloy deposition is of this type.

v) **Induced Codeposition:** Induced codeposition is characterized by the deposition of alloy containing metals, such as Mo, W or Ge, which cannot be deposited alone. However, these metals readily codeposit with the iron group metals. Metals which stimulate deposition are called inducing metals and the metals which do not deposit by themselves are called reluctant metals. The effects of the plating variables on the composition of the alloys of induced codeposition are more vagarious and unpredictable than the effects on the composition of alloys or any of the other types of codeposition.

2.4 Purposes of Electrodeposition

The purposes for which articles are electroplated have already been mentioned in the introduction, but they are worth repeating: electrodeposited coatings may be applied for (1) appearance, (2) protection, (3) special surface properties, or (4) engineering or mechanical properties. The distinctions between these aims are not, of course, clear-cut, and there are many overlapping categories. A deposit applied purely for appearance must be, at least to some extent, protective as well. But the classification is convenient.

2.4.1 Decorative Plating

Many metals do not possess much "eye appeal" or lose such pleasing appearance as they do possess rather quickly on exposure to ordinary conditions: zinc die castings and ordinary steels, which are the least expensive metals available for most articles, are dull and not very attractive. A thin coating of a metal such as chromium enhances their

appearance and adds to their sales value. Chromium can be plated in a bright condition, and when properly applied, it maintains its brightness over long periods. For this reason chromium is the most common electroplate for decorative purposes. But since coatings of chromium thick enough to retain some measure of their original appearance are difficult to apply and very expensive, decorative chromium deposits are almost universally applied over undercoats of copper and nickel or nickel alone, and the final chromium coating is very thin. (Chromium plate is often called chrome plate, and this usage is now legitimized by some dictionaries. Here "chrome" is used for chromium ore, the metal is chromium.)

Other electroplated metals used for decorative effects include gold, silver, brass, bronze, nickel, copper and rhodium. Lead and tin are sometimes used for special effects.

2.4.2 Protective Plating

The function of protecting the basis metal from degradation overlaps that of improving its appearance. The common copper/nickel/chromium composite applied to automotive hardware and numerous other items not only imparts a pleasing appearance, but also protects the substrate from corrosion. However, when corrosion prevention is the only, or principal, aim of the coating, zinc is the most economical and most effective metal available. Although zinc can be plated in a bright condition, or brightened after plating by so-called conversion coatings, this coating does not retain its brightness very long in service and would not be chosen where decorative appeal is the main consideration. However, zinc is the most economical coating for preventing steel from rusting. Cadmium is far more expensive than zinc, but is superior to it for some environments, especially marine

Tin is not normally protective to steel, but in the particular conditions obtaining inside the sanitary can (sanitary meaning containing foods or beverages) the usual potentials of tin and iron are reversed and tin becomes protective. Tin plating of steel for use in the "tin can" is the largest single use of electroplating, in terms of tonnage of product.

2.4.3 Special Surface Properties

This category cannot be characterized by generalities: each use has its own particular reason for being. Soft solder, a tin-lead alloy sometimes containing other minor constituents, is used widely in the communications and electronics industry for making electrical connections, and for this purpose the parts to be joined must be easily and quickly wetted by the molten solder, often without the use of any corrosive fluxes. Although copper, almost universally used as the electrical conductor, is wetted by solder when its surface is fresh and untarnished, as it quickly tarnishes and becomes difficult to solder. A coating of tin or tin-lead alloy renders the surface far more solderable. Light reflection is another surface property that can be modified by coating. Both silver and rhodium are used for this application. In electrical and electronic industry, Gold plating is used to keep the resistance minimum of the mating surface.

2.5 The Plating Bath

The plating bath is practically always an aqueous solution containing a compound of the metal to be deposited. Nonaqueous solutions, in which the solvent may be an organic or inorganic liquid or a fused salt, are of great theoretical interest. But there is hardly any commercial use of such solutions; the only present exception is the plating of aluminium from an organic electrolyte, practiced by only a few highly specialized shops. A few of the so-called refractory metals such as tantalum, niobium, zirconium, and tungsten, have been plated in adherent and coherent form from fused electrolytes on a large scale, but again only by a few specialists. Otherwise all electroplating baths are aqueous.

2.5.1 Ingredients of a Plating Bath

Every plating bath contains ingredients which serve one or more of the following functions.

1. To provide a source of the metal or metals being deposited. i.e., the bath must contain the metal to be deposited.

2. To form complexes with ions of the depositing metal: Complex formation is not always required, and some metals are plated from simple salt solutions. In many cases, however, it is found that the deposits obtained from complex ions are superior to those from simple ions.

3. To provide conductivity: Any ionic solution conducts electricity, but many metal salts are rather poor conductors (their ions have low mobilities), and to avoid the necessity for the employment of high voltages, "conducting salts" are often added.

4. To stabilize the solution, e.g., against hydrolysis: Most metal salts are subject to hydrolysis, since most metal hydroxides are insoluble:



In some alkaline baths, absorption of carbon dioxide from the air would precipitate metal compounds unless acceptors for carbon dioxide were present.

5. To act as a buffer, i.e., to stabilize the pH: Many plating solutions are highly acidic or highly alkaline, and for this pH control is a minor concern. For that class of solutions known as "neutral," i.e., with pH between about 5 and 8, control of pH within prescribed limits is important, and buffering is usually necessary.

6. To modify or regulate the physical form of the deposit: When direct current is passed from an anode to a cathode through a solution containing a depositable metal ion, the metal will deposit on the cathode but frequently the deposit will be useless, consisting of trees and nodules, either nonadherent or noncoherent, unless additives are present to control its physical form.

7. To aid in dissolving the anodes. Unless anodes are deliberately inert i.e., act merely to introduce current into the solution, it is desired that they replenish the metal deposited at the cathode so that the composition of the bath remains relatively stable. Anodes of some metals tend to become "passive," i.e., to act as inert anodes, unless specific ions are present that tend to break down this passivity.

8. To modify other properties, either of the solution or of the deposit, peculiar to the specific case: Finally, some baths require specific additives for specific purposes. An example is the addition to most zinc cyanide baths of sulfur compounds such as sodium polysulfide to precipitate impurities that would interfere with satisfactory plating.

This does not mean that all plating baths contain eight ingredients, since some compounds perform more than one of these functions, and in some instances not all of the listed functions are necessary.

2.6 Bulk Behavior of Nanostructured Materials

Bulk nanostructured materials are defined as bulk solids with nanoscale or partly nanoscale microstructures. This category of nanostructured materials has historical roots going back many decades but has a relatively recent focus due to new discoveries of unique properties of some nanoscale materials.

Early in the century, when “microstructures” were revealed primarily with the optical microscope, it was recognized that refined microstructures, for example, small grain sizes, often provided attractive properties such as increased strength and toughness in structural materials. A classic example of property enhancement due to a refined microstructure with features too small to resolve with the optical microscope was age hardening of aluminium alloys. The phenomenon, discovered by Alfred Wilm in 1906, was essentially explained by Merica, Waltenberg, and Scott in 1919 (Mehl and Cahn 1983, 18) and the microstructural features responsible were first inferred by the X-ray studies of Guinier and Preston in 1938. With the advent of transmission electron microscopy (TEM) and sophisticated X-ray diffraction methods it is now known that the fine precipitates responsible for age hardening, in Al-4% Cu alloys, for example, are clusters of Cu atoms Guinier-Preston (GP) zones and the metastable partially coherent θ' precipitate (Silcock et al 1953-54) [100], (Cohen 1992). Maximum hardness is observed with a mixture of GP II (or θ') (coarsened GP zones) and θ' with the dimensions of the θ' plates, typically about 10 nm in thickness by 100 nm in diameter.

Therefore, the important microstructural feature of age-hardened aluminium alloys is nanoscale. There are a number of other examples of nanoscale microstructures providing optimized properties. The critical current density J_c of commercial superconducting Nb_3Sn is controlled by grain size and is inversely proportional to grain size, with grain sizes of 50-80 nm providing high values of J_c (Scanlan et al. 1975).

The field of nanocrystalline (or nanostructured, or nanophase) materials as a major identifiable activity in modern materials science results to a large degree from the work in the 1980s of Gleiter and coworkers (Gleiter 1990), who synthesized ultrafine-grained materials by the in situ consolidation of nanoscale atomic clusters. The ultrasmall size (< 100 nm) of the grains in these nanocrystalline materials can result in dramatically improved or different properties from conventional grain-size ($> 1 \mu m$) polycrystalline or single crystal materials of the same chemical composition. This is the stimulus for the tremendous appeal of these materials.

While there are a number of bulk properties that may be dramatically changed when the microstructure is nanoscale, this chapter focuses on those for which the recent work with nanostructured materials has been most extensive. These are (1) the mechanical properties of nanostructured materials for a variety of potential structural applications, and (2) ferromagnetic materials with nanoscale microstructures for potential applications as soft magnetic materials and permanent magnet materials, and for other special applications such as information storage, magnetoresistance spin valves, and magnetic nanocomposite refrigerants. Other bulk applications such as hydrogen storage are discussed briefly.

2.6.1 Mechanical Behavior

2.6.1.1 Structural Nanostructured Materials

The great interest in the mechanical behavior of nanostructured materials originates from the unique mechanical properties first observed and/or predicted for the materials prepared by the gas condensation method. Among these early observations/predictions were the following:

- lower elastic moduli than for conventional grain size materials by as much as 30 -50%
- very high hardness and strength—hardness values for nanocrystalline pure metals (~ 10 nm grain size) are 2 to 7 times higher than those of larger grained (>1 μm) metals
- a negative Hall-Petch slope, i.e., decreasing hardness with decreasing grain size in the nanoscale grain size regime
- ductility perhaps superplastic behavior at low homologous temperatures in brittle ceramics or intermetallics with nanoscale grain sizes, believed due to diffusional deformation mechanisms

While some of these early observations have been verified by subsequent studies, some have been found to be due to high porosity in the early bulk samples or to other artifacts introduced by the processing procedures. The following summarizes the author's understanding of the state of the art of the mechanical behavior of nanostructured materials, as determined from the literature, presentations at the U.S. workshop (Siegel et al. 1998) [33], and the WTEC panel's site visits in Japan and Europe.

2.6.1.2 Elastic Properties

Early measurements of the elastic constants on nanocrystalline (nc) materials prepared by the inert gas condensation method gave values, for example for Young's Modulus, E , that were significantly lower than values for conventional grain size materials. While various reasons were given for the lower values of E , it was suggested by Krstic and coworkers (1993), that the presence of extrinsic defects pores and cracks, for example was responsible for the low values of E in nc materials compacted from powders. This conclusion was based on the observation that nc NiP produced by electroplating with

negligible porosity levels had an E value comparable to fully dense conventional grain size Ni (Wong et al. 1994, 85). Subsequent work on porosity-free materials has supported these conclusions, and it is now believed that the intrinsic elastic moduli of nanostructured materials are essentially the same as those for conventional grain size materials until the grain size becomes very small, e.g., < 5 nm, such that the number of atoms associated with the grain boundaries and triple junctions becomes very large. This is illustrated in Fig. 2.10 for nanocrystalline Fe prepared by mechanical attrition and measured by a nano-indentation technique. Thus, for most nanostructured materials (grain size > 10 nm), the elastic moduli are not unique properties and not a “negative”.

2.6.1.3 Hardness and Strength

Hardness and strength of conventional grain size materials (grain diameter, $d > 1 \mu\text{m}$) is a function of grain size. For ductile polycrystalline materials the empirical Hall-Petch equation has been found to express the grain-size dependence of flow stress at any plastic strain out to ductile fracture. In terms of yield stress, this expression is $\sigma_0 = \sigma_1 + kd^{-1/2}$, where σ_0 = yield stress, σ_1 = friction stress opposing dislocation motion, k = constant, and d = grain diameter. Similar results are obtained for hardness, with $H_0 = H_1 + kd^{-1/2}$. To explain these empirical observations, several models have been proposed, which involve either dislocation pileups at grain boundaries or grain boundary dislocation networks as dislocation sources. In all cases the Hall-Petch effect is due to dislocation motion/generation in materials that exhibit plastic deformation. Most of the mechanical property data on nc materials have pertained to hardness, although some tensile test data are becoming available. Several recent reviews have summarized the mechanical behavior of these materials (Siegel and Fougere 1994, 233–261), (Siegel 1997) [34], (Morris and Morris 1997) [35], (Weertman and Averbach 1996, 323–345) [36]. It is clear that as grain size is reduced through the nanoscale regime (< 100 nm), hardness typically increases with decreasing grain size and can be factors of 2 to 7 times harder for pure nc metals (10 nm grain size) than for large-grained ($> 1 \mu\text{m}$) metals.

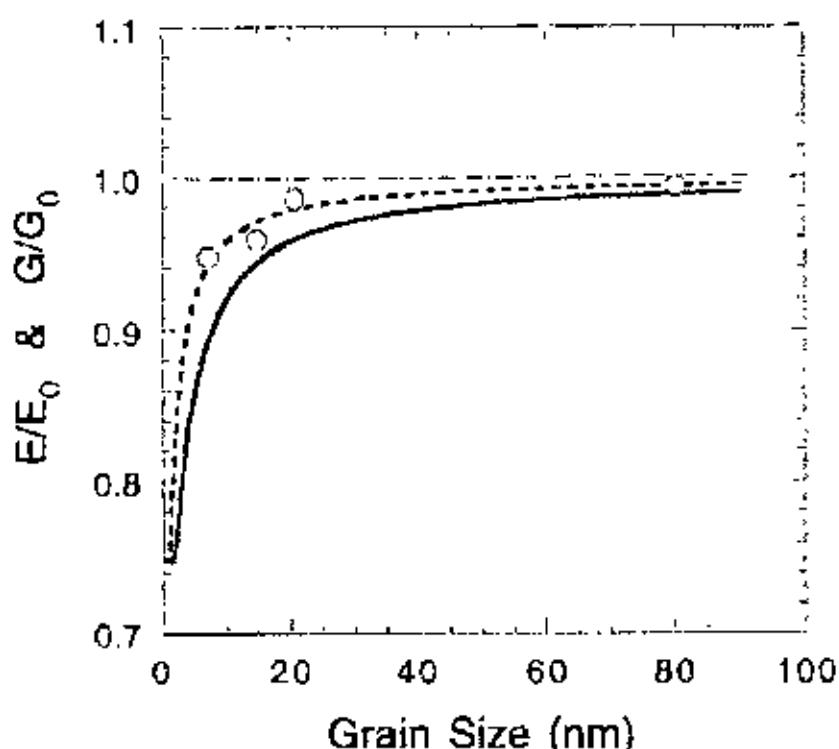


Fig. 2.10 Ratio of the Young's (E) and shear (G) moduli of nanocrystalline materials to those of conventional grain size materials as a function of grain size. The dashed and solid curves correspond to a grain boundary thickness of 0.5 and 1 nm, respectively (Shen et al. 1995).

The experimental results of hardness measurements, summarized previously, show different behavior for dependence on grain size at the smallest nc grains (< 20 nm), including (a) a positive slope ("normal" Hall-Petch behavior), (b) essentially no dependence (\sim zero slope), and (c) in some cases, a negative slope (Siegel and Fougere 1994, 233–261), (Siegel 1997), (Morris and Morris 1997), (Weertman and Averback 1996, 323–345).

Most data that exhibit the negative Hall-Petch effect at the smallest grain sizes have resulted from nc samples that have been annealed to increase their grain size. It is suggested that thermally treating nanophase samples in the as-produced condition may result in such changes in structure as densification, stress relief, phase transformations, or grain boundary structure, all of which may lead to the observed negative Hall-Petch behavior (Siegel and Fougere 1994, 233–261).

Only a few cases of negative Hall-Petch behavior have been reported for as-produced nanocrystalline samples with a range of grain sizes. These include electrodeposited nc alloys and devitrified nc alloys (Erb et al 1996, 93-110 and Alves et al. 1996) [37]. Nanocrystalline thin films with grain sizes ≤ 6 nm are also observed to exhibit a negative Hall-Petch effect (Veprék 1998). While it seems likely that in many cases the observed negative Hall-Petch slopes are due to artifacts of the specimen preparation methods, it is also likely that conventional dislocation-based deformation is not operable in nanocrystalline materials at the smallest grain sizes ($< \sim 30$ nm). At these grain sizes, theoretically, mobile dislocations are unlikely to occur; nor have they been observed in TEM deformation experiments (Siegel and Fougere 1994, 233-261), (Milligan et al 1993), (Ke et al. 1995). Thus, the hardness, strength, and deformation behavior of nanocrystalline materials is unique and not yet well understood.

2.6.1.4 Ductility and Toughness

It is well known that grain size has a strong effect on the ductility and toughness of conventional grain size ($> 1 \mu\text{m}$) materials. For example, the ductile/brittle transition temperature in mild steel can be lowered about 40°C by reducing the grain size by a factor of 5. On a very basic level, mechanical failure, which limits ductility, is an interplay or competition between dislocations and cracks (Thomson 1996, 2208-2291) [38]. Nucleation and propagation of cracks can be used as the explanation for the fracture stress dependence on grain size (Nagpal and Baker 1990). Grain size refinement can make crack propagation more difficult and therefore, in conventional grain size materials increase the apparent fracture toughness. However, the large increases in yield stress (hardness) observed in nc materials suggest that fracture stress can be lower than yield stress and therefore result in reduced ductility.

The results of ductility measurements on nc metals are mixed and are sensitive to flaws and porosity, surface finish, and method of testing (e.g., tension or compression testing). In tension, for grain sizes < 30 nm, essentially brittle behavior has been observed for pure nanocrystalline metals that exhibit significant ductility when the grain size is conventional. This is illustrated in Fig. 2.11. In some metals, Cu for example, ductile

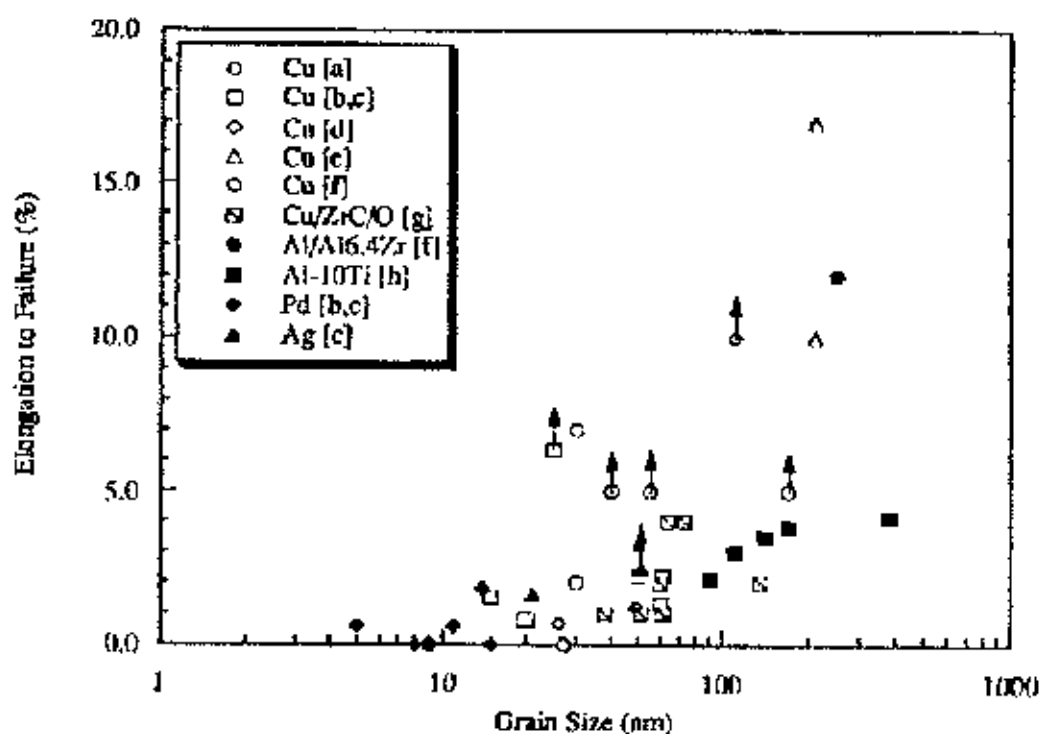
behavior is observed in compression, along with yield strengths about twice those observed in tension. While it is likely that the flaws and porosity present in many nc samples seriously affect the results of mechanical tests and may be partly responsible for the asymmetry of results in compression compared to tension tests, the nature of the deformation process in terms of shear banding (shown below) may also be important.

The above behavior is presumably due to the inability of usual dislocation generation and motion to occur at these smallest nc grain sizes. An intriguing suggestion based on early observations of ductile behavior of brittle nc ceramics at low temperatures is that brittle ceramics or intermetallics might exhibit ductility with nc grain structures (Karch et al. 1987), (Bohn et al. 1991). Karch and colleagues (1987) observed apparent plastic behavior in compression in nc CaF₂ at 80°C and nc TiO₂ at 180°C. These observations were attributed to enhanced diffusional creep providing the plasticity at these temperatures, where conventional grain-size materials would fail in the elastic regime. It was assumed that diffusional creep was responsible for the plasticity; observations were rationalized, with boundary diffusion dominating the behavior such that the strain (creep) rate is defined as

$$\frac{d \epsilon}{dt} = \frac{B \sigma \Omega \Delta D_b}{d^3 k T} \dots \dots \dots (2.12)$$

where σ is the applied stress, Ω the atomic volume, d the grain size, k the Boltzmann constant, T the temperature, B a constant, and D_b the grain boundary diffusion coefficients. Going from a grain size of 1 μm to 10 nm should increase $d\epsilon/dt$ by 106 or more if D_b is significantly larger for nc materials. However, these results on nc CaF₂ and nc TiO₂ have not been reproduced, and it is believed that the porous nature of these samples was responsible for the apparent ductile behavior.

In addition, the idea of unusually high creep rates at low temperatures has been refuted. Recent creep measurements of nc Cu, Pd, and Al-Zr at moderate temperatures by Sanders et al. (1997) find creep rates comparable to or lower than corresponding coarse-grain rates. The creep curves at low and moderate homologous temperatures (0.24 – 0.48 T_M) could be fit by the equation for exhaustion (logarithmic) creep.



Key to Sources

a. Gunther et al. 1990 [39]	e. Gertsman et al. 1994 [43]
b. Nieman et al. 1991a [40]	f. Eastman et al. 1997, 173-182 [44]
c. Nieman et al. 1991b [41]	g. Morris and Morris 1991 [45]
d. Sanders et al. 1996, 379-386 [42]	h. Liang et al. 1996 [46]

Fig. 2.11. Elongation to failure in tension vs. grain size for some nanocrystalline metals and alloys

One explanation is that the observed low creep rates are caused by the high fraction of low energy grain boundaries in conjunction with the limitation on dislocation activity by the small grain sizes. In sum, the predicted ductility due to diffusional creep in nc brittle ceramics or intermetallics at temperatures significantly less than $0.5 T_M$ has not been realized.

2.6.1.5 Superplastic Behavior

Superplasticity is the capability of some polycrystalline materials to exhibit very large tensile deformations without necking or fracture. Typically, elongations of 100% to >1000% are considered the defining features of this phenomenon. As grain size is decreased it is found that the temperature is lowered at which superplasticity occurs, and the strain rate for its occurrence is increased. As discussed previously, Equation 2.12 suggests that creep rates might be enhanced by many orders of magnitude and superplastic behavior might be observed in nc materials at temperatures much lower than $0.5 T_M$. As mentioned above, actual creep experiments have not borne out this prediction, but instead have shown creep rates comparable to or lower than those in coarse-grained samples of the same material. This is presumably why little enhancement in ductility or superplastic behavior has been observed for nc materials at temperatures $< 0.5 T_M$. However, there is evidence of enhancement of superplastic behavior in nc materials at temperatures $> 0.5 T_M$. Superplasticity has been observed at somewhat lower temperatures and at higher strain rates in nc materials. The evidence for tensile superplasticity is limited and observed typically at temperatures greater than $0.5 T_M$ and in materials that exhibit superplasticity in coarser grain sizes (1–10 μm). For example, Mishra et al. (1997) [47] observed superplastic behavior in nc Pb-62%Sn at $0.64 T_M$ and nc Zn-22%Al at 0.52 to $0.60 T_M$. However, Salishev et al. (1994) observed superplastic behavior in submicron 200 nm Ti and several Ti and Ni base alloys. Here, superplasticity (190% elongation, $n = 0.32$) was observed in Ti at $0.42 T_M$. This was at a temperature 50°C lower than for 10 μm grain size Ti. The flow stress for the 200 nm Ti at 550°C was 90 MPa, compared to 120 MPa for 10 μm Ti at 600°C .

Mishra and Mukherjee (1997) [47] have observed superplastic behavior in Ni_3Al with a 50 nm grain size at temperatures of 0.56 to $0.60 T_M$ to strains of 300 - 600%, but with unusual stress-strain behavior and significant apparent strain-hardening. These new results suggest very different mechanisms may be causing superplastic behavior in these nc materials.

2.7 Unique Mechanical Properties of Nanocrystalline Materials

While there are still only limited data on the mechanical behavior especially tensile properties of nc materials, some generalizations may be made regarding the deformation mechanisms. It is likely that for the larger end of the nanoscale grain sizes, about 50 - 100 nm, dislocation activity dominates for test temperatures $< 0.5 T_M$. As grain size decreases, dislocation activity apparently decreases. The essential lack of dislocations at grain sizes below 50 nm is presumably the result of the image forces that act on dislocations near surfaces or interfaces. The lack of dislocations in small, confined spaces such as single-crystal whiskers has been known for many years (Darken 1961). Creation of new dislocations is also made difficult as the grain size reaches the lower end of the nanoscale (< 10 nm). Stresses needed to activate dislocation sources, such as the Frank-Read source, are inversely proportional to the distance between dislocation pinning points. Since nanoscale grains will limit the distance between such pinning points, the stresses to activate dislocation sources can reach the theoretical shear stress of a dislocation-free crystal at the smallest grain sizes (~ 2 nm). Thus, at the smallest grain sizes we may have new phenomena controlling deformation behavior. It has been suggested that such phenomena may involve grain boundary sliding and/or grain rotation accompanied by short-range diffusion-assisted healing events (Siegel 1997) [34].

Several examples of deformation by shear banding have been reported for nc materials. Carsley et al (1997, 183-192) [48] have studied nc Fe-10% Cu alloys with grain sizes ranging from 45 to 1,680 nm. In all cases, deformation in compression proceeds by intense localized shear banding. The stress-strain curves exhibited essentially elastic, perfectly plastic behavior; that is, no measurable strain hardening was observed. Shear banding is also the deformation mode observed in amorphous metallic alloys and amorphous polymers. The deformation shear banding in nc Fe-10% Cu was compared to that for metallic glasses, amorphous polymers, and coarse grained polycrystalline metals after significant plasticity and work hardening had taken place. While this suggests a close similarity between deformation in nc materials and amorphous materials, not all tensile data on nc materials exhibit a lack of strain hardening. The Fe-10% Cu samples of Carsley et al. (1997, 183-192) [48] showed shear bands even in their larger grained specimens (i.e., about 1,000 nm).

2.8 Ferromagnetic Nanostructured Materials

2.8.1 Soft Magnetic Nanocrystalline Alloys

The discovery of nanocrystalline Fe-based soft magnetic materials is less than ten years old. The first class of such materials was the melt-spun Fe-Si-B alloys containing small amounts of Nb and Cu (Yoshizawa et al. 1988). The Fe-Si-B-Nb-Cu amorphous phase transforms to a body-centered cubic (bcc) Fe-Si solid solution with grain sizes of about 10 nm during annealing at temperatures above the crystallization temperature. The presence of small amounts of Cu helps increase the nucleation rate of the bcc phase while Nb retards the grain growth. These "Finemet" alloys provide low core losses (even lower than amorphous soft magnetic alloys such as Co-Fe-Si-B), exhibit saturation induction of about 1.2 T, and exhibit very good properties at high frequencies, comparable to the best Co-based amorphous alloys. These were first developed in Japan and have stimulated a large amount of research and development worldwide to optimize the magnetic properties. There has been relatively little work in the United States in this area, however.

While many of the soft magnetic properties of Finemet-type nanocrystalline alloys are superior, they exhibit lower saturation inductions than Fe-metalloid amorphous alloys, mainly because of the lower Fe content to attain amorphization and because of the addition of Nb and Cu (or other elements to control the nucleation and growth kinetics). In order to remedy this problem, another class of Fe-based nanocrystalline alloys was developed by Inoue and coworkers at Tohoku University (Makino et al 1997) [49], which is commercialized by Alps Electric Co., Ltd., of Nagaoka, Japan. These "Nanoperm" alloys are based on the Fe-Zr-B system; they contain larger concentrations of Fe (83-89 at.%) compared to the Finemet alloys (~ 74 at.% Fe) and have higher values of saturation induction (~ 1.6-1.7 T). The Nanoperm alloys have very low energy losses at power frequencies (60 Hz), making them potentially interesting for electrical power distribution transformers. The issues of composition modification, processing, and the brittle mechanical behavior of these nanocrystalline/amorphous alloys are discussed by V.R. Ramanan [33] in the first volume of this WTEC study, the proceedings of the May 8-9, 1997 panel workshop on the status of nanostructure science

and technology in the United States (Ramanan 1998, 113-116) [33]. Fig. 2.12 compares the soft magnetic properties of Finemet, Nanoperm, and other materials. While there has been extensive research on these alloys, particularly in Japan and Europe, most of the development has been carried out in Japan. The Finemet family of alloys is marketed by Hitachi Special Metals. Vacuumschmelze GmbH (Germany) and Impky (France) also market similar alloys. The Nanoperm alloys are being commercialized by Alps Electric Co. (Japan). No extensive research or any commercialization of these materials has been carried out in the United States

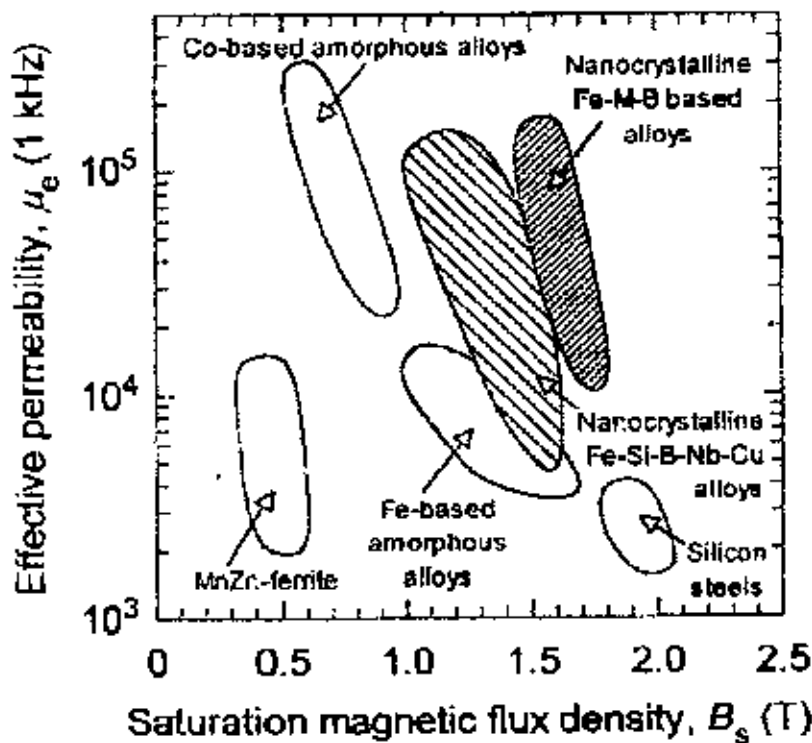


Fig. 2.12 Effective permeability, μ_e , vs. saturation magnetic flux density, B_s , for soft ferromagnetic materials (after A. Inoue 1997).

The small single-domain nanocrystalline Fe particles in the amorphous matrix gives these alloys their unique magnetic behavior, the most dramatic being the lowest energy losses (narrowest B/H hysteresis loop) of any known materials, along with very high permeabilities. These alloys can also exhibit nearly or exactly zero magnetostriction. To date, these materials have been made by crystallization of rapidly solidified amorphous ribbons. Other methods that might provide geometrically desirable products should be

explored or developed. Electrodeposition is one such method that requires further work. Electrodeposited Fe-Ni soft magnetic alloys are being developed in Canada.

2.8.2 Magnetic Properties Derived from Hysteresis Loops

The magnetization / demagnetization curve for a given ferromagnetic material provides a great deal of information during magnetic characterization. The full magnetization curve, shown in Fig. 2.13 , and known as a hysteresis loop, illustrates the methodology as well as which properties of the material under scrutiny are revealed. The hysteresis loop has the axes of applied field (H) and magnetization of the material (M). Often the magnetic induction (B) is displayed as a function of applied field (H) but B is related to M by the following equation (2.13).

$$B = \mu_0(M + H) \dots\dots\dots(2.13)$$

Where μ_0 is the permeability of free space

The hysteresis loop is generated in the following fashion as show in Fig. 2.13. At point (a) the material is in the virgin or demagnetized state and incurs an applied field (H) until the material achieves magnetic saturation at point (b). From point (b) the field is reduced to zero and the magnetization remaining in the material with zero applied field (remanence) is shown at point (c). From point (c) a negative field is applied to the sample and the induced magnetization is reduced from (c) to (d) which corresponds to the amount of field required to reach zero magnetization in a particular sample. Point (d) is known as the coercive point. The sample is negatively magnetized to point (e) corresponding to magnetic saturation in the opposite direction. When the field is decreased to zero and the magnetization falls to the value at point (f).

Lastly, the field is applied in the positive direction to bring the sample back to positive magnetic saturation crossing the applied field axis at point (g) and joining the initial saturation at point (b). The area enclosed from point (b) counterclockwise to point (b) is the hysteresis loop.

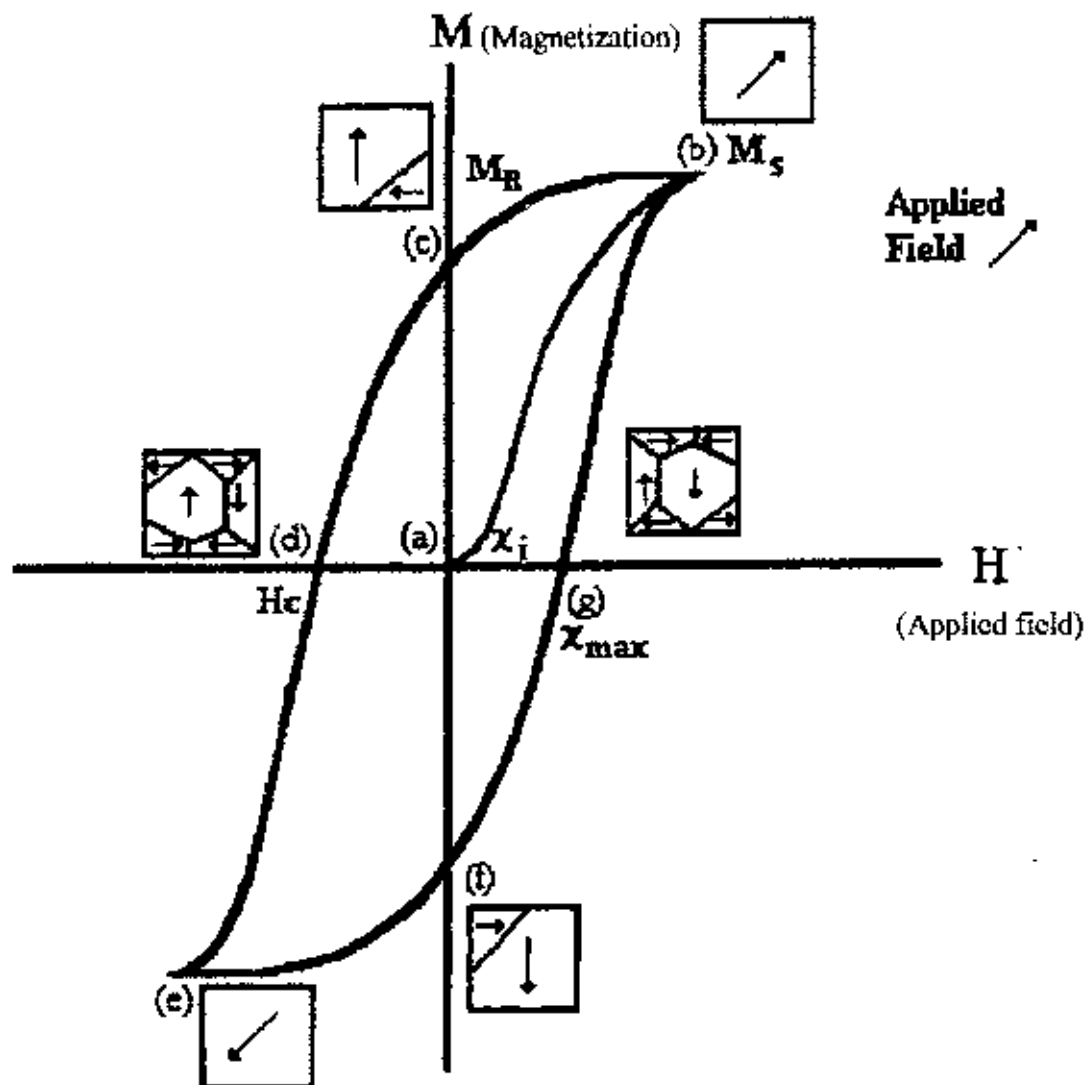


Fig. 2.13 Schematic diagram of M vs. H or hysteresis loop showing magnetic properties and domain structures during different stages of magnetization.

Hysteresis comes from the Latin verb 'hyster', meaning 'to lag'. The area enclosed by the hysteresis loop represents a property known as the energy loss (W_H) in cycling the magnetic field. There are several mitigating factors that determine the shape and size of the hysteresis loop and all of the properties revealed by the hysteresis loop. An important property for characterizing ferromagnetic materials and their subsequent application is determined in part by the susceptibility or permeability of a material. The susceptibility (χ) is defined by the following:

$$\chi = \frac{M}{H} \dots\dots\dots(2.14)$$

Where M is the magnetization and H is the applied field.

Similarly, the permeability (μ) is defined in the following equation:

$$\mu = \frac{B}{H} \dots\dots\dots(2.15)$$

The susceptibility and permeability are defined as the slopes of M vs. H or B vs. H respective behavior on hysteresis loops. As these slopes change throughout the magnetization process, the most useful information is the initial susceptibility (initial permeability), χ_i (μ_i) which occurs at point (a) in Fig 2.13 and the maximum susceptibility (permeability) χ_{max} (μ_{max}) which occurs at points (d) and (g) corresponding to the coercive points. The susceptibilities give us important information regarding the ease at which a material may be magnetized.

Saturation magnetization (M_s) describes the limit of magnetization in any given material. This occurs when all of the dipole moments in the material are aligned in the direction of the applied magnetic field. Magnetic saturation occurs at point (b) in Fig. 2.13. It should be noted the saturation magnetization depends only on the volume of atoms being magnetized and is expected to be a structure insensitive property [36]. Retentivity (M_R) or remanent induction (B_R) is the amount of magnetization remaining in a material after a saturating field has been removed. The retentivity is given by point (c) in Fig. 2.13. Permanent magnet theory makes use of this property sometimes called the retention of magnetization to distinguish ferromagnetic materials from paramagnetic materials [50].

The coercivity (H_C) is defined, as the applied field required to demagnetize or to bring the magnetization of a saturated material to zero. The coercivity or coercive point is given by point (d) in Fig. 2.13. It should be noted that the width of the hysteresis loop is defined as twice the coercivity and as such, the coercivity will determine to a great deal the magnetic properties of a material. The domain structure of the material is magnetically saturated in the direction of the applied field at point (b) in Fig. 2.13. The

domain structure changes when the magnetic field is applied in the opposite direction to have zero net magnetization at point (d) as shown in Fig. 2.13. At point (e) in Fig. 2.13, all dipole moments are aligned in the direction of the applied field.

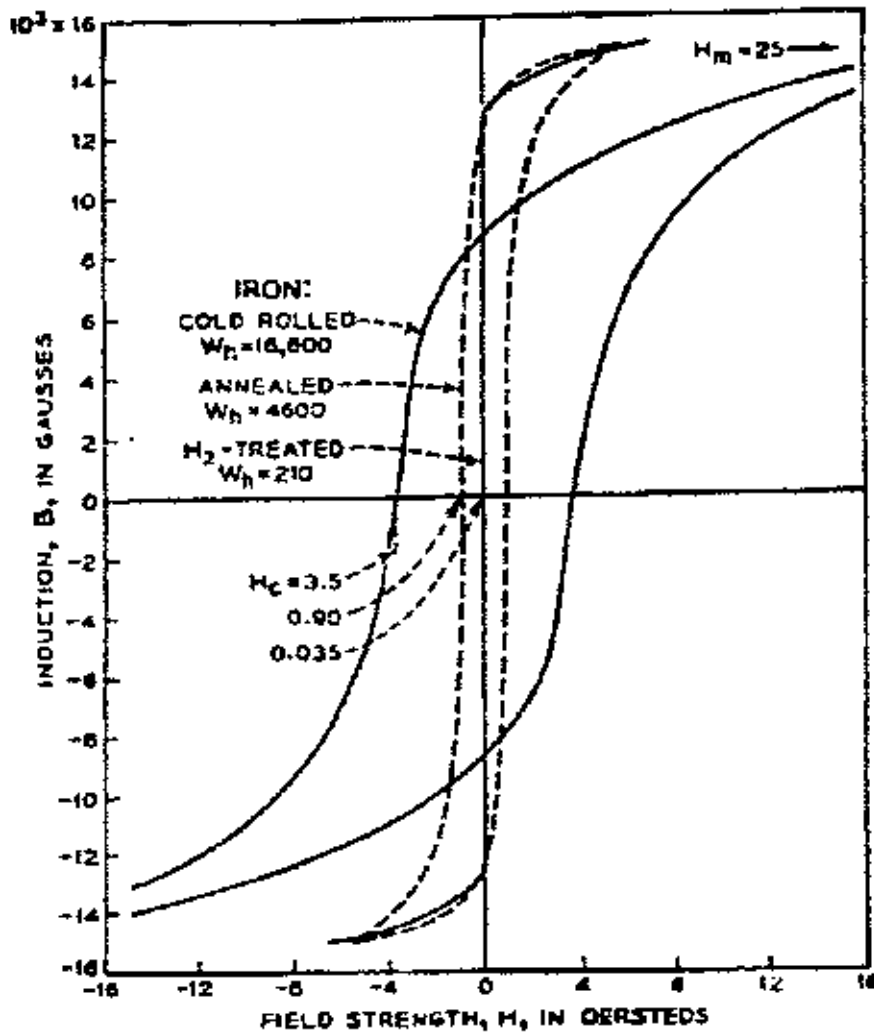


Fig. 2.14 Hysteresis loop behavior for soft iron and hardened steel [36].

There are various contributions to the hysteresis of a ferromagnetic material. For instance, a cold worked specimen will increase the hysteresis core loss (W_H) and coercivity (H_c) as show in Fig. 2.14. Impurities, inclusions and dislocations in material act as pinning sites for domain wall movement. This in turn provides an 'internal friction' during the magnetization process that subsequently increases the hysteresis.

2.8.3 Hard and Soft Magnetic Materials

It is possible to broadly classify, ferromagnetic materials as either hard or soft magnetic materials based on their permeabilities and coercivities. Fig. 2.15 illustrates the relative permeabilities and coercivities along with the year of discovery for both hard and soft magnetic materials. A hard magnetic material is one in which the material, once magnetized is difficult to demagnetize. Materials, which fall into this category, are used for permanent magnets and magnetic data storage or recording media. Hard magnetic materials typically have coercivities greater than 10kA/m [50].

Permanent magnetic materials are chosen for applications based on their 2nd quadrant hysteresis loop properties or what is known as the demagnetization curve. The magnetic properties of permanent magnets are determined not only by their composition but heat treatments and processing treatments during fabrication. One important permanent magnet class, which was discovered in 1984, is the neodymium-iron-boron class of magnets. The Nd-Fe-B magnet is known for its extraordinarily high coercivity, which can reach values of 1.12×10^6 A/m.

The other important magnetic property that determines the suitability of a permanent magnet material is the maximum energy product (BH_{max}). For Nd-Fe-B magnets the energy product can be as high as 320×10^3 J/m³ [50]. Recording media require high remanence and coercivity not unlike permanent magnet materials. Another requirement of materials for recording is a square hysteresis loop, which means that the material has a high remanence and coercivity but is able to switch from one state to another quickly. Typical materials used for recording media are oxides of iron, chromium and cobalt.

Soft magnetic materials find use in entirely different applications. Typical soft magnetic applications include: transformer cores, relays, recording heads, electric motors and electromagnets. Soft magnetic materials are materials, which can be easily magnetized and demagnetized with minimal coercivity (H_c) and core loss (W_H) in cyclic applications. Soft magnetic materials typically have coercivities lower than 1 kA/m.

105892

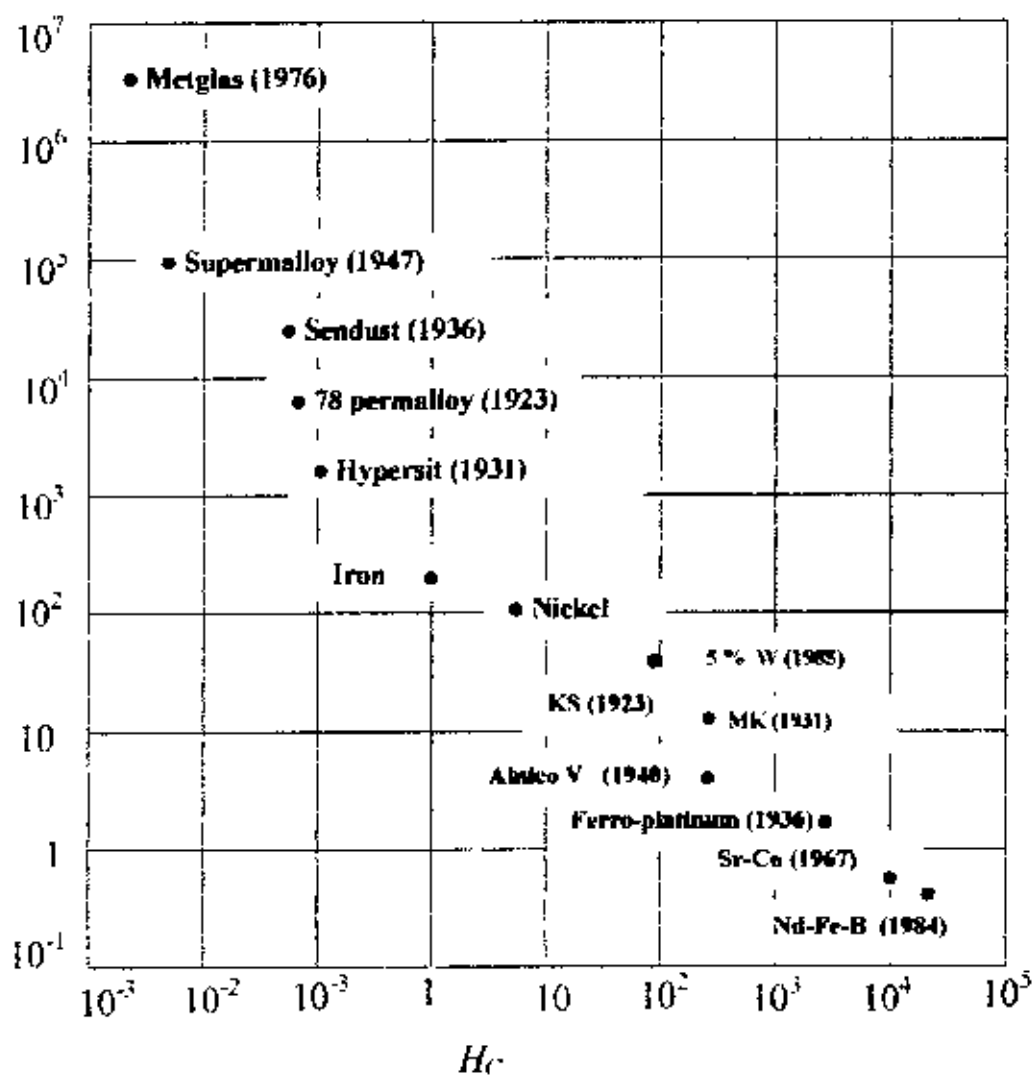


Fig. 2.15 Relative permeabilities and coercivities of ferromagnetic materials [36].

Electromagnets must have a high permeability and saturation but low coercivity so that the field direction may be easily reversed. Soft iron and alloys of cobalt and iron are used almost exclusively which provide a saturation magnetization as high as 1.7×10^6 A/m and 1.95×10^6 A/m respectively. As transformers operate in an alternating current environment they must minimize core losses which are generated as a result of magnetic hysteresis and eddy current formation. Laminated structures comprising, grain oriented iron-silicon alloys are usually used for transformers as they have a high magnetization combined with a low conductivity (due to Si) which reduces losses due to eddy currents.

2.8.4 Permanent Magnet Materials

The first attempts to produce nanoscale microstructures to enhance the magnetic properties of the Nb-Fe-B permanent magnetic materials used mechanical alloying of blended elemental powders followed by heat treatment (Schultz et al. 1987). Since the grain structure so obtained does not exhibit any crystallographic texture and limits the energy product special processing methods such as die-upsetting were used by Schultz and coworkers (1989) to provide the crystallographic anisotropy. While the coercivities of these nanocrystalline alloys are high, the remanent magnetization is decreased.

Recent approaches to increasing the magnetic induction have utilized exchange coupling in magnetically hard and soft phases. The Fe-rich compositions (e.g., $\text{Fe}_{90}\text{Nd}_7\text{B}_3$) result in a mixture of the hard $\text{Fe}_{14}\text{Nd}_2\text{B}$ phase and soft $\alpha\text{-Fe}$ phase. The nanoscale two-phase mixtures of a hard magnetic phase and a soft magnetic phase can exhibit values of remanent magnetization, M_r , significantly greater than the isotropic value of $0.5 M_s$. This "remanence enhancement" is associated with exchange coupling between the hard and soft phases, which forces the magnetization vector of the soft phase to be rotated to that of the hard phase (Smith et al. 1996) [51]. Two important requirements for alloys to exhibit remanence enhancement are a nanocrystalline grain size and a degree of coherence across interphase boundaries sufficient to enable adjacent phases to be exchange-coupled. The significant feature of the exchange coupling is that it allows crystallographically isotropic materials to exhibit remanence values approaching those achieved after full alignment. Such two-phase nanoscale ferromagnetic alloys have been prepared by nonequilibrium methods such as melt-spinning, mechanical alloying, and sputter deposition. Besides the high reduced remanence, the material cost is reduced by reduction in the content of the expensive hard rare earth-containing magnetic phase. The theoretical understanding of remanence enhancement appears to be developed to a degree enabling prediction of magnet performance; however, this performance, while a significant improvement over single-phase isotropic magnets, does not reach predicted values. Work is required on optimizing the orientation relationships between the hard and soft phases and the interphase properties (coherency) between them.

Research on nanocrystalline hard magnetic alloys has received attention worldwide. The U.S. efforts are summarized in the article by G.C. Hadjipanayis (1998, 107-112) [52]. While less research seems to be carried out in the world on these materials compared to the nanocrystalline soft magnetic alloys, some efforts exist in most countries. Notable programs are those of L. Schultz and coworkers at the Institut für Festkörper und Werkstofforschung (IFW) in Dresden and P.G. McCormick and coworkers at the University of Western Australia.

While the very low losses of the nc soft magnetic materials (Finemet or Nanoperm) are dependent on grain size for their properties, the hard magnetic nc alloys with remanence enhancement provide flexibility in processing, especially with powder materials. These remanence-enhanced nc hard magnetic alloys may find many applications as permanent magnet components.

2.8.5 Giant Magnetoresistance (GMR)

The phenomenon of giant magnetoresistance (GMR), the decrease of electrical resistance of materials when exposed to a magnetic field was first reported in a number of multilayer ferromagnetic/nonferromagnetic thin film systems (Baibich et al. 1988) [53]. More recently, GMR was observed in equiaxed granular nanocrystalline materials (Berkowitz et al. 1992) [54]. In particular, GMR systems with low saturation fields offer a wide area for application in magnetoresistive devices. GMR sensors have a higher output than conventional anisotropic magnetoresistive sensors or Hall effect sensors. They can operate at higher magnetic fields than conventional magnetoresistive sensors. In multilayer systems the antiferromagnetic alignment of the ferromagnetic layers in zero field becomes ferromagnetic as the field is applied and causes a decrease in resistance. Granular materials that show GMR consist of small ferromagnetic single-domain particles with randomly oriented magnetic axes in a nonmagnetic matrix. An external field rotates the magnetic axes of all magnetic particles. The rotation towards complete alignment of all magnetic axes again reduces the resistance in a similar way as for multilayers. The GMR in granular systems is isotropic. The explanation for the GMR is spin-dependent scattering of the conduction electrons at the

ferromagnetic/nonmagnetic interfaces and, to a lesser extent, within the magnetic grains. The GMR scales inversely with the average particle diameter.

There is worldwide research on the GMR effect. U.S. programs are reviewed by R. Shull and G.C. Hadjipanayis in the proceedings of the WTEC U.S. nanotechnologies workshop (Shull 1998, 43-58) [55], (Hadjipanayis 1998, 107-112). The NIST work described by Shull has provided material with the largest GMR values for the smallest switching fields. Japanese research on GMR includes studies in Prof. Fujimori's group at Tohoku University.

While the theory for GMR of spin-dependent scattering referred to above has been used as an explanation, other explanations taking into account interaction between magnetic regions have been proposed (El-Hilo et al. 1994) [56]. Combined theoretical and experimental studies should help to clarify the mechanism for this effect.

2.9 Other Ferromagnetic Nanocrystalline Materials

Magnetic nanocomposite refrigerants, which have four times the magnetocaloric effects of the best low temperature magnetic refrigerant, were developed by NIST and described by R. Shull (1998, 43-58). The entropy change at a given (low) temperature for a system of magnetic spins is enhanced when the isolated spins are clustered. Shull et al. (1993) [57] have shown that the nanocomposite $Gd_3Ga_{5-x}Fe_xO_{12}$ gives superior magnetocaloric effects, which increase with x up to $x = 2.5$ and can be extended to higher temperatures than conventional materials.

Magnetostrictive materials such as Terfenol-D ($Tb_{0.3}Dy_{0.7}Fe_2$) have been of scientific and technological interest in recent years. It is suggested by G.C. Hadjipanayis (1998, 107-112) [52] nanostructured magnetostrictive materials can have improved properties, such as lower saturation fields, with reduced anisotropy and in multilayers with alternate layers of magnetostrictive and soft magnetic materials that are exchange-coupled. Hadjipanayis states that most of the research in this area is carried out in Japan and Europe.

2.10 Other Bulk Applications of Nanostructured Materials

2.10.1 Nanocrystalline Hydrogen Storage Materials

R.B. Schwarz (1998, 93-95) [58] has pointed out that nanostructured materials offer several potential advantages for hydrogen storage materials. Rapid kinetics of absorption/desorption can be aided by refining the microstructure to the nanoscale. For example, nanoscale inclusions of Mg_2Ni in Mg catalyze the decomposition of the molecular hydrogen, increasing the hydrogen absorption/desorption kinetics. Another advantage of the nanoscale microstructure is that the alloy powder does not comminute on repeated charging/discharging with hydrogen. This is not strictly a bulk material, since powder agglomerates or green compacts can be used, thus obviating the need for compaction to theoretical density.

2.10.2 Nanocrystalline Corrosion-Resistant Materials

The limited work to date on corrosion resistance of nanocrystalline materials indicates that no generalizations can be made. Superior localized corrosion resistance in HCl was observed for nanocrystalline 304 stainless steel (Fe-18%Cr-8%Ni) prepared by sputter deposition (Inturi and Szklavska-Smialowska 1991 and 1992) was attributed to the fine grain size and homogeneity of the nc material. However, the average dissolution rate of nc Ni was found to be higher than that for coarse-grained material (Rofagha et al. 1991)

2.10.2.1 Corrosion of Metals and Their Alloys

Corrosion involves the interaction (reaction) between a metal or alloy and its environment. Corrosion is affected by the properties of both the metal or alloy and the environment. In this discussion, only the environmental variables will be addressed, the more important of which include:

- pH (acidity)
- Oxidizing power (potential)
- Temperature (heat transfer)
- Velocity (fluid flow)

- Concentration (solution constituents)

The concept of pH is complex. It is related to, but not synonymous with, hydrogen concentration or amount of acid. While corrosion obeys well-known laws of electrochemistry and thermodynamics, many variables that influence the behavior of a metal in its environment can result in accelerated corrosion or failure in one case and complete protection in another, similar case. Avoiding detrimental corrosion requires the interdisciplinary approach of the designer, the metallurgist, and the chemist. Sooner or later, nearly everyone in these fields will be faced with major corrosion issues. It is necessary to learn to recognize the forms of corrosion and the parameters that must be controlled to avoid or mitigate corrosion. The theory of corrosion from the thermodynamic and kinetic points of view covers the principles of electrochemistry, diffusion, and dissolution as they apply to aqueous corrosion and high-temperature corrosion in salts, liquid metals, and gases. We can face the various forms of corrosion, and we must know how to recognize them, as well as the driving conditions or parameters that influence each form of the corrosion, for it is the control of these parameters which can minimize or eliminate corrosion. All corrosion processes show some common features. Thermodynamic principles can be applied to determine which processes can occur and how strong the tendency is for the changes to take place. Kinetic laws then describe the rates of the reactions. There are, however, substantial differences in the fundamentals of corrosion in such environments as aqueous solutions, non-aqueous liquids, and gases.

2.10.2.2 Forms of Corrosion

Over the years, corrosion scientists and engineers have recognized that corrosion manifests itself in forms that have certain similarities and therefore can be categorized into specific groups. However, many of these forms are not unique but involve mechanisms that have overlapping characteristics that may influence or control initiation or propagation of a specific type of corrosion

The most familiar and often used categorization of corrosion is: uniform attack, crevice corrosion, pitting, intergranular corrosion, selective leaching, erosion corrosion, stress corrosion, and hydrogen damage. This classification of corrosion was based on visual characteristics of the morphology of attack. Other prominent corrosion authors have avoided a classification format and have simply discussed the classical types of corrosion (for example, pitting and crevice corrosion) as they relate to specific metals and alloys.

Forms of corrosion are:

1. General corrosion

- Atmospheric corrosion
- Galvanic corrosion
- Stray-current corrosion
- General biological corrosion
- Molten salt corrosion
- Corrosion in liquid metals

2. High-temperature corrosion

- Oxidation
- Sulfidation
- Carburization
- Other forms

3. Localized corrosion

- Filiform corrosion
- Crevice corrosion
- Pitting corrosion
- Localized biological corrosion

4. Metallurgically influenced corrosion

- Intergranular corrosion
- Dealloying corrosion

5. Mechanically assisted degradation

- Erosion corrosion
- Fretting corrosion
- Cavitation and water drop impingement
- Corrosion fatigue

6. Environmentally induced cracking

- Stress-corrosion cracking
- Hydrogen damage
- Liquid metal embrittlement
- Solid metal induced embrittlement

2.11 Applications of the Thin Films of Electrodeposited Iron- Nickel Alloy

Iron-Nickel alloys are of great commercial interest as a result of their soft magnetic and thermal expansion properties. Due to their unique low coefficient of thermal expansion (CTE) and soft magnetic properties, iron-nickel alloys have been used in industrial applications for over 100 years [59]. Typical examples of applications that are based on the low CTE of Fe-Ni alloys include: thermostatic bimetals, glass sealing, integrated circuit packaging, cathode ray tube shadow masks, composite molds/tooling and membranes for liquid natural gas tankers [59]; applications based on the soft magnetic properties include: read-write heads for magnetic storage, magnetic actuators, magnetic shielding and high performance transformer cores. Nanostructured Fe-Ni alloys made by electrodeposition provide material with significantly improved strength, increased wear resistance, and good soft magnetic properties, without compromising the CTE. Nickel Ferrite is mostly used as gas sensing, magnetoresistance and used in electronic industries

2.11.1 Low Thermal Expansion Applications

Two applications in particular are for use in integrated circuit packaging and shadow masks for cathode ray tubes. Integrated circuit packaging requires materials with thermal expansion coefficients matched to those of silicon to prevent the formation of cracks, delamination and/or de-bonding of the different materials during thermal cycles to which the component is exposed. In colour cathode ray tube televisions and computer monitors, the shadow mask is a perforated metal sheet that the electrons from the electron gun must pass through before reaching the phosphor screen. The role of the

shadow mask is to ensure that the electron beam hits only the correct coloured phosphor dots and does not illuminate more than the one that was intended. Only 20% of the electrons pass through the shadow mask, thereby absorbing the other 80%, which leads to an increase in temperature in the mask. The resulting thermal expansion can disturb the alignment between the apertures and the phosphor tracks, leading to a distorted image. This effect is known as “doming”. To minimize the “doming” effect, Fe-Ni (Invar) alloys have recently replaced aluminium-killed (AK) plain carbon steel for use in shadow masks in high-resolution televisions and computer monitors [60].

2.11.2 Microelectromechanical Systems

In addition, the increased strength and low CTE of the Fe-Ni alloys can improve the overall performance of the component in terms of specific strength, elastic energy storage capacity and thermal shock resistance [61].

2.11.3 Magnetic Applications

For soft magnetic applications, ranging from electromagnetic shielding, transformer materials, read-write heads, high efficiency motors or emerging microelectromechanical system components, magnetic materials that exhibit small hysteresis losses per cycle are required. More specifically, materials with: (i) high permeability (the parameter which describes the flux density in very small fields), (ii) low coercivity, (iii) high saturation and remnant magnetization, (iv) high electrical resistivity (to minimize losses due to eddy current formation) and (v) high Curie temperatures are required. Electrodeposited nanocrystalline Fe-Ni alloys fulfill the above requirements with the added benefit of high strength and good wear resistance. In the case of magnetic shielding, the ability of producing high strength net shape components with good soft magnetic properties is highly desirable.

2.11.4 Other Applications

Electrodeposited nanocrystalline Fe-Ni alloys would be ideal for hardfacing coatings where corrosion is not an issue (such as machine parts operating in an oil environment). The wear resistance of the coatings could be further improved by co-depositing hard

ceramic particles such as B [62]. As the composition of Fe-Ni can be varied to match the low Coefficient of Thermal Expansion (CTE) of the ceramic particles, a nanocrystalline Fe-Ni composite electrodeposit would be an excellent hardfacing coating in applications where large thermal gradients exist and close dimensional tolerance is required.

3.1 Materials

Commercial copper sheets were used as substrates in this investigation. As anodes for electrodeposition platinum sheets were used. The size of platinum anodes was 35 mm x 15 mm x 0.4 mm and that of copper substrate was 50 mm x 15mm x 1 mm.

3.2 Preparation of Specimen for Electrodeposition

Removal of sharp edges: This is done by grinding the sharp edges. Current density becomes larger at sharp edges and this in turn results thicker deposition at the edges. In order to get uniform deposition, sharp edges were removed.

Cleaning with detergent: The sample may contain grease, oil, drawing compounds and other substances which come during its fabrication. If these contaminants are present, they will weaken the subsequent pickling action on the sample. So, these were removed. For this operation, a solution of commercial Na_2CO_3 powder was used.

Pickling: Pickling was done for the chemical removal of surface oxides (scale) and other contaminants such as dirt from metal by immersion in an aqueous acid solution. Particulars of pickling operation are given in Table 3.1.

Rinsing: Thorough rinsing was done for obtaining the clean, stain-free and smut-free surface necessary for the subsequent operation. In order to get optimum rinsing conditions, maintenance of the high pressure cold water sprays were provided. Thus, acid contamination is eliminated or minimized.

Acid dipping: Plating is initiated on an active surface. So, samples were acid dipped to neutralize any residual film, remove oxides and smuts and to activate the work piece for subsequent electroplating. Various parameters of this treatment are given in Table 3.1. The sample is now ready for electrodeposition.

The flow diagram of sample preparation is as follows:

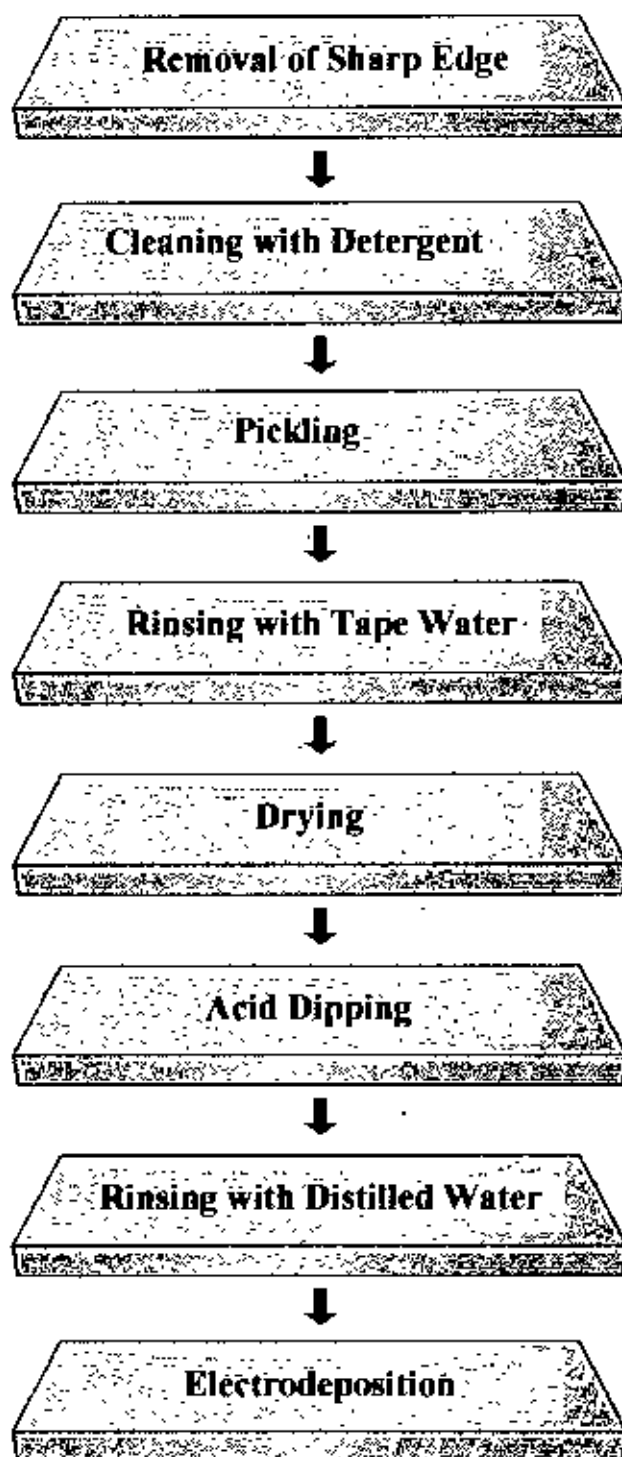


Table 3.1 Particulars of Pickling and Acid Dipping Operations

Name of operation	Reagents used (wt.%)	Operating conditions	
		Temperature (°C)	Time
Pickling	HCl : 20 H ₂ O : 80	70	10 minutes
Acid dipping	HCl : 10 H ₂ O : 90	Room	15 seconds

3.3 Electrodeposition Set-up

Electrodeposition was carried out in a laboratory type electrodeposition set-up consisting of a beaker, a D.C. power supply, a thermometer, a magnetic stirrer, a stand and perspex holder. The beaker containing the electroplating solution and magnetic stirrer was placed on a magnetic hot plate so as to be able to agitate the electrolyte automatically. Anode and cathode were connected to the D.C power supply via a multimeter. Two anodes were used on both sides of the cathode for uniform deposition on the both sides. Schematic of the set-up used for electrodeposition is shown in Fig. 3.1.

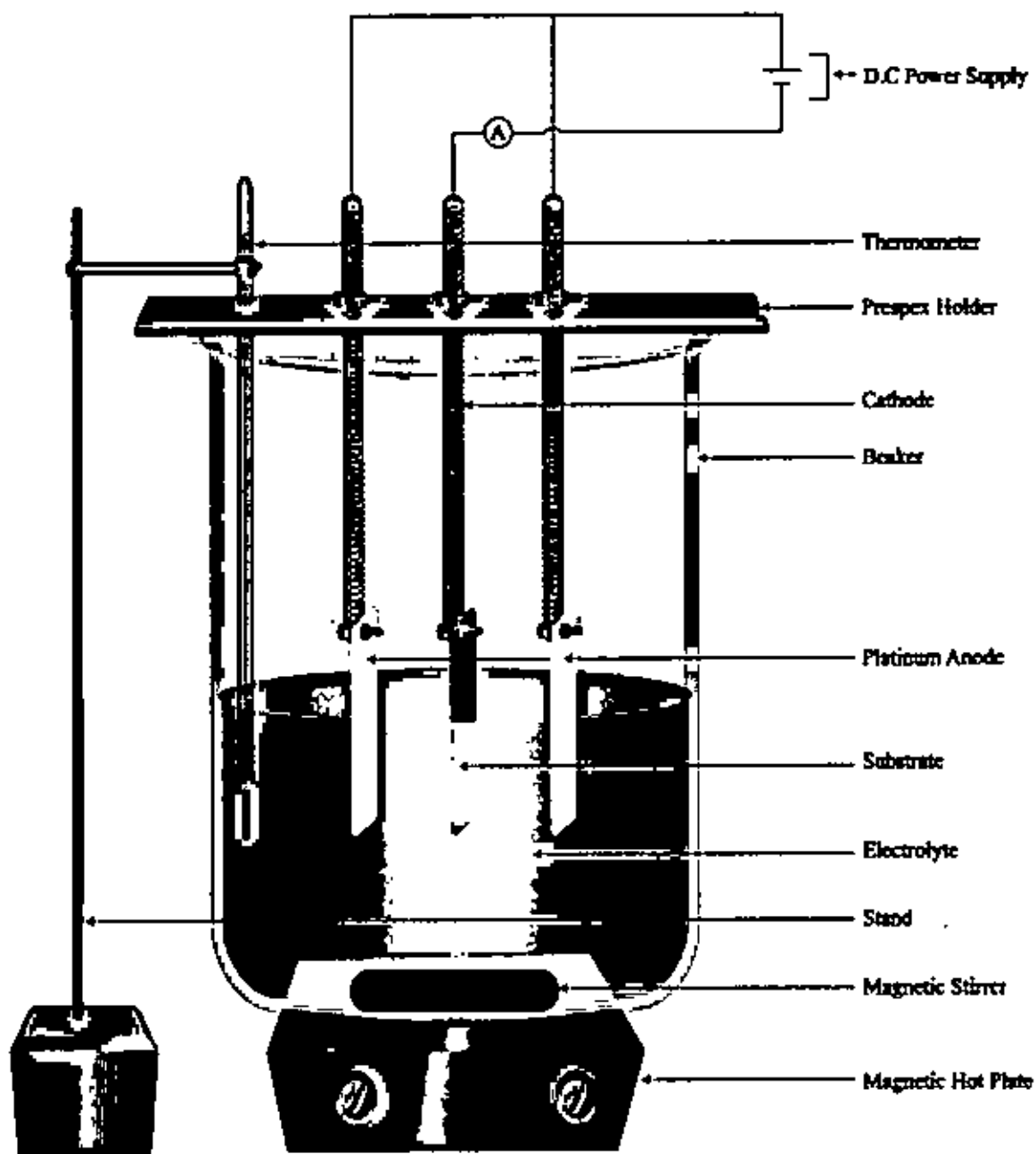


Fig. 3.1 Electrodeposition set-up

3.4 Electroplating Operation

The beaker was filled to approximately two thirds of its marking point with bath solution. The pH value of the solution before electrodeposition was measured by pH meter. The pre-treated substrate and two anodes were immersed into bath solution upto the mark. All the accessories were set-up. The substrate was then connected to the negative terminal and two platinum anodes to the positive terminal of a D.C. power supply. A digital multimeter was also placed in the circuit in series connection to measure the current. Deposition was carried out at room temperature and constant current densities viz. 20, 30, 40, 50, 60, 70, 100, 120 and 140 mA/cm². Each electrodeposition was continued for a predetermined time period of two hours. At the end of each deposition, the power supply was switched off and the work piece was taken out. The coated specimens were thoroughly rinsed in distilled water to remove surplus electrolyte, dried and stored in a desiccator for further investigation. The pH value of the bath solution after electrodeposition was again measured and the change of pH was recorded. Compositions of different simple and complex baths used are given in Table 3.2a and Table 3.2b respectively.

Table 3.2a: Composition of simple baths used in the study

Bath identification	Bath concentration (g/l)	Ni/Fe ratio
B- 1	NiSO ₄ . 7 H ₂ O : 28.1	1.04
	FeSO ₄ . 7 H ₂ O : 27.8	
	H ₃ BO ₃ : 12.4	
B- 2	NiSO ₄ . 7 H ₂ O : 15.5	2.84
	FeSO ₄ . 7 H ₂ O : 5.6	
	H ₃ BO ₃ : 12.4	
	Na ₂ SO ₄ : 49.7	

Table 3.2b: Composition of complex baths used in the study

Bath identification	Concentration of principal ingredients (g/l)	Concentration of Complexing ingredients (g/l)			Ni/Fe ratio
		Ascorbic acid	Saccharin	Citric acid	
B-3a	NiSO ₄ ·7H ₂ O : 28.1	1.5	1.5	2.1	1.04
	FeSO ₄ ·7H ₂ O : 27.8				
B-3b	H ₃ BO ₃ : 12.4	2.0	3.0	4.2	
B-3c	Na ₂ SO ₄ : 49.7	3.0	4.5	8.4	
	H ₂ SO ₄ : 9.8				
B-4a	NiSO ₄ ·7H ₂ O : 28.1	—	—	4.2	
	FeSO ₄ ·7H ₂ O : 27.8				
B-4b	H ₃ BO ₃ : 12.4	2.0	—	4.2	
B-4c	Na ₂ SO ₄ : 49.7	—	3.0	4.2	
	H ₂ SO ₄ : 9.8				

3.5 Methods of Investigation

In the present study, the following tests have been conducted on the deposit.

- i) Chemical analysis of the coating.
- ii) Micro-hardness measurement of the deposited coating.
- iii) Measurement of corrosion properties of the Fe-Ni alloy coating.
- iv) Study of coating morphology by Scanning Electron Microscope (SEM).
- v) Measurement of magnetization by Vibrating Sample Magnetometer (VSM).

3.5.1 Chemical Analysis of the Fe-Ni Alloy Deposit

Chemical analysis of the deposit was carried out by the conventional wet method. Weight of the electrodeposited sample was taken first (say w_1). The deposit was allowed to dissolve in 40 c.c. aqua regia solution (HCl : HNO₃ = 3:1). Precaution was taken here so that HCl and HNO₃ do not react with the substrate. The sample was rinsed with tap water, dried in acetone and weighted (say w_2). So, $w = w_1 - w_2$ gives the weight of the

deposit dissolved in aqua regia solution. The solution was heated to expel the oxides of N_2 and then diluted to 100 cc with hot water.

20 ml. of 25% citric acid solution was added into the solution. Neutralization with NH_4OH was done and 1 ml. in excess was added. Few drops of HCl were added until the neutral solution is slightly acidic. After this, 50-70 ml. of a 1% ammoniacal solution of dimethyl glyoxime ($C_4H_8N_2O_2$) was added. Ni-glyoxime precipitate of blood red color was formed; again some NH_4OH was added to make the solution slightly alkaline and digested for 30 minutes. The precipitate was then separated by filtering through pulp. The precipitate was washed several times with hot water and ignited carefully at 650-700°C. Both ash and NiO were obtained after burning and %Ni was determined by the following formula:

$$\% Ni = NiO \times 78.58 / w$$

Iron estimation for Fe-Ni alloy coating was determined by volumetric method by using potassium dichromate. For this, some solution (coating dissolved in aqua regia) was heated to expel the oxides of N_2 and then a few drops of HCl was added. After then it was diluted to 25 cc with hot water and transferred into a conical flask. The solution was then heated to boiling. Stannous chloride solution was added to it drop by drop with constant shaking till the yellow color changes to almost colorless. It was then cooled quickly to avoid oxidation. 20 ml of $HgCl_2$ solution was added, a silky white precipitate was formed. 2-3 drops of diphenylamine indicator was added and the solution was titrated with 1N $K_2Cr_2O_7$ solution. The end point was indicated by the appearance of deep blue color. % Fe was calculated as follows:

$$1 \text{ ml of } 1N \text{ } K_2Cr_2O_7 \cong 0.05585 \text{ g of Fe.}$$

$$\% Fe_{total} = 11.17 \times (V_2 - V_1) \text{ (ml)}$$

Where,

V_1 = Initial volume of $K_2Cr_2O_7$

V_2 = Final volume of $K_2Cr_2O_7$

3.5.2 Microhardness Measurement

Microhardness indentations were imposed on the coating surface by using a Shimadzu Microhardness Tester. The indenter was used in the form of a right pyramid with a square base and an angle of 136 degrees between opposite faces subjected to a load of 50 g. The full load was applied for 10 seconds on unetched specimen surface of Fe-Ni alloy coating. The two diagonals of the indentation after removal of the load were measured using Scanning Electron Microscope (SEM) and the Vicker Hardness Number (VHN) was calculated from the conventional conversion table.

3.5.3 Corrosion Test

The Salt Immersion Corrosion Test was adopted to measure the corrosion resistance of Fe-Ni films on Cu substrate. The immersion test was performed at room temperature using a solution of 5 % NaCl and sections of Fe-Ni films on Cu substrate were used as test samples (Fig. 3.2).

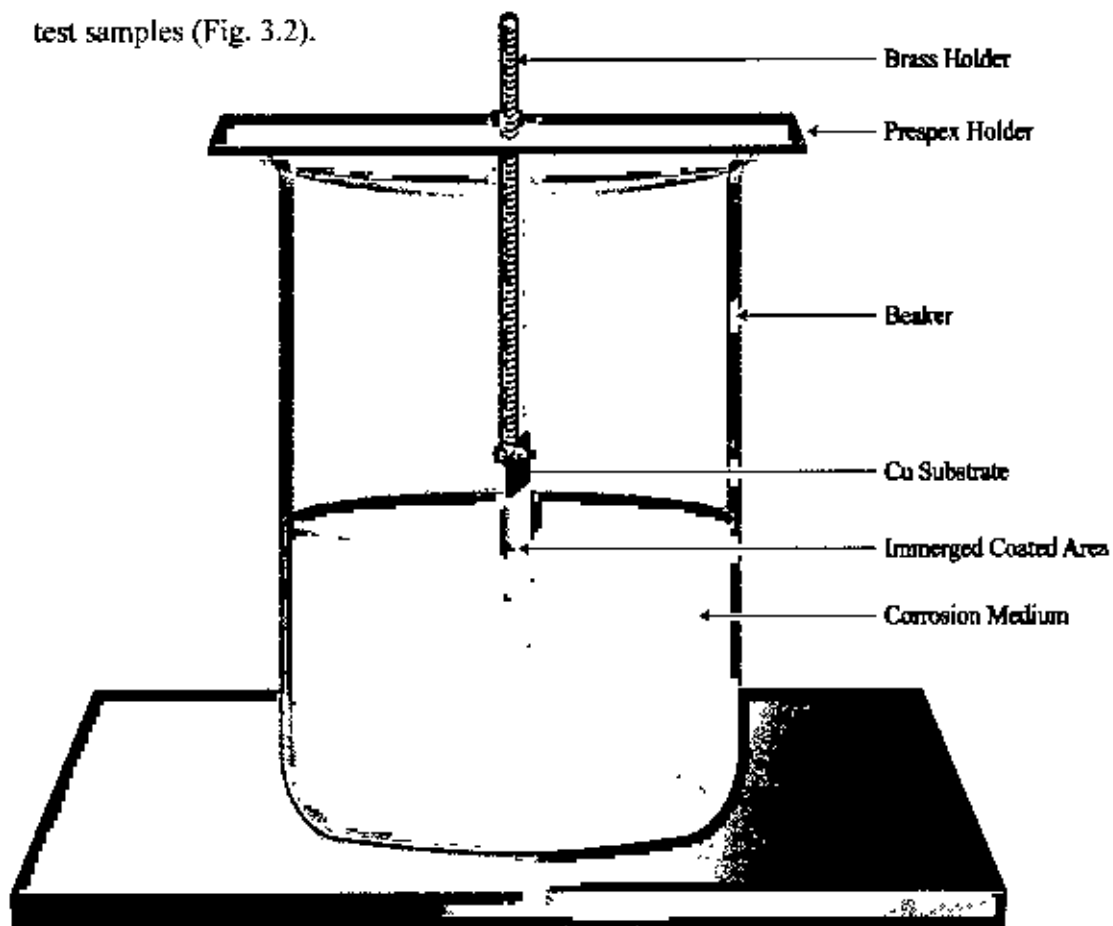


Fig. 3.2 Salt Immersion Test

The test samples were weighed and recorded before the immersion and then immersed in the prepared fresh salt water solution and they were kept there for 48 hours. When the test time was completed the samples were taken out of NaCl solution. After rinsing with tap water and drying with acetone, weight of the samples was taken. The difference in initial and final weight was the measure of weight loss which indicates the amount of corrosion occurred in the test. The section of Fe-Ni films on Cu substrate that was used for the corrosion test is shown in Fig. 3.3.

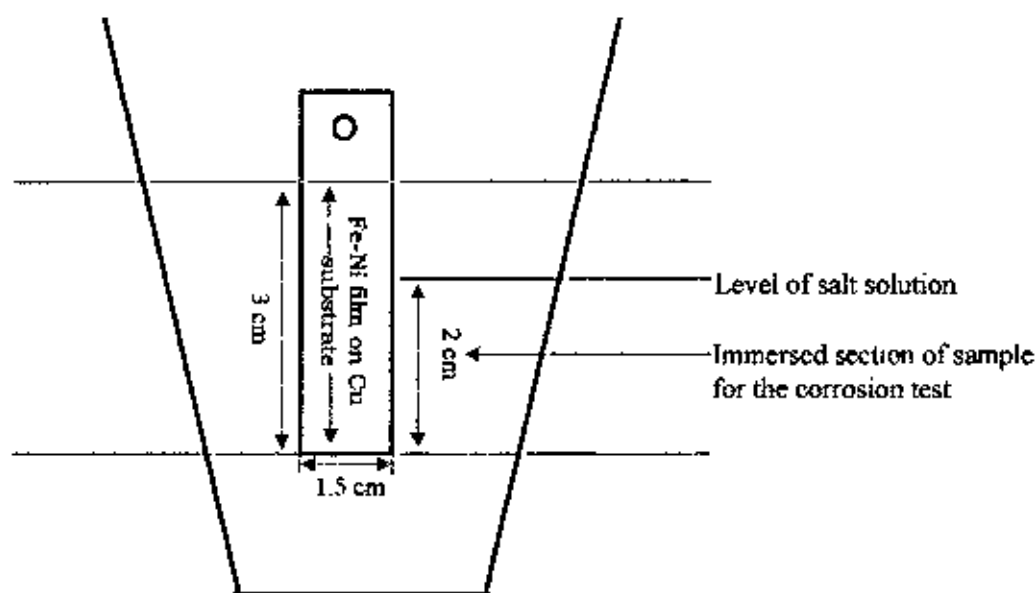


Fig. 3.3 Section of electrodeposited film used for the corrosion test

The expression $\text{mg}/\text{dm}^2/\text{day}$ (mdd) was used to express the corrosion rates throughout the whole study. This expression was readily calculated in accordance with the weight loss and the immersed surface area using the following formula:

$$\text{mdd} = \frac{\text{Weight loss (mg)}}{[\text{Specimen area (dm}^2) \times \text{time (days)}]}$$

3.5.4 Investigation of Surface Morphology of Fe-Ni Alloy Coating

The surface morphology of the Fe-Ni coating was studied by Scanning Electron Microscope (SEM). The deposited specimen was cut into pieces of 1 cm x 1.5 cm. Each sample was cleaned in methanol (CH₃OH) for 10 minutes using the ultrasonic cleaner. Ultrasonic cleaning of the samples was done to remove unwanted dirt and fines if present onto the coating surface. The sample was then ready for observing under SEM. The specimens were sealed with aluminum foil to protect it from environment whenever required.

The surfaces of the Fe-Ni alloy deposited coatings were investigated by means of scanning electron microscope (SEM) at X500 and X1000 magnifications to analyze the surface characteristics. The observed images were recorded and then studied. The operating condition of SEM is shown in Table 3.3.

Table 3.3 Operating conditions of Scanning Electron Microscope (SEM)

Radiation	Fine electron beam
Emission type	Thermionic
Filament	Tungsten (W)
Voltage	10 kV
Current	About 50 μ A

3.5.5 Investigation of Magnetic Properties of Fe-Ni Alloy Coating

Magnetic properties of the Fe-Ni films were characterized by a vibrating sample magnetometer (VSM). VSM was used to generate hysteresis loops at room temperature (20°C). The VSM was carefully calibrated using the standard calibration sample of nickel with a purity of 99.999%. The calibration was done at an applied magnetic field of 2500 Oe and a temperature of 20°C. Hysteresis loops were generated using a sweep time of 20 minutes and a maximum field of 2500 Oe. The VSM was then ready (calibrated) to measure the magnetization of the coated experimental samples.

Magnetization loop spectra of the experimental samples were taken with the magnetic field applied parallel and perpendicular to the film plane using VSM at room temperature. The dimensions of the Fe-Ni coated samples used in the VSM measurements were 3mm x 4mm. The sample was fixed to a small sample holder located at the end of a sample rod mounted in an electromechanical transducer as shown in Fig. 3.4.

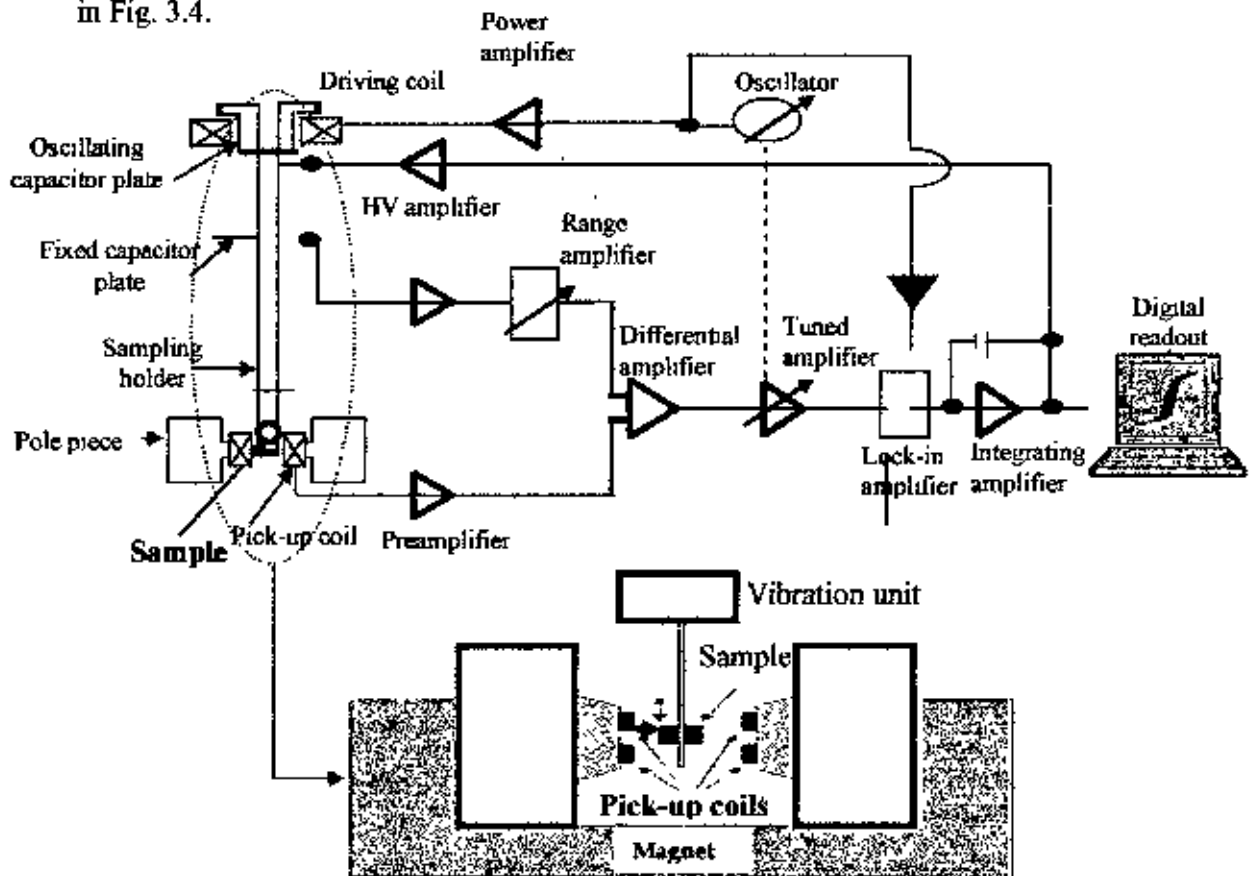


Fig. 3.4 Schematic diagram of Vibrating Sample Magnetometer (VSM)

The transducer is driven by a power amplifier which itself is driven by an oscillator at a frequency of 90 Hz. So, the sample vibrates along the Z axis perpendicular to the magnetizing field. The induced signal in the pick-up coil system is fed to a differential amplifier. The output of the differential amplifier is subsequently fed into a tuned amplifier and an internal lock-in amplifier receives a reference signal supplied by the oscillator. The output of this lock-in amplifier, or the output of the magnetometer itself, is a DC signal proportional to the magnetic moment of the sample and is obtained from the digital readout.

4 RESULTS AND DISCUSSION

4.1 Electrodeposition of Fe-Ni Alloy Coating

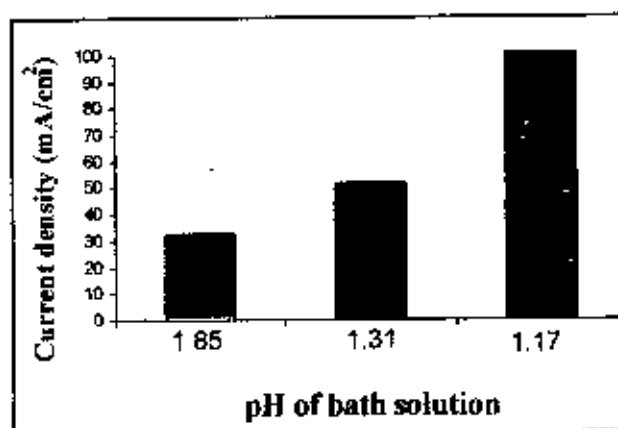
The Fe-Ni films were deposited from eight different baths. Two of them were simple baths containing the main ingredients NiSO_4 , FeSO_4 , Na_2SO_4 , H_3BO_3 of varying composition with different Ni/Fe ratio in each bath. Another six were complex baths containing ascorbic acid, saccharin and citric acid in varying concentration as complexing agents in addition with the main ingredients.

The bath pH and applied current density had a profound effect on the nature of Fe-Ni alloy deposit. The deposit quality was identified by visual inspection. Uniform, adherent and bright coatings from all the baths were obtained at higher pH range with lower current density and at lower pH range with higher current density. A unique relation between current density and pH of bath solution for uniform and bright coating from complex bath is shown in Table 4.1. An applied current density of 100 mA/cm^2 produced blackish rough deposit from bath B-3a having electrolyte solution of 1.85 pH while uniform, adherent and bright coatings were obtained from the same bath B-3a at current density of 30 mA/cm^2 and pH 1.85 of the bath.

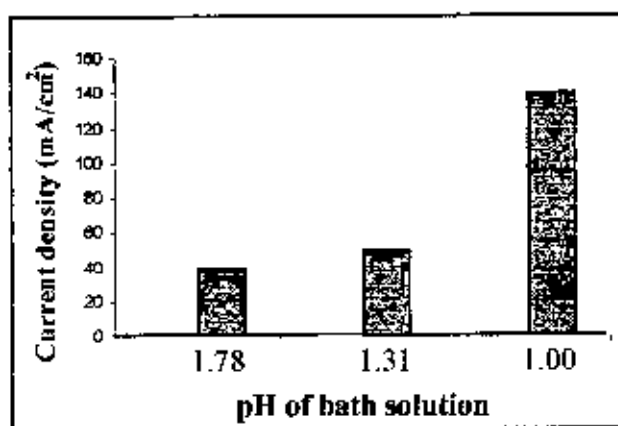
Table 4.1: Current density (cd) and bath pH for uniform and bright coating deposited from complex bath.

Bath identification	pH and cd (mA/cm^2) for uniform and bright deposition											
	1		2		3		4		5		6	
	pH	cd	pH	cd	pH	cd	pH	cd	pH	cd	pH	cd
B-3a	1.85	30	—	—	1.31	50	—	—	1.17	100	—	—
B-3b	—	—	1.78	40	1.31	50	—	—	—	—	1.00	140
B-3c	—	—	—	—	1.78	50	1.31	60	—	—	1.00	140

Fig. 4.1 represents the pH and current density matching for uniform and bright deposition of Fe-Ni coatings from complex baths B-3a and B-3b. Similar trend was also observed in all other complex as well as simple baths.



(a)



(b)

Fig. 4.1: Relation between pH and current density for bright deposition obtained from baths (a) B-3a and (b) B-3b.

No deposition was seen in cases the pH < 1.90 for simple baths and pH < 1.00 for complex baths. From baths with pH less than these lower limit, deposit could form only near the edges while major portion of the substrate surface remained bare. At this low pH Fe-Ni plating baths became too corrosive and therefore the newly deposited Fe-Ni

alloy is chemically attacked and dissolved. At the mid portion of the sample where current density is lower than the average, rate of this chemical attack is higher than the deposition rate. On the other hand, at areas near the edges which receive more current than the average, the deposition rate is higher than the rate of chemical attack. As a result, significant amount of deposit could only be seen near the edges at pH < 1.90 for simple baths and pH < 1.00 for complex baths [64]. No good deposition was obtained at a current density > 120 mA/cm² for simple baths and > 140 mA/cm² for complex baths. At these higher current densities deposited coating tend to peeling due to developing of stress and some times curved surface was observed. Thus, no electrodeposition was carried out at any current density > 120 mA/cm² and 140 mA/cm² for simple and complex baths respectively.

4.2 Chemical Analysis

Chemical analysis of the coatings was carried out by the conventional wet method. Fe-Ni films obtained at different current density from baths with varying Ni/Fe ratio show the variation of Ni content in it. Electrodeposition was performed at room temperature with no agitation where current density had been varied from 50 to 120 mA/cm² for simple baths B-1 and B-2 while 20 to 140 mA/cm² for complex baths B-3a, B-3b, B-3c, B-4a, B-4b, & B-4c. The variation of Ni content in the coatings with current density for different Ni/Fe ratio in simple and complex baths is given in Table 4.2 and Table 4.3 respectively.

Table 4.2: % Ni in coatings deposited from simple baths at different current density.

Bath identification	Ni/Fe in bath solution	% Ni in coatings			
		50 mA/cm ²	70 mA/cm ²	100 mA/cm ²	120 mA/cm ²
B-1	1.04	9.38	11.09	10.38	15.11
B-2	2.84	16.12	15.21	21.02	21.80

Table 4.3: % Ni in coatings deposited from complex baths at different current density.

Bath identification	Ni/Fe in bath solution	% Ni in coatings						
		20 mA/cm ²	30 mA/cm ²	40 mA/cm ²	50 mA/cm ²	60 mA/cm ²	100 mA/cm ²	140 mA/cm ²
B-3a	1.04	44.13	40.38	—	39.29	—	34.38	—
B-3b		—	47.52	44.38	37.48	—	—	31.43
B-3c		—	—	39.27	35.48	29.78	—	26.19
B-4a	1.04	—	28.37	—	—	—	—	—
B-4b		—	32.13	—	—	—	—	—
B-4c		—	30.43	—	—	—	—	—

Fe content of the coatings was also analyzed to check the co-deposition of Fe-Ni alloy in the coating. The variation of Fe content in the coatings with current density for different Ni/Fe ratio in simple and complex baths is given in Table 4.4 and Table 4.5 respectively. Summation of Ni and Fe content close to 100% for the same coating confirms the co-deposition of Fe-Ni alloy in it.

Table 4.4: % Fe in coatings deposited from simple baths at different current density.

Bath identification	Ni/Fe in bath solution	% Fe in coatings			
		50 mA/cm ²	70 mA/cm ²	100 mA/cm ²	120 mA/cm ²
B-1	1.04	89.60	—	—	82.72
B-2	2.84	—	82.74	—	75.20

Table 4.5: % Fe in coatings deposited from complex baths at different current density.

Bath identification	Ni/Fe in bath solution	% Fe in coatings						
		20 mA/cm ²	30 mA/cm ²	40 mA/cm ²	50 mA/cm ²	60 mA/cm ²	100 mA/cm ²	140 mA/cm ²
B-3a	1.04	—	57.59	—	—	—	64.62	—
B-3b		—	50.48	—	—	—	—	65.55
B-3c		—	—	—	62.73	—	—	—
B-4a	1.04	—	69.57	—	—	—	—	—
B-4b		—	—	—	—	—	—	—
B-4c		—	66.87	—	—	—	—	—

Percentage Ni in the deposit as a function of applied current density is shown in Fig.4.2 for simple baths and in Fig. 4.3 for complex baths. Neglecting a small deviation, an increase of % Ni in the deposit with increasing applied current density is observed for simple baths while the reverse trend is seen for complex baths. Bath B-2 contains higher Ni/Fe ratio in its composition than the other baths

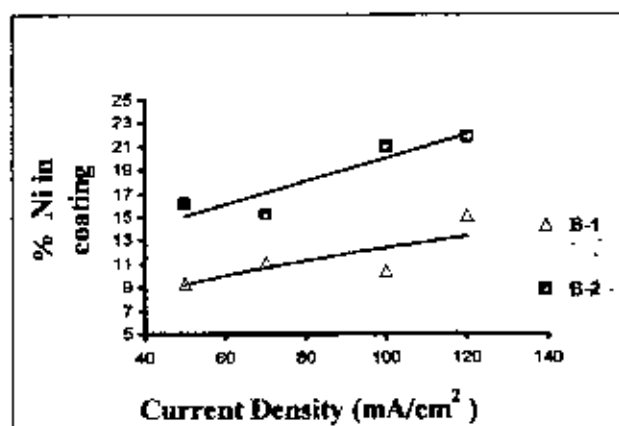


Fig. 4.2: Effect of current density on % Ni in coating deposited from simple baths.

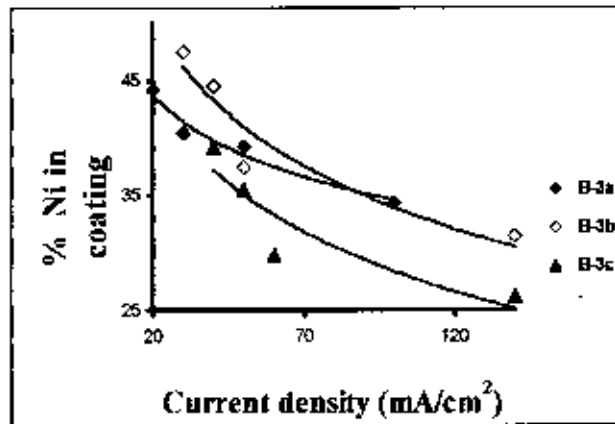


Fig. 4.3: Effect of current density on % Ni in coating deposited from complex baths B-3a, B-3b and B-3c.

(Table 4.2 and 4.3). The highest Ni content in the deposit was measured 21.80 wt% for bath B-2 while 15.11 wt% for bath B-1 at the same current density of 120 mA/cm². This is supported by the alloy deposition principle that an increase in the metal percentage (or ratio) of a parent metal in an alloy plating bath results in an increase in its percentage (or ratio) in the deposit [65]. Moreover, the electrolyte conductance increases as a result of addition of Na₂SO₄ in bath B-2 and consequently it significantly increased Ni²⁺ in the deposit if compared with bath B-1 [65].

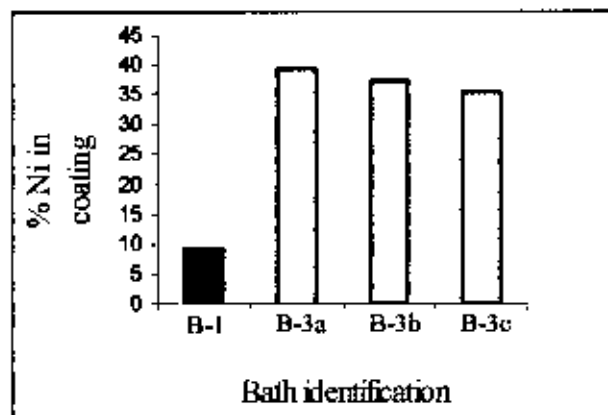


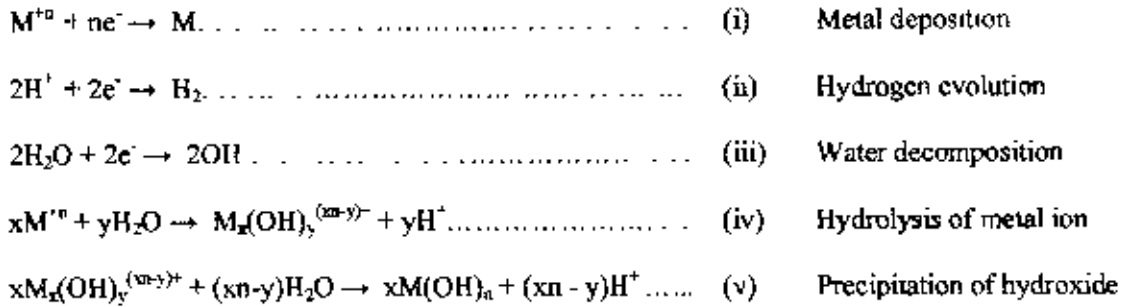
Fig. 4.4: % Ni deposited from simple bath B-1 and complex baths B-3a, B-3b and B-3c. All depositions were carried on at 50 mA/cm².

Decrease in Ni content with increasing current density is observed in coatings obtained from complex baths (Fig 4.3). 47.52 wt% Ni content obtained from complex bath B-3b which was higher than all the simple and complex baths studied. Ni/Fe ratio in all the baths except bath B-2 is 1.04.

Figure 4.4 shows the %Ni in the coating deposited from simple bath B-1 and complex baths B-3a, B-3b and B-3c at the same current density of 50 mA/cm². Higher %Ni in coatings deposited from complex baths than from simple baths is observed. The standard electrode potential for reduction of pure Ni²⁺ (-0.257 V) is relatively more positive than that of Fe²⁺ (-0.44 V). According to normal deposition theory, an element with a higher positive standard electrode potential is expected to deposit preferentially than the one with a less positive standard electrode potential [66]. Thus with the progress of deposition, availability of Ni²⁺ for deposition on cathode surface decreases and the relative %Fe in deposition increases in the baths. Again according to Brenner's definition of anomalous codeposition [67], the less noble metal (here Fe) is deposited preferentially and its percentage in the deposit become higher than that in electrolytes. In general, the anomalous codeposition is attributed to hydrogen evolution (the side reaction of metal reduction at the cathode surface) that depletes protons and results in increasing the local concentration of hydroxyl ions [68]. This increase in the concentration of hydroxyl ion, however, leads to the formation and adsorption of metal monohydroxide ions or metal hydroxides on cathode surface, favoring the anomalous codeposition. According to the proposed model (Gangasingh et. al.), the formation of FeOH⁺ and NiOH⁺ near the cathode has a critical role in the occurrence of anomalous deposition phenomena. But, higher %Ni (more noble) in coatings deposited from complex baths than the simple bath concludes that addition the complexing agents suppresses the anomalous characteristics of the Fe-Ni alloy electrodeposition.

pH of the complex baths was as low as 2 which might prevent the generation of hydroxide and therefore could suppress the anomalous characteristics of Fe-Ni coatings.

Typical reactions which may take place during the deposition of metals having a negative standard electrode potential are as follows [69]:



- Electrochemical reactions (ii) and (iii) tend to consume H^{+} or generate OH^{-} . Hence, when they take place at the cathode, the pH of the cathode will increase.
- Reactions (iv) and (v) tend to produce H^{+} and will counteract the pH rise at the cathode produced by reactions (ii) and (iii).
- When the pH near the surface becomes such that hydrolysis and precipitation reactions occur, any further pH rise will be slowed by reactions (iv) and (v).
- If the hydrolysis reaction (iv) is not able to slow the pH rise, the deposit may contain hydroxide inclusions because of reaction (v).

Ni electrodeposition proceeds via a nickel monohydroxide species ($NiOH^{+}$) and that the surface pH may reach values at which nickel hydroxide [$Ni(OH)_2$] would precipitate at the surface and would inhibit metal deposition [70]. So, complexing agent was supposed to enhance the hydrolysis reaction during electrodeposition which might increase the Ni content of the coatings in bath B-3a, B-3b and B-3c.

Effect of different complexing agents on %Ni in the deposit is shown in Fig. 4.5. Addition of ascorbic acid and citric acid shows a major impact (bath B-4b) to increase %Ni in the deposit than addition of saccharin with citric acid (bath B-4c) or only with citric acid in the bath (bath B-4a).

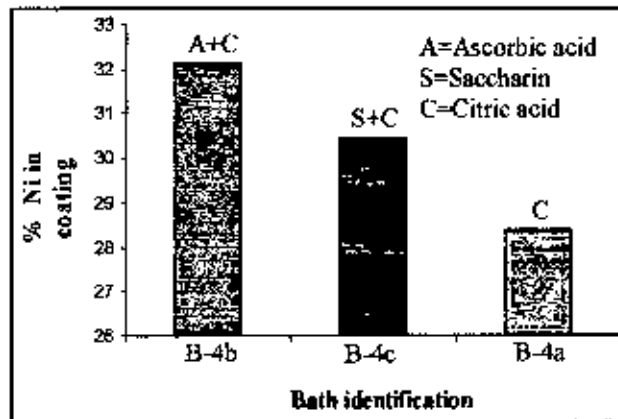
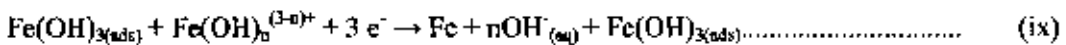
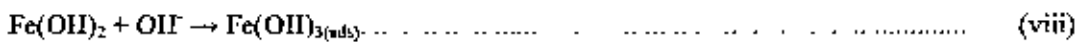
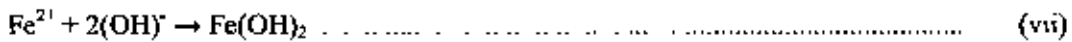
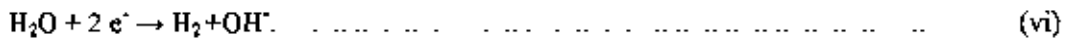


Fig. 4.5: Effect of complexing agent on % Ni in coating deposited from complex baths B-4a, B-4b and B-4c. All depositions were carried on at 30 mA/cm².

Ascorbic acid prevents oxidation of ferrous to ferric ions [71] in the bath and thus the Ni content of the films was higher. The reaction mechanism may be proposed as following [56-58]:



According to these reactions, if it is inhibited to convert Fe(OH)₂ to Fe(OH)₃, then Fe(OH)₃ was not able to act as a positive catalyst to produce Fe. So, inhibition of ferrous to ferric ions might increase the Ni content of the coatings obtained from bath B-4b by reducing Fe content of the deposited films. Saccharin increases the Ni content of the films. Citric acid increases the side reaction rate [72] that decreases the alloy current efficiency due to the increase of the hydrogen ions adsorption which consequently, might decrease the Ni content in coatings.

4.3 Microhardness (VHN)

Vickers Hardness Number (VHN) of the freestanding deposits was evaluated by microhardness testing using a shimadzu microhardness machine. Several factors may contribute to the variation in hardness of coating. The factors include applied current density, % Ni content of deposited films, pH of the electrolytes, presence of internal stresses and grain size distribution of the deposited thin films. The microhardness test results of coatings deposited from simple baths are summarized in Table 4.6 and those deposited from complex baths in Table 4.7. Test result shows the variation of microhardness of the deposited films with relation to its %Ni content and the applied current density.

Table 4.6: Microhardness and % Ni of Fe-Ni coatings deposited from simple baths at different current density.

Bath identification	Microhardness (VHN) and %Ni of coatings deposited at different current density (mA/cm ²)							
	50 mA/cm ²		70 mA/cm ²		100 mA/cm ²		120 mA/cm ²	
	VHN	% Ni	VHN	% Ni	VHN	% Ni	VHN	% Ni
B-1	85.91	9.38	110.08	11.09	107.69	10.38	120.17	15.11
B-2	118.37	16.12	116.32	15.21	123.22	21.02	133.37	21.80

Table 4.7: Microhardness and % Ni of Fe-Ni coatings deposited from complex baths at different current density

Bath identification	Microhardness (VHN) and % Ni of coatings deposited at different current density (mA/cm ²)													
	20 mA/cm ²		30 mA/cm ²		40 mA/cm ²		50 mA/cm ²		60 mA/cm ²		100mA/cm ²		140mA/cm ²	
	VHN	% Ni	VHN	% Ni	VHN	% Ni	VHN	% Ni	VHN	% Ni	VHN	% Ni	VHN	% Ni
B-3a	166.1	44.13	155.7	40.38	—	—	146.5	39.29	—	—	139.8	34.38	—	—
B-3b	—	—	171.7	47.52	166.3	44.38	138.3	37.48	—	—	—	—	132.3	31.43
B-3c	—	—	—	—	157.2	39.27	144.9	35.48	143.5	29.78	—	—	126.6	26.19
B-4a	—	—	110.2	28.37	—	—	—	—	—	—	—	—	—	—
B-4b	—	—	133	32.13	—	—	—	—	—	—	—	—	—	—
B-4c	—	—	118.3	30.41	—	—	—	—	—	—	—	—	—	—

Neglecting a small deviation, VHN of the coating obtained from simple baths B-1 and B-2 increases with increasing applied current density as shown in Fig. 4.6. Maximum VHN of the film deposited from the simple bath B-1 is 120.17 and the same deposited from the bath B-2 is 133.4 at same current density. Hardness of the coatings deposited from bath B-2 is slightly higher than that deposited from bath B-1. This may be due to the compositional variations of the coatings deposited from the two baths. Coating obtained from bath B-2 contains higher %Ni than obtained from bath B-1 (Fig. 4.6)

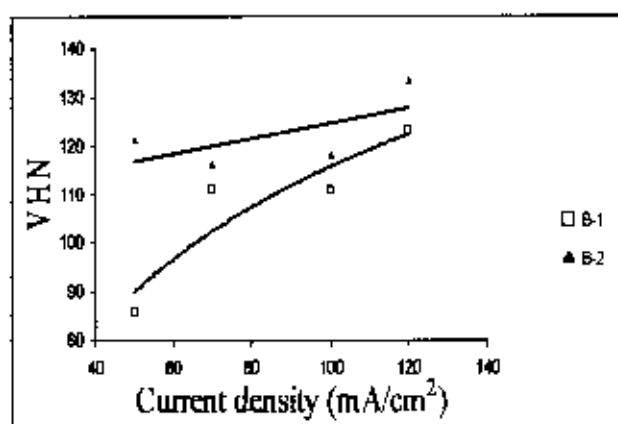


Fig.4.6: Effect of current density on microhardness of coating deposited from simple baths.

On the contrary, decreasing VHN with increasing current density for complex baths is observed in Fig. 4.7. Trend of these changes is not linear. Even the extent of changes for various simple baths as well as complex baths is different.

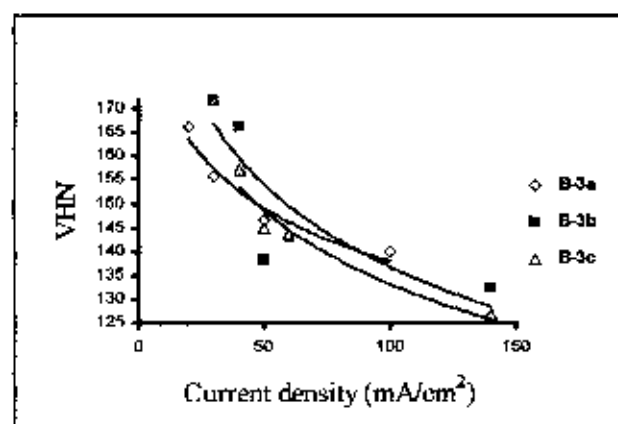


Fig. 4 7: Effect of current density on microhardness of coating deposited from complex baths.

This changes might be the effect of complexing agent which could reduce VHN with the current density. The highest VHN of coatings obtained from bath B-3a, B-3b and B-3c is 171.7, 166.1 and 157.2 respectively.

The change of VHN is also related with %Ni content in films as shown in Fig. 4.8. The highest VHN 120.17 is observed on coating with 15.11 %Ni content for bath B-1 while the value 133.37 is observed on coating with 21.80 %Ni content for bath B-2. Thus higher %Ni favors high VHN value of Fe-Ni coatings.

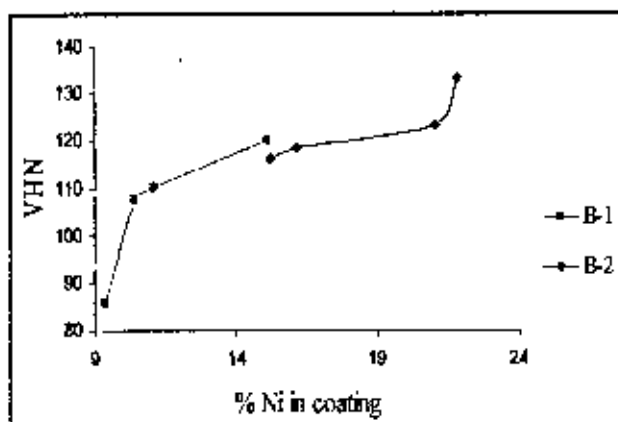


Fig. 4.8: Effect of % Ni in coating on its microhardness deposited from simple baths.

Figure 4.9 shows the VHN increase with the % Ni content of the films in complex baths which is similar as simple baths. Maximum VHN of the film deposited from the simple

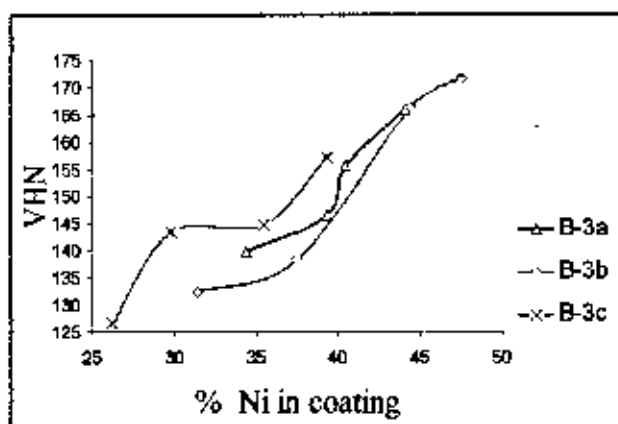


Fig. 4.9: Effect of % Ni in coating on its microhardness deposited from complex baths.

bath B-2 is 133.4 and the same deposited from the complex bath B-3b is 172. So, complexing agent increases the % Ni as well as VHN of the deposited films.

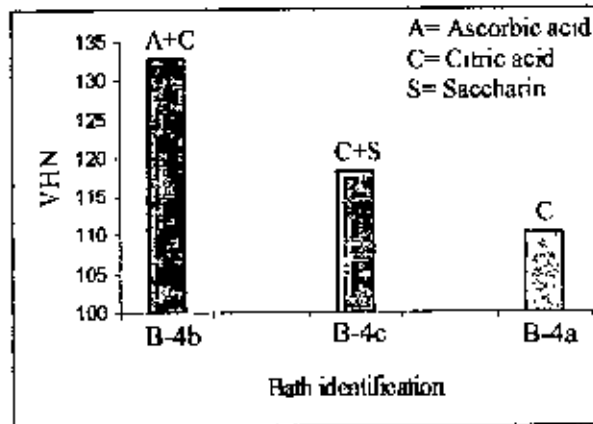


Fig.4.10: Effect of complexing agent on microhardness of coating deposited from complex baths.

That complexing agent used in bath B-4a, B-4b and B-4c has a great influence on VHN of the Fe-Ni coatings is shown in Fig.4.10. Addition of ascorbic acid with citric acid to bath B-4b showed the higher VHN than the combined effect of saccharin and citric acid or only addition of citric acid. The variation of VHN might be affected by Ni content as well as grain size distribution of the coatings which could again be influenced by the addition of different complexing agent(s) in the bath constituents. Effect of grain size distribution will be discussed in the latter sections.

Electrodeposition was carried out in the current density ranges from 50 to 120 mA/cm² for simple baths and 20 to 140 mA/cm² for complex baths. In case of simple baths, VHN of the coating increased with %Ni in it and the %Ni in coatings again increased with the applied current density. For, complex baths, VHN increased with %Ni in the coatings which is a similar observation obtained from simple baths. But a different result is found from complex baths that %Ni in coatings decreased with the applied current density. Thus complexing agents have a role to decrease the more noble constituent (here Ni) in the coating with increasing current density although we got another finding in chemical analysis that complexing agents suppress the anomalous characteristics of Fe-Ni alloy electrodeposition at the same current density (Fig. 4.4).

4.4 Corrosion Properties

Fe-Ni alloys are of interest in applications involving high temperature oxidation due to their ability to form protective Ni-rich oxide scales. High performance alloys are defined, in the present context, as Ni, Fe-Ni and Co base alloys able to operate at higher temperatures than 550°C and high pressures [73]. The use of Fe-Ni coatings is a cost effective means of providing oxidation resistance at the surface while maintaining the mechanical properties of the underlying substrate [74]. Salt immersion corrosion test was conducted in the present study. Coated samples were kept immersed in 5% NaCl solution for 48 hours. The corrosion rate expressed in mg/dm²/day (mdd) of Fe-Ni coatings deposited from simple baths and complex baths are shown in Table 4.8 & Table 4.9 respectively.

Table 4.8: Corrosion rate (mdd) and %Ni of coatings deposited at various current density from simple baths.

Bath identification	Corrosion rate (mdd) and %Ni of coatings for different current density (mA/cm ²)							
	50 mA/cm ²		70 mA/cm ²		100 mA/cm ²		120 mA/cm ²	
	mdd	% Ni	mdd	% Ni	mdd	% Ni	mdd	% Ni
B-1	20.51	9.38	19.69	11.09	—	—	16.59	15.11
B-2	15.48	16.12	—	—	15.02	21.02	14.54	21.80

Table 4.9: Corrosion rate (mdd) and %Ni of coatings deposited at various current density from complex baths.

Bath identification	Corrosion rate (mdd) and %Ni of coatings for different current density (mA/cm ²)													
	20 mA/cm ²		30 mA/cm ²		40 mA/cm ²		50 mA/cm ²		60 mA/cm ²		100 mA/cm ²		140 mA/cm ²	
	mdd	% Ni	mdd	% Ni	mdd	% Ni	mdd	% Ni	mdd	% Ni	mdd	% Ni	mdd	% Ni
B-3a	6.02	44.13	6.15	40.38	—	—	—	—	—	—	11.59	34.38	—	—
B-3b	—	—	1.55	47.52	—	—	10.37	37.48	—	—	—	—	12.21	31.43
B-3c	—	—	—	—	9.63	39.27	—	—	12.74	29.78	—	—	11.41	26.19
B-4a	—	—	11.69	28.37	—	—	—	—	—	—	—	—	—	—
B-4b	—	—	10.13	32.13	—	—	—	—	—	—	—	—	—	—
B-4c	—	—	11.31	30.43	—	—	—	—	—	—	—	—	—	—

Effect of %Ni in the deposit on its corrosion rate is shown in Fig. 4.11. Decreasing corrosion rate with increase in %Ni in the deposits is observed. In contrast, 21.80 wt.% Ni showed much lower corrosion rate in bath B-2. This might be the higher Ni content of the deposited films which lowers the corrosion rate. Corrosion rate decreases rapidly with increase of %Ni in coatings in the range of 9-15% Ni (bath B-1) and the corrosion decrease rate becomes slow in the range of 16-21% Ni (bath B-2). If a protective NiO layer is formed at the surface, the coating corrosion rate is decreased. When the Ni level at the surface drops, the coating is no longer able to form NiO scale in corrosive environment. As a result, corrosion rate of Fe-Ni thin films is increased. [74].

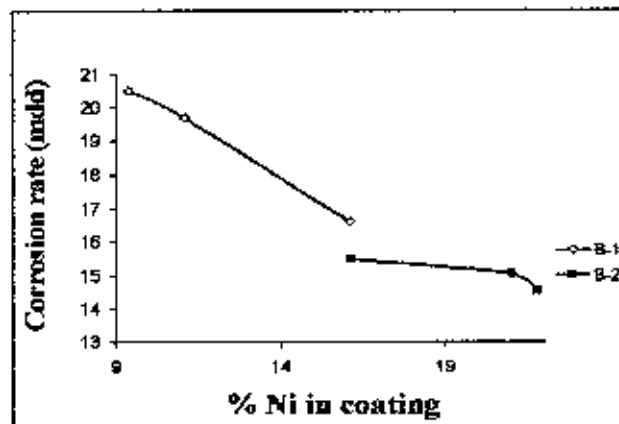


Fig. 4.11: Effect of % Ni in coating on its corrosion rate deposited from simple baths B-1 and B-2.

The effect of complexing agents on the corrosion resistance of the alloys was investigated. The results are summarized in Fig.4.12 and Fig.4.13. Similar observation that decrease in corrosion rate with increasing %Ni in coating is observed. It is known that complexing agents are usually added in the bath to form complexes with metal ions to ensure the plating bath stability, reasonable metal deposition rate and acceptable quality of alloys [75]. The variation of the complexing agent changes the composition and structure of coating which might lead to the change of corrosion rate of the alloys. In presence of complexing agent, it was found from SEM morphology (shown in the latter section) that the deposits were pore-free which reveals good adhesion of alloy deposit to the substrate. Moreover, the presence of optimum concentration of all addition agents

might improve the corrosion resistance properties. Previous studies have reported that the effects, such as pH and mole ratios of Ni/Fe in the bath, the deposition rate, composition, structure and microhardness of Fe-Ni alloy may change the corrosion properties of the films [75].

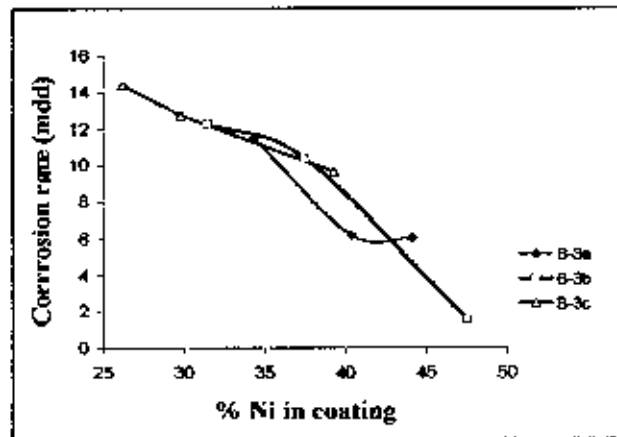


Fig. 4.12: Effect of % Ni in coating on its corrosion rate deposited from Complex baths B-3a, B-3b and B-3c

Figure 4.13 clears the effect of different complexing agents on the corrosion resistance of Fe-Ni thin film. The three coatings were deposited from the three different baths B-4a, B-4b and B-4c at a same current density of 30 mA/cm^2 . The coating deposited from bath B-4b containing ascorbic acid and citric acid shows better corrosion resistance than that deposited from bath B-4c containing saccharin and citric acid or from bath B-4a containing only citric acid as complexing agent. Ascorbic acid and citric acid provides higher Ni content (32.13%) in coating than the other two combinations of complexing agents in baths B-4a and B-4c. The film deposited with composition of 47.52 wt% Ni (bath B-3h) showed the best corrosion resistance throughout the whole study.

This can be attributed to the increase of Ni content of the deposited films. It is known that the corrosion resistance of any alloy depends largely on the ability to form a surface protective film which depends largely on the ability of noble metal of the films. Addition of saccharin with citric acid or only citric acid as complexing agent is supposed not to

facilitate to form stable passivation films (NiO) and this might increase the corrosion rate of the coatings.

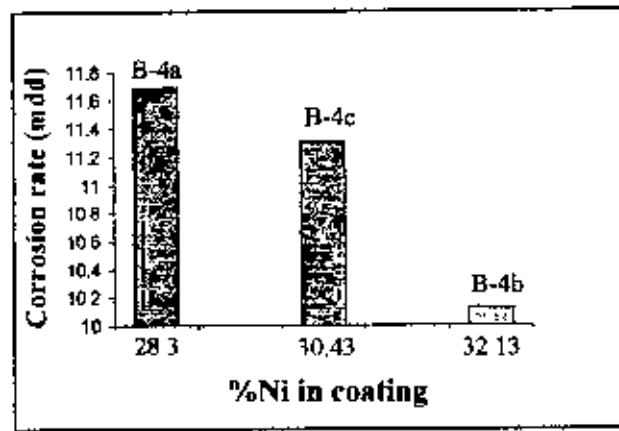


Fig. 4.13: Effect of % Ni in coating on its corrosion rate. Coatings were deposited from complex baths B-4a, B-4b and B-4c at the same current density of 30 mA/cm².

Figure 4.14 shows the %Ni in the coating deposited from simple bath B-1 and complex baths B-3a, B-3b and B-3c at the same current density of 50 mA/cm². Higher %Ni in coatings was obtained from complex baths than from simple bath. So, the complexing

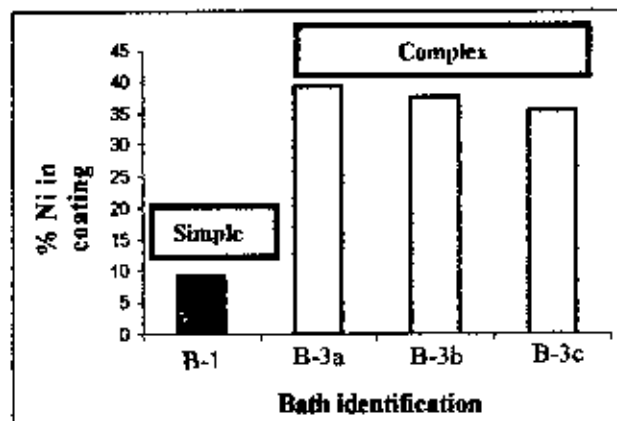


Fig. 4.14: % Ni deposited from simple bath B-1 and complex baths B-3a, B-3b and B-3c. All depositions were carried on at 50 mA/cm².

agent helps to increase the Ni content in the coatings obtained from complex baths which favors the higher corrosion resistance properties than the coatings obtained from simple baths.

After the salt water immersion test, the extent of corrosion was also evaluated qualitatively by visual inspection of the corroded samples. Photograph of the corroded samples for simple and complex baths at different parameters are shown in Fig. 4.15 Fig.4.16 respectively.

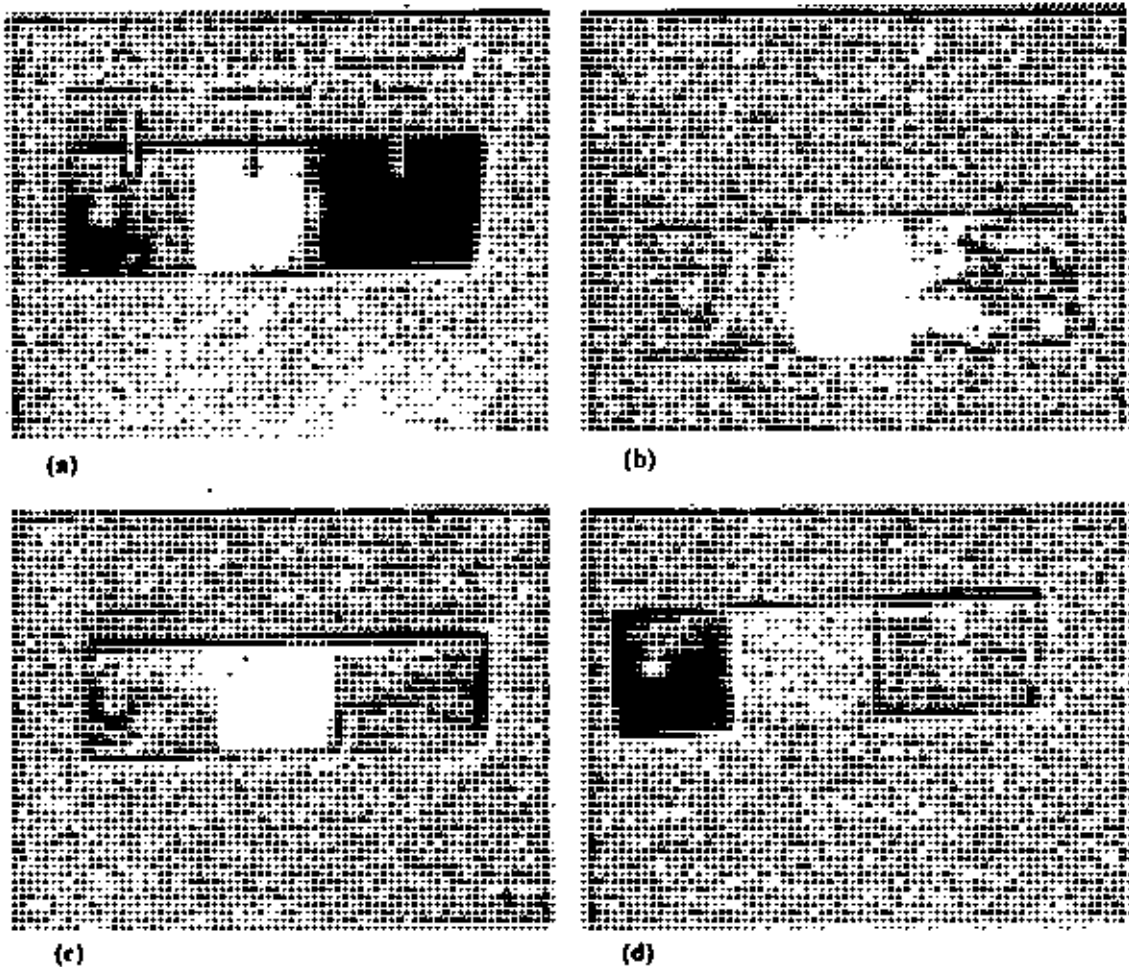


Fig.4.15 Photograph of corroded samples obtained from baths and at current densities of (a) B-1 and 50 mA/cm^2 (b) B-1 and 120 mA/cm^2 (c) B-2 and 50 mA/cm^2 (d) B-2 and 120 mA/cm^2 respectively.

The coatings deposited from simple baths corroded and almost the entire coating disappeared after 48 hours of immersion as is seen in Fig.4.15 whereas for the coatings deposited from complex baths, the progress of corrosion was much lower as shown in Fig. 4.16.

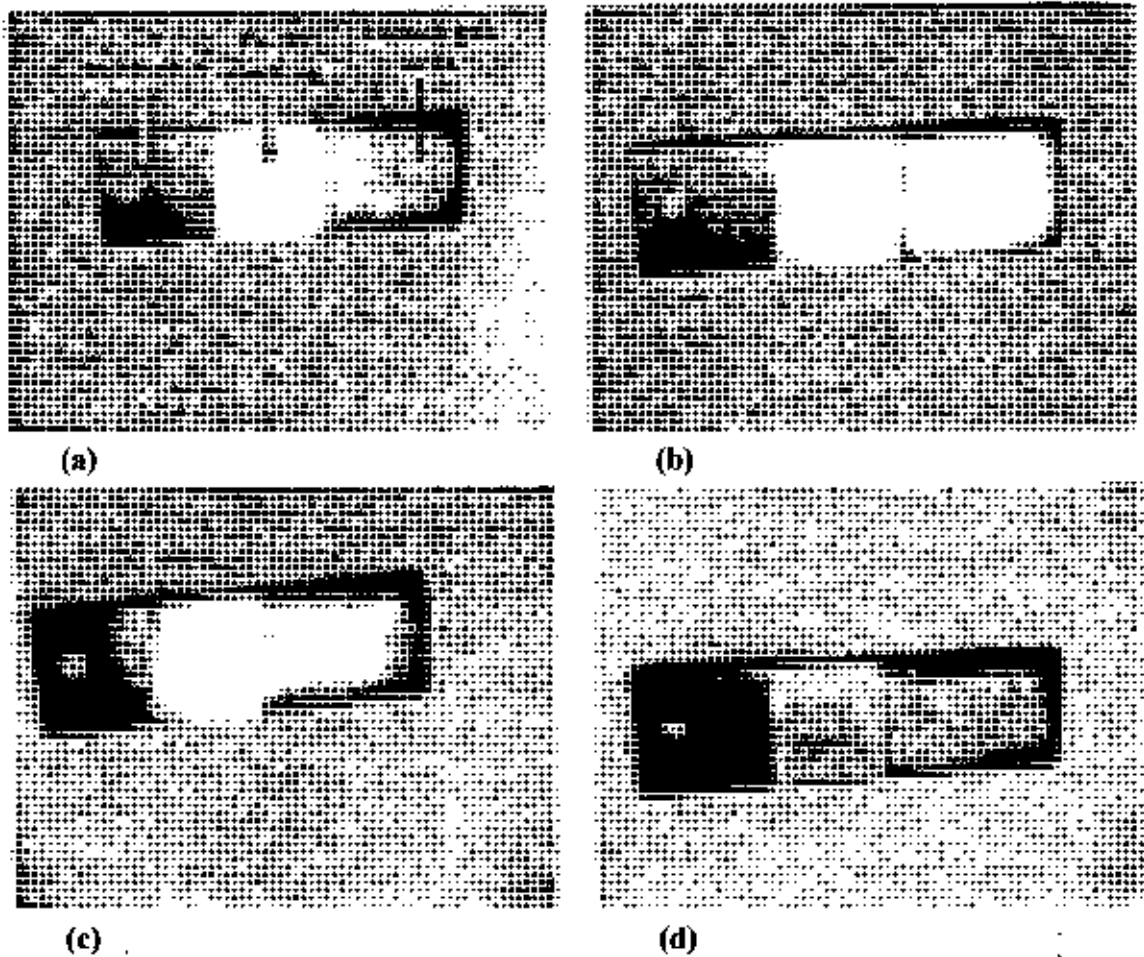


Fig. 4.16 Photograph of corroded samples obtained from baths and at current densities of (a) B-3a and 50 mA/cm^2 (b) B-3b and 50 mA/cm^2 (c) B-3c and 50 mA/cm^2 (d) B-4b and 30 mA/cm^2 respectively.

Porosity in the films might develop during electrodeposition from simple baths. The four possible mechanisms that can make the films porous during electrodeposition [76] are (i) the ionization-redeposition mechanism in which both elements of the binary alloy dissolve but the more noble element is redeposited (ii) the surface diffusion mechanism whereby only the less noble element is dissolved and the remaining more noble element aggregates by surface diffusion (iii) the volume diffusion mechanism where the less noble element is dissolved but both atoms move in the solid phase by volume diffusion and (iv) the percolation model of selective dissolution which expands upon the surface diffusion model to account for the pre-existing interconnected paths of like elements in the binary alloy.

4.5 Morphology

The Fe-Ni alloy was electrodeposited under different deposition conditions on Cu substrate. The influence of current density, bath composition and pH on the morphology of Fe-Ni coatings was evaluated by Scanning Electron Microscope (SEM). The topographies of Fe-Ni coatings were analyzed concerning their uniformity, porosity and the presence of cracks. The SEM images of Fe-Ni coatings obtained from simple bath B-1 at different current density is shown in Fig. 4.17.

The morphology of the electrodeposited Fe-Ni alloy deposited from bath B-1 at current density of 50, 70, 100, 120 mA/cm² does not exhibit smooth surface. Coarse-grained deposits are observed at low current density and typical river or vein pattern surface of deposits are seen at all current density. Sulphate baths of varying composition were used in the present study. Directional patterns seen on the deposits are supported by the

information available in the literature that coatings produced in sulphate electrolytes usually reveal lamellar microstructures [77].

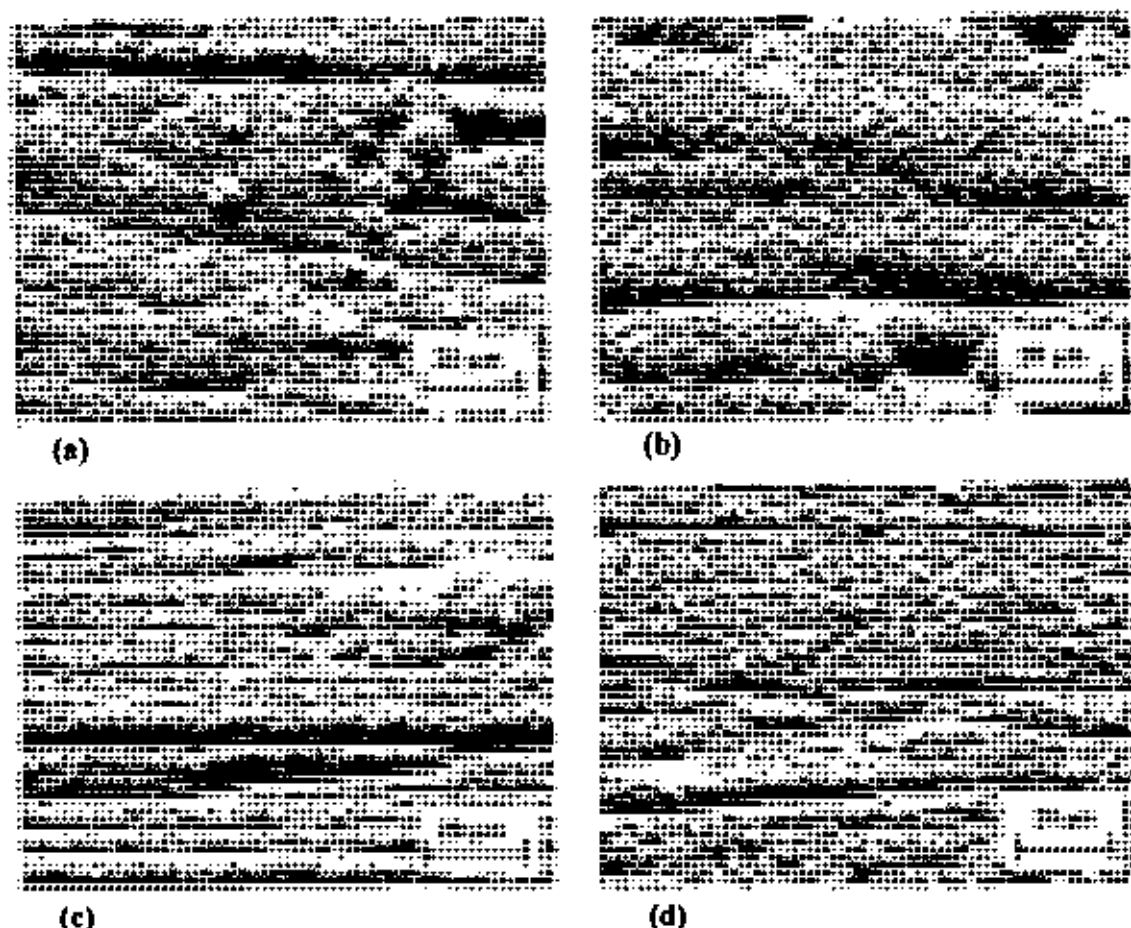


Fig. 4.17 SEM images of the deposit obtained from bath B-1 at current density of (a) 50 mA/cm² (b) 70 mA/cm² (c) 100 mA/cm² (d) 120 mA/cm²

Fig. 4.18 shows SEM images of Fe-Ni alloy coatings obtained from bath B-2 at different current density. The morphology is similar to that obtained from bath B-1. Grains are roughly spherical and average grain size decreased with increasing current density.

Thus structure of the Fe-Ni coatings is strongly influenced by current density. N. V. Myung et. al. [78] reported similar observations to binary Fe-Ni thin films. It is known that high current density give rise to a high degree of adatoms saturation at the electrode surface [79] and high degree of adatoms decreases the grain size.

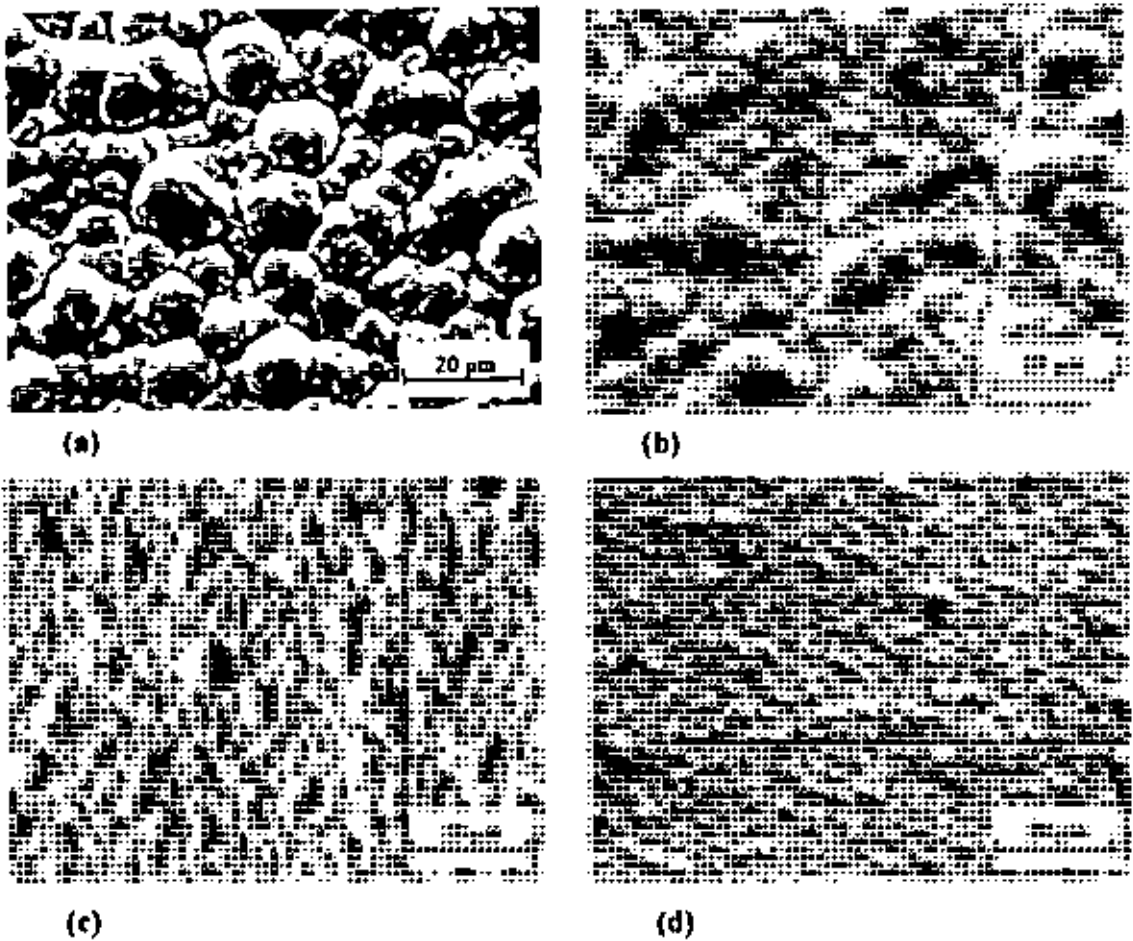


Fig. 4.18 SEM images of the deposit obtained from bath B-2 at current density of (a) 50 mA/cm² (b) 70 mA/cm² (c) 100 mA/cm² (d) 120 mA/cm²

N. Elezovi et. al. reported that the stress changes in the Fe-Ni films on varying deposition current density may mainly be attributed from the changes of the average grain sizes. As the average grain sizes decreased with increasing current density, the deposit stress might be increased. Thus morphology of the Fe-Ni alloys is characterized by the presence of microcracks. In this study, stressed films at high current density revealed the presence of sharp line microcracks distributed over the deposits [Fig.4.18(c), 4.18(d)]. The detail mechanisms of stress changes by varying the deposited current density have yet not been clear.

Complexing agent used in complex baths with varying composition contributed to decrease the coating roughness and improve the uniformity of the films. Moreover, it was observed that high current density with high pH led to black deposition (examined with the naked eye) while lower current density with higher pH or higher current density with lower pH resulted in uniform and bright coatings. Fig. 4.19 shows SEM images of Fe-Ni alloy coatings obtained from bath B-3a at different current density.

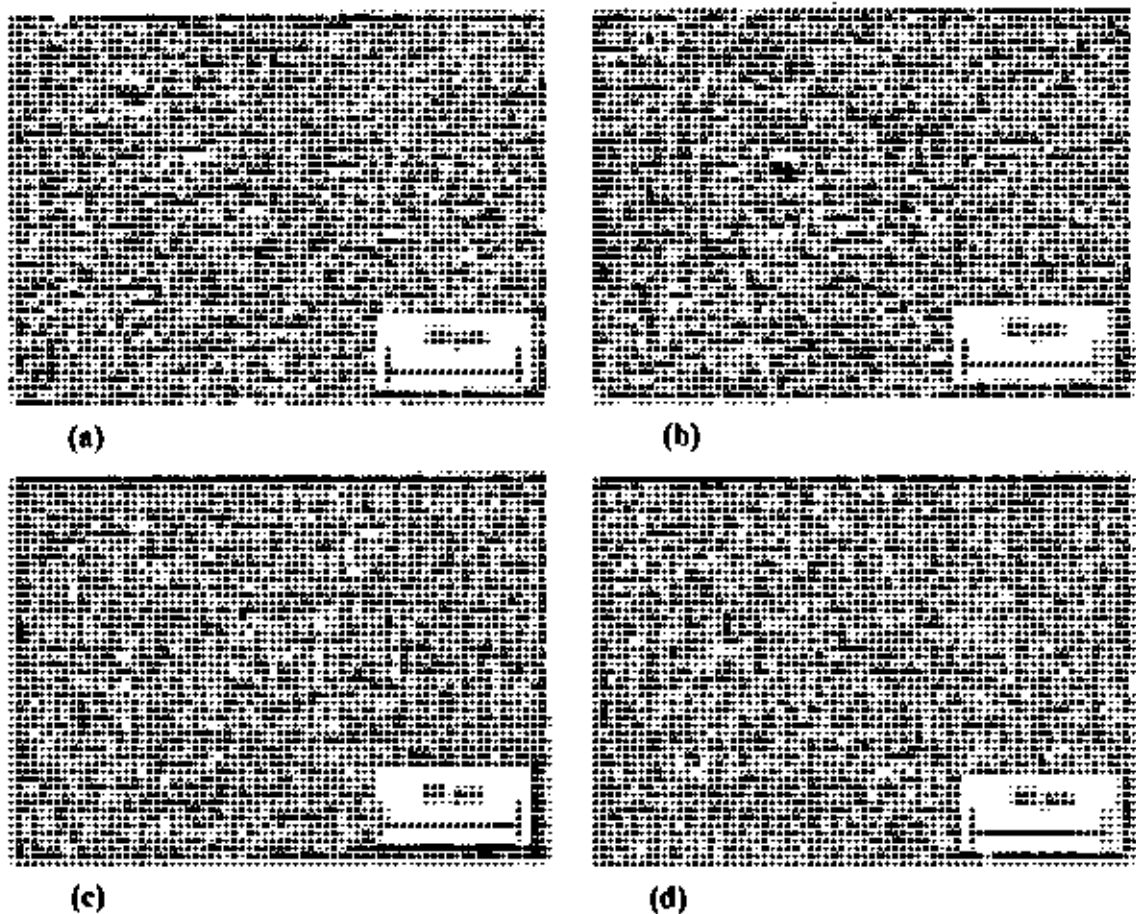


Fig. 4.19 SEM images of the deposit obtained from bath B-3a at current density and pH value of (a) 30 mA/cm² and 1.85 (b) 40 mA/cm² and 1.78 (c) 50 mA/cm² and 1.31 (d) 100 mA/cm² and 1.40 respectively.

The films had high apparent film density however the charging effect (bright spots in SEM images), which might be metallic oxide, is seen elsewhere. Metallic alloys and their oxides were produced simultaneously during the electrochemical reduction process [80]. Since the Ni deposition rate was higher in complex baths than simple baths [Fig. 4.4], such behavior can be attributed to the formation of a more stable Ni oxide in the presence of complexing agent.

By varying the plating parameters (including but not limited to bath pH, current density and bath additions), the morphology of the deposits can be controlled to some large extent by using electrolytes containing complexing agent/agents with proper compositions. For complexing agent, the crystallization of the electrodeposited layer is very important, since it influences directly the structure of the deposit and therefore its properties [81]. Crystallization occurs either by the buildup of old crystals or by the formation and growth of new ones. These two processes are in competition and can be influenced by different factors. High surface diffusion rates, low population of adatoms and low over-potentials are factors enhancing the buildup of old crystals. On the contrary, low surface diffusion rates, high population of adatoms and high over-potentials on the surface enhance the creation of new nuclei [82]. From the SEM observations, it can be said that addition of complexing agent of 2.0 g/l ascorbic acid, 3.0 g/l saccharin and 4.2 g/l citric acid in bath B-3h increased nucleation rates that helped to form crack-free, uniform and fine grained structures as is seen in Fig. 4.20.

The coatings obtained from bath B-3c produced little refined microstructure but scattered porosity in the deposits is seen (Fig. 4-21). The presence of pores, voids in Fe-

Ni alloy coatings can be the result of an additional effect of complexing agent and evolution of H_2 in the films [83-85].

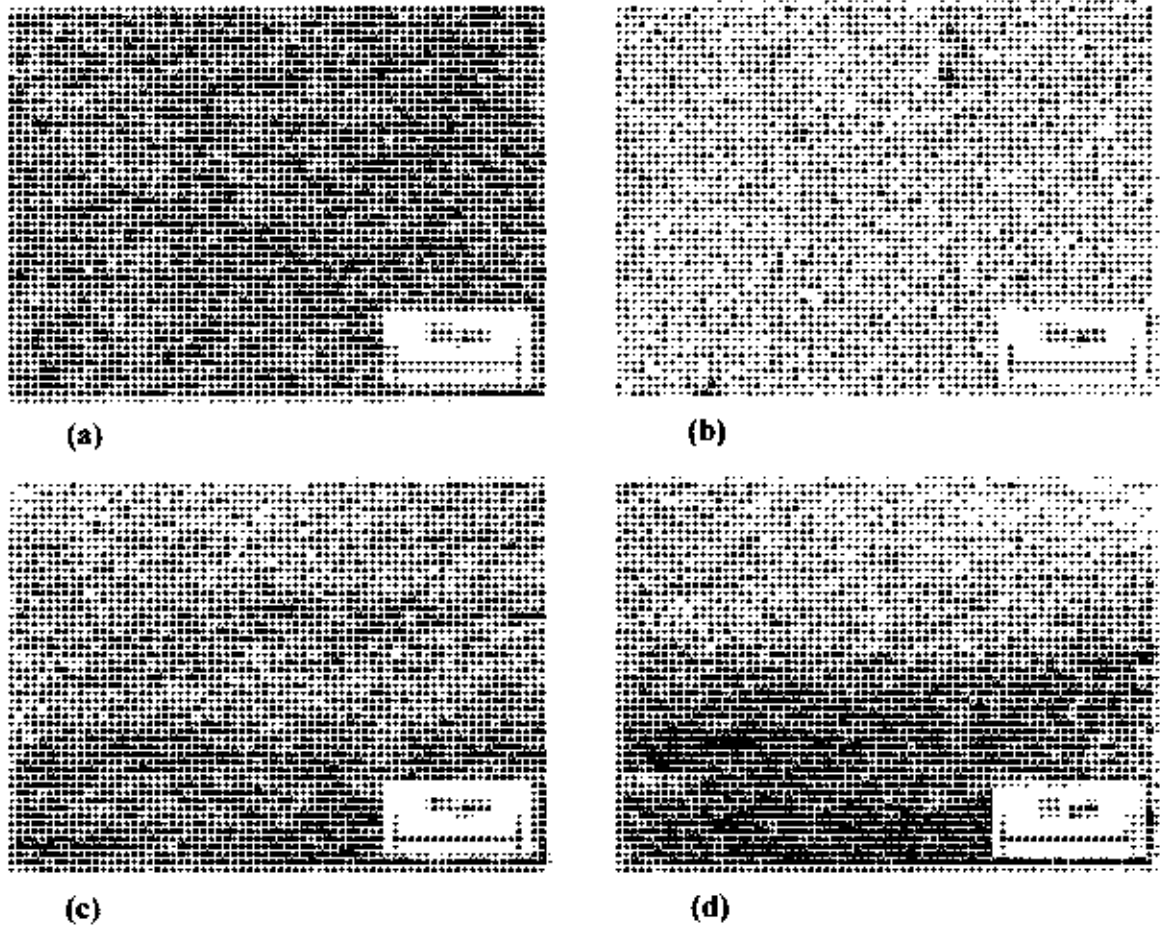


Fig. 4.20 SEM images of the deposit obtained from bath B-3b at current density and pH value of (a) 50 mA/cm^2 and 1.31 (b) 40 mA/cm^2 and 1.78 (c) 100 mA/cm^2 and 1.31 (d) 140 mA/cm^2 and 1.00 respectively.

A clear morphological modification was observed due to the addition of only citric acid, combined addition of ascorbic acid and citric acid or saccharin with citric acid as complexing agents in bath B-4a, B-4b and B-4c respectively. The images are shown in Fig. 4.22. All images were taken from coatings deposited from the same current density

of 30 mA/cm^2 but from different baths having different complexing agent with varying compositions.

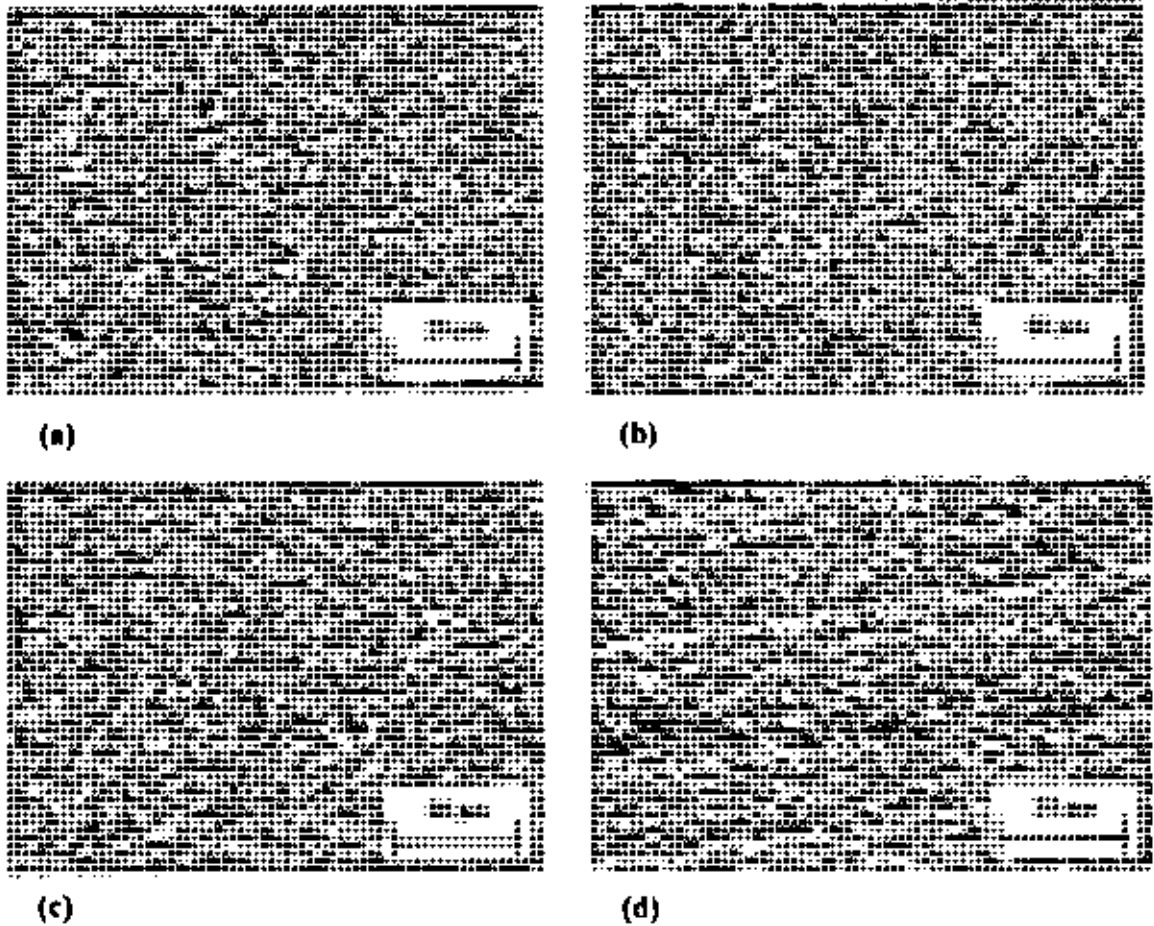


Fig. 4.21 SEM images of the deposit obtained from bath B-3c at current density and pH value of (a) 50 mA/cm^2 and 1.80 (b) 60 mA/cm^2 and 1.78 (c) 100 mA/cm^2 and 1.31 (d) 140 mA/cm^2 and 1.00 respectively

With the presence of only citric acid as complexing agent, the film was highly porous [Fig. 4.22 (a)] probably due to the hydrogen bubbles formed during co-deposition. Deposits obtained from the combined presence of citric acid and ascorbic acid in the bath displayed a few but large pores [Fig. 4.22 (b)]. Addition of saccharin with citric

acid into the bath B-4c resulted smooth, bright deposit with a little / no porosity in it [Fig. 4.22(c)].

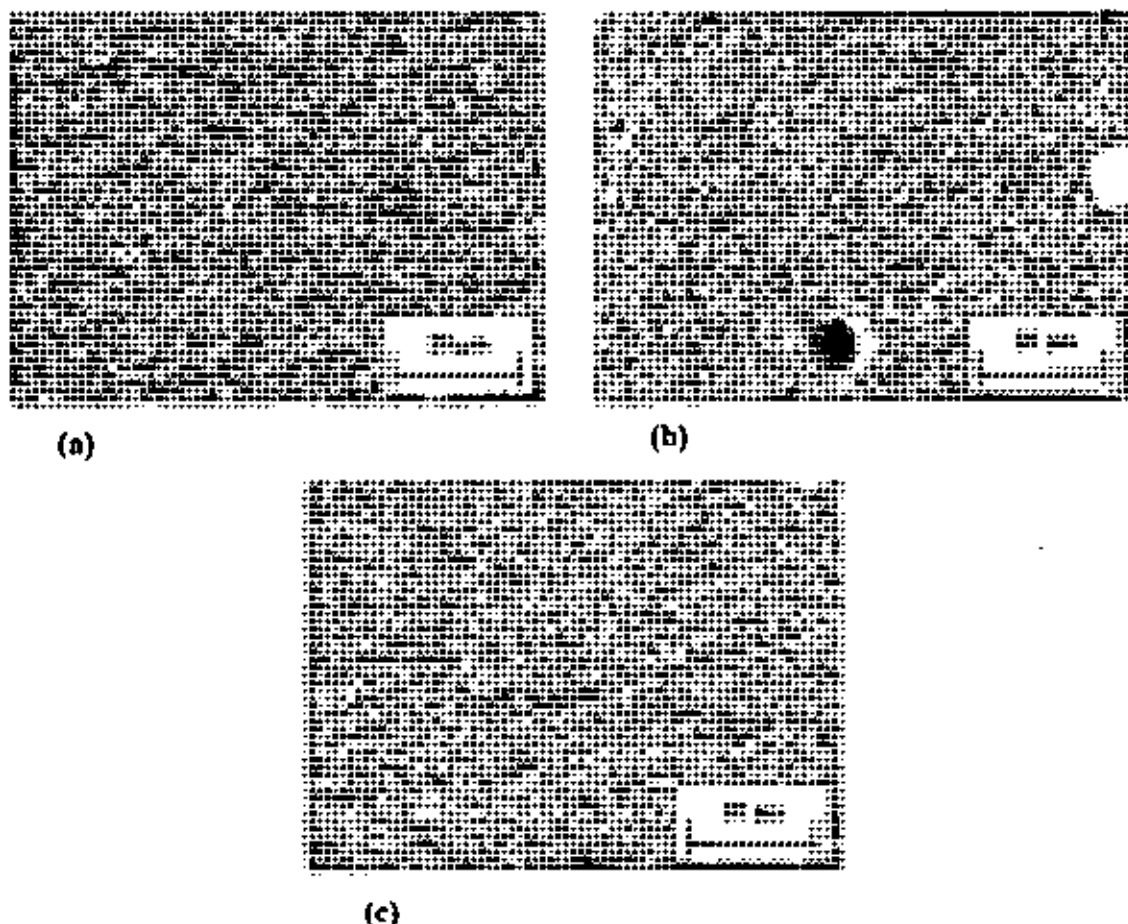


Fig 4.22 SEM images of the deposit obtained at a current density of 30 mA/cm^2 from baths (a) B-4a (b) B-4b and (c) B-4c

Saccharin, as a leveling agent, might reduce H_2 evolution causing less porous, fine grained smooth deposit. However, a more detailed study concerning the mechanism of saccharin as a leveling agent should be carried out to reach a final conclusion.

4.6 Magnetic Properties

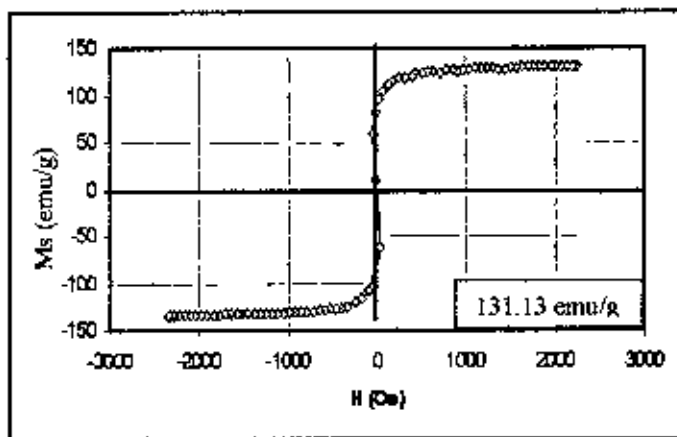
Soft magnetic thin films with high saturation magnetization are highly desired in a wide range of applications from magnetic write heads to high frequency inductors. However, soft magnetic thin-film materials with a saturation magnetization >21 kG and a low coercivity <1 Oe are still not available. Discovering new soft magnetic materials with very high saturation magnetization still remains to be a major challenge [86]. The magnetic anisotropy and coercivity are important properties of soft magnetic materials which find applications in the magnetic recording and reading technology [87]. Magnetization loops of the Fe-Ni films deposited from various simple and complex baths were measured using a vibrating sample magnetometer (VSM) with a magnetic field applied both parallel and perpendicular to the film plane at room temperature. The variation of saturation magnetization (M_s) with %Ni of coatings from simple baths is shown in Table 4.10.

Table 4.10: The saturation magnetization (emu/g) and %Ni obtained from simple baths.

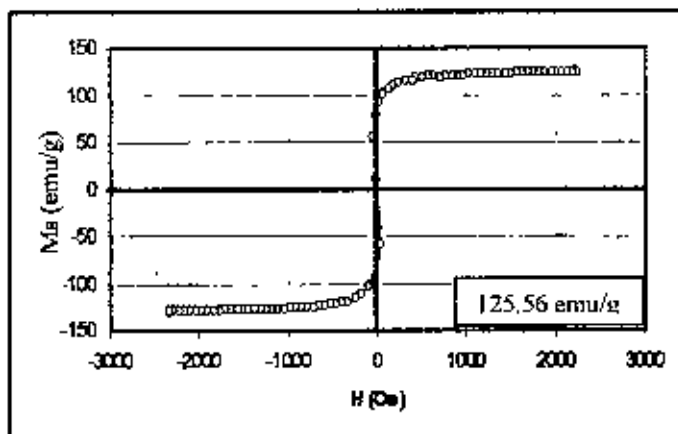
Bath identification	M_s (emu/g)	% Ni
B-1	131.13	9.38
	125.56	10.38
	118.38	11.09
B-2	104.92	15.21
	94.34	16.12
	68.32	21.80

As shown in Table 4.10, the saturation magnetization (M_s) for bath B-1 is higher than that of films for bath B-2. 9.38 %Ni containing coating displays the highest saturation magnetization and it decreases with increase in Ni content in the coating. Figure 4.23 shows saturation magnetization curves of Fe-Ni films for bath B-1. The M_s -H (Saturation magnetization vs applied field) curves clearly show that the curves are mostly straight lines with a small easy axis hysteresis which occur by domain translation and rotation. This shows that the uniaxial anisotropy, which is dependent on the film

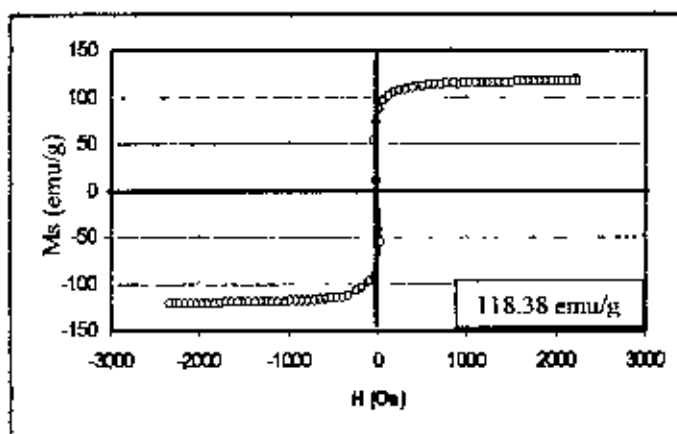
microstructure such as grain size, preferred orientation and stress, is mostly confined in-plane [88]



(a) 9.38% Ni coating



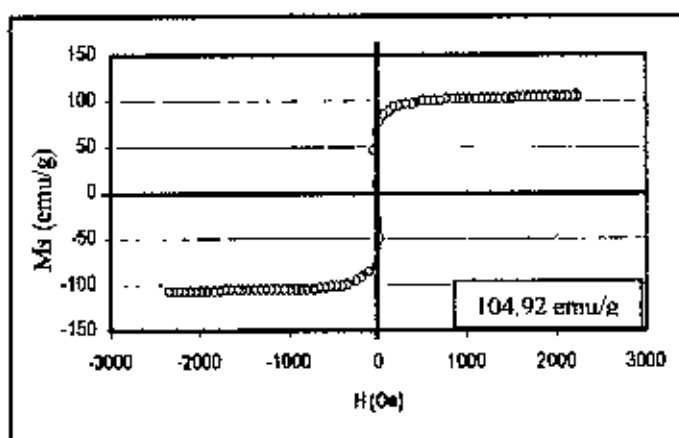
(b) 10.38% Ni coating



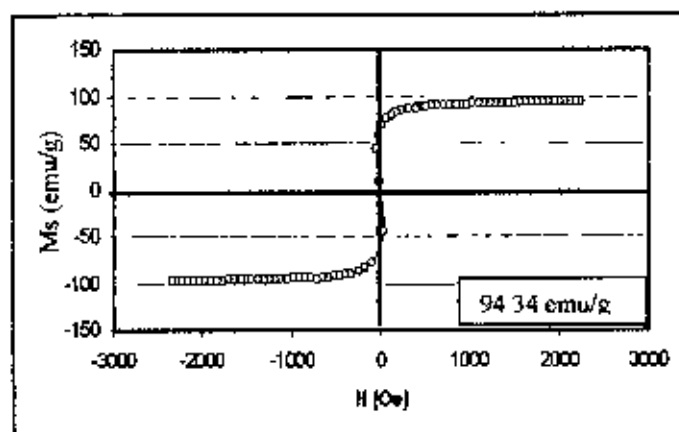
(c) 11.09% Ni coating

Fig. 4.23 Magnetic hysteresis loops of Fe-Ni coatings obtained from simple bath B-I.

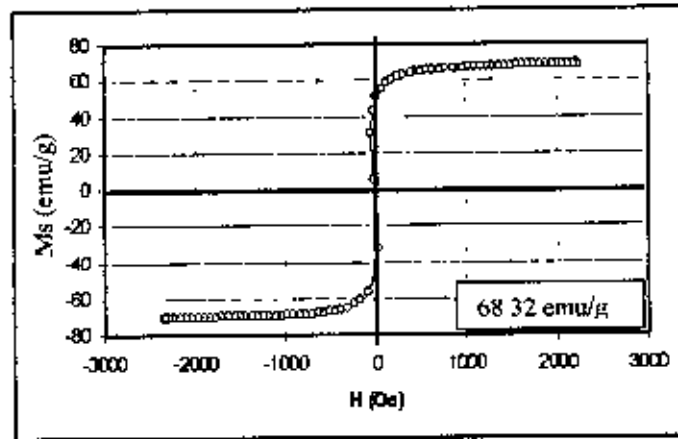
The saturation magnetization curves of Fe-Ni coatings obtained from bath B-2 are shown in Fig. 4.24. The highest saturation magnetization for bath B-2 is seen 104.92 emu/g among the coatings studied. Similar results that magnetic saturation decreases with increasing %Ni content in coatings and the uniaxial anisotropy is mostly confined in plane were observed for coatings obtained from bath B-1 as well as bath B-2. Thus no major difference in magnetic saturation property is found due to the variation of bath composition from simple baths. The demand of saturation magnetization for soft magnetic materials are increasing steadily and that the saturation magnetization 135 emu/g is satisfactorily acceptable for the write head materials [89].



(a) 15.21% Ni coating



(b) 16.12% Ni coating



(c) 21.80% Ni coating

Fig. 4.24 Magnetic hysteresis loops of the Fe-Ni coatings deposited from simple bath B-2.

The saturation magnetization (M_s) of the as-deposited Fe-Ni coatings obtained from simple baths is shown in Fig. 4.25 as a function of %Ni of the films. The fast decreasing M_s with the increasing %Ni within the lower range Ni content (9-11%) and relatively slow decreasing M_s with the increasing %Ni within the higher range Ni content (15-22%) was observed.

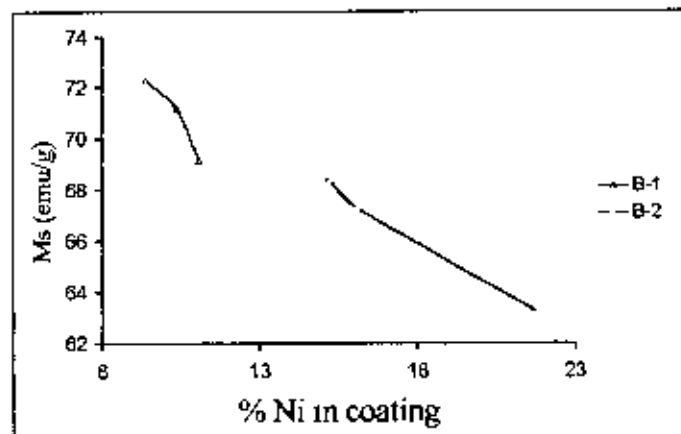


Fig. 4.25 Variation of magnetization saturation with Ni content for simple baths.

The saturation magnetization of the Fe-Ni coating is shifted to higher saturation magnetization values with increasing Fe content in it which is expected as magnetic

moment of pure Fe (221.9 emu/g) is greater than that of pure Ni (57.5 emu/g) [73]. The saturation magnetization of these Fe-Ni thin films is apparently limited by that of pure iron which is 221.9 emu/g.

Magnetization loop curves of the films obtained from baths with complexing agent did not show normal magnetization behavior. This is clear from Fig.4.26 which may be due to the structural and compositional characteristics in the thin films, such as grain size, crystallographic texture, strain and stress state. Coating from simple baths are characterized by coarse-grained with some microcracks onto it but those from complex baths are characterized by fine-grained smooth deposits.

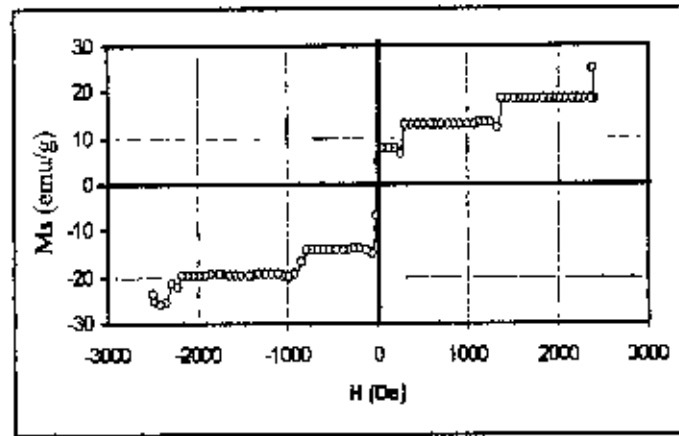


Fig. 4.26 Magnetic hysteresis loop of the Fe-Ni coating (44.13 %Ni) deposited from complex bath B-3a.

Magnetic softness of polycrystalline thin films is an extrinsic property of the magnetic materials, and is closely related to the structural and compositional characteristics in the thin films [89-91]. These characteristics can also affect anisotropy and magnetostriction, which are in turn correlated with the magnetic softness. However, it is still not well established how these structural characteristics affect the magnetic softness [92]. It would be of great scientific as well as technological interests to make this alloy soft while keeping its high saturation magnetization at the same time.

5.1 Conclusions Drawn from the Present Work

Electrodeposition of Fe-Ni thin films has been carried on copper substrate under various electrodeposition conditions from simple as well as complex baths. The influence of complexing agents on anomalous characteristics as well as the morphology and other properties of Fe-Ni thin films are investigated. The properties include coating composition, microhardness, corrosion resistance and magnetization. In the present electroplating system, the electrolytic composition, current density, pH and relationship between current density and pH for bright deposition are examined. The conclusions drawn from the study are:

- a. Bright Fe-Ni coating can be deposited from higher current density with lower pH value or higher pH value with lower current density both from simple and complex baths.
- b. Addition of ascorbic acid, saccharin, citric acid as complexing agents in the plating bath suppresses the anomalous nature of Fe-Ni alloy electrodeposition.
- c. Plating current density and pH value of plating bath are the two major parameters affecting composition as well as VHN of the Fe-Ni alloy coating. Percentage Ni and hence VHN of the coating increased with increasing current density for simple baths whereas the reverse occurred for complex baths.
- d. The corrosion rate decreased with increasing Ni content of the Fe-Ni alloy coating.
- e. The morphology of the Fe-Ni films obtained from simple baths is characterized by coarse-grained, non-smooth surface with presence of microcracks onto it. On the contrary, coatings from complex baths are fine-grained with smooth surfaces.

- f) The saturation magnetization (M_s) of the electrodeposited Fe-Ni coating is found to decrease with increasing Ni content which is in good agreement with suppression of ferromagnetic character of the films. The highest saturation magnetization is seen 131.13 emu/g among the coatings studied which is very close to the acceptable limit (135 emu/g). Coating obtained from complex baths did not show normal magnetization behavior possibly due to its different morphological character with those deposited from simple baths.

5.2 Suggestions for Future Work

Characterizing Fe-Ni alloy electrodeposition and study of the property were performed on the coatings obtained from two simple as well as six complex baths. Coatings from complex baths revealed superior properties in terms of morphology, microhardness and corrosion properties. Magnetic behavior of the coatings were inferior than those obtained from the simple baths. Thus recommendations for future work are:

- i) A more detail study on the behavior of complexing agents should be done in order to get further information on the properties of Fe-Ni alloy coating. Fine tuning of the content and composition of complexing agents should be performed to get normal magnetic behavior as well as an acceptable saturation magnetization of the Fe-Ni alloy coatings.
- ii) Further study should be carried out to measure the coating thickness and its effect on other properties.
- iii) Wear property of the Fe-Ni alloy coating should be studied in order to get more optimized quality coating of Fe-Ni alloy.

REFERENCES

1. H. Li and F. Ebrahimi, *Mater. Sci. Eng.*, Vol. 93, p. 347, (2003).
2. G. Beranger, F. Duffaut, J. Morlet and J. F. Tiers, 'The Iron-Nickel Alloys' Lavoisier Publishing, New York, (1996).
3. P. Egberts, P. Brodersen, G. D. Hibbard, *J. of Mat. Sci. and Engg.*, Vol. 441, p. 336, (2006).
4. J. A. Abrikosov, O. Eriksson, P. Soderlind, H. L. Skriver and B. Johansson, *J. Phys. Rev.*, Vol 51, pp.1058 -1995.
5. V. C. Kieling, *Surf. Coat. Technol.*, Vol. 96, p. 135, (1997).
6. R. Wczyk, A. Bienkowski, J. Salach, E. Fazakas and L. K. Varga, *J Optoelectron. Adv. Mater.*, Vol. 5, p. 705, (2003).
7. A. Brenner, 'Electrodeposition of Alloys', Academic Press, Vol. 2, New York, (1963).
8. W. C. Grande and J. B. Talbot, 'Electrodeposition of Thin Films of Nickel-Iron Alloy', *J. Electrochem. Soc.*, Vol. 140, p. 699, (1993).
9. T. P. Moffat, D. Wheeler and D. Josell, *Electrochem. Soc. Interface*, Vol 13, p. 46, (2004).
10. P. N. Bartlett, *Electrochem. Soc.*, Vol 13, p. 28, (2004).
11. K. Y. Sasaki, J. B. Talbot, *J. Electrochem. Soc.*, Vol. 145, p. 981, (1998).
12. C. Koch 'Bulk Behavior of Nanostructured Materials' North Carolina State University, (2003).
13. N. V. Myung and K. Nobe, *J. Electrochem. Soc.*, Vol. 148, p. 136, (2001)
14. A. Kohn, M. Eizenberg, Y. Shacham-Diamand, B. Israel and Y. Sverdlov, *Microelectron. Eng.*, Vol. 55, p. 297, (2001).
15. D. Y. Park, N. V. Myung, M. Schwartz and K. Nobe, *Electrochim. Acta*, Vol. 47, p. 2893, (2002).
16. M. Schwartz, R. F. Bunshah, 'Handbook of Deposition Technologies for Films and Coatings', Noyes Publ, p. 524, (1994).
17. J. J. Kelly, S. H. Goods and N. Y. C. Yang, 'Electrochem. Solid State Lett.', Vol. 6, p. 88, (2003).

18. A. Brenner, 'Electrodeposition of Cu-Bi Alloys from a Perchlorate Bath', Ph. D. Thesis, University of Maryland, (1939).
19. S.G. Clarke, W.N. Bradshaw and E.E. Longhurst, 'Studies on Brass Plating Electrodepositors', Tech. Soc., Vol. 19, p 63, (1994).
20. K. Iwase and N. Nasu, 'X-ray study on the electrolytic Fe-Ni alloy', Bull. Chem. Soc. Japan, Vol. 7, pp.305-314, (1932).
21. S. Glasstone and T.E. Symes, 'The Electrodeposition of Fe-Ni alloy', I. Trans. Faraday Soc., Vol. 23, pp 213-226, (1927).
22. S. Glasstone and T.E. Symes, 'The Electrodeposition of Fe-Ni alloys', II. Trans. Faraday Soc., Vol. 24, pp.370-378, (1928).
23. N. V. Korovin, 'Cathode Process in the Electrodeposition of an Fe-Ni alloy', Zhur. Khim., Vol. 2, pp.2259-2263,(1957).
24. K. Engemann, 'Über das abblättern des elektrolytnickels', Z. Elektrochem., Vol. 17, pp.910-917,(1911).
25. H. W. Toepffer, 'Über galvanische Ausfällung Von Legierungen des Eisens und verwandter Metalle', Z. Elektrochem. Vol 6 pp.342-344, (1899).
26. R. Kremann and R. Mass, 'Die bei höherer Temperatur aus Sulfatbarden abgechiedenen Nickel-Eisen-Legierungen Monatsh', Vol. 35, pp.731-753, (1914).
27. S. Glasstone and J.C. Speakman, 'The Electrodeposition of Co-Ni alloys', I. Trans. Faraday Soc , Vol .26 p.565, (1930).
28. C.G. Fink and K.H. Loh, 'The deposition of Ni-Co alloys', Trans. Am. Electrochem. Soc., Vol. 58, p.373, (1930).
29. F. Marschak, D. Stepanow and L. Lewius. 'Zur. Frage der elektrolytischen Abscheidung von Fe-Ni Legierungen. II Z. Elektrochem Vol 41 p. 596-597. (1935).
30. A. I. Chernilovskaya and G. A. Tsyganov, 'Determination of distribution coefficient of the iron-group metals by electro-coprecipitation', Uzbek. Khim. Zhur., Akad. Nauk Uzbek. S.S.R. No. 4 p.25-32. (1958).
31. K. Aotani, 'Studies on electrodeposited alloys (2nd report), 'Structure and Electrode Potentials o electrodeposited Fe-Ni, Ni-Co and Co-Fe alloys', J. Japan Inst. Metals (Sendai) B 14, No. 5, pp.55-58, (1950).

32. V. V. Sysoeva, Production of Fe-Ni alloys by Electrodeposition from chloride electrolytes, *Zhur. Prikladn, Khim.* Vol. 32, pp. 128-132. (1959).
33. E. J. Podlaha and D. Landolt, *J. Electrochem. Soc.*, Vol. 144, p. 1672, (1997).
34. V. R. Ramanan and E. D. Siegel, 'Nanocrystalline Soft Magnetic Alloys for Applications in Electrical and Electronic Devices', In *R&D Status and Trends*, (1998).
35. R. W. Siegel, *Materials Science Forum*, Vol. 851, pp. 235-238, (1997).
36. D. G. Morris and M. A. Morris, *Materials Science Forum*, Vol. 861, pp. 235-238, (1997).
37. J. R. Weertman, R. S. Averback, A. S. Edlestein and R. C. Cammarata, 'In *Nanomaterials: Synthesis, Properties and Applications*', Institute of Physics Pub., Bristol, (1996).
38. U Erb, G. Palumbo, R. Zugic, K. T. Aust, C. Suryanarayana, J. Singh, and F. H. F. Warrendale, 'In *Processing and Properties of Nanocrystalline Materials*', PA: TMS, (1996).
39. R. M. Thomson, R. W. Cahn and P. Haasen, 'In *Physical metallurgy*' Elsevier Science BV, 4th ed., (1996).
40. B. Günther, A. Baalmann and H. Weiss, *Mater. Res. Soc. Symp. Proc.*, Vol. 195, pp. 611-615, (1990).
41. G. W. Nieman, J. R. Weertman and R. W. Siegel, *Mater. Res. Soc. Symp. Proc.*, Vol. 206, pp. 581-586, (1991).
42. G. W. Nieman, J. R. Weertman and R. W. Siegel, *J. Mater. Res.*, Vol. 6, pp. 1012-1027, (1991).
43. P. G. Sanders, J. A. Eastman and J. R. Weertman, 'In *Processing and properties of nanocrystalline materials*', (1996).
44. V. Y. Gertsman, M. Hoffman, H. Gleiter and R. Birringer, *Acta Metall. Mater.*, Vol. 42, pp. 3539-3544, (1994).
45. J. A. Eastman, M. Choudry, M. N. Rittner, C. J. Youngdahl, M. Dollar, J. R. Weertman, R. J. Dimelfi and L. J. Thompson, 'In *Chemistry and Physics of Nanostructures*', (1997).

46. D. G. Morris and M. A. Morris, *Acta Metall. Mater.*, Vol. 39, pp. 1763-1779, (1991).
47. G. Liang, Z. Li and E. Wang, *J. Mater. Sci.*, (1996).
48. R. S. Mishra and A. K. Mukherjee, 'Mechanical Behavior of Bulk Nano-Materials', *Proceedings of Symp.*, (1997).
49. J. F. Carsley, R. Shark, W. W. Milligan, E. C. Aifantis, E. Ma, B. Fultz, R. Shull, J. Morral, and P. Nash, 'In Chemistry and Physics of Nanostructures and Related Non-equilibrium Materials', PA: TMS (1997).
50. A. Makino, A. Inoue, T. Hatanai and T. Bitoh, *Materials Science Forum*, Vol. 723, p. 235-238, (1997).
51. D. Jiles, 'Introduction to Magnetism and Magnetic Materials', London, (1991).
52. P. A. I. Smith, J. Ding, R. Street and P. G. McCormick, *Scripta Materialia*, Vol. 34, p. 61, (1996).
53. C. G. Hadjipanayis and E. D. Siegel, 'Nanostructured Magnetic Materials', (1998).
54. M. N. Baibich, J. M. Broto, A. Fert, F. Nguyen Van Dau, F. Petroff, P. Etienne, and G. Creuzet, *J. Phys. Rev Lett*, Vol. 61, p. 2472, (1998).
55. A. E. Berkowitz, J. R. Mitchell, M. J. Carey, A. P. Young, S. Zhang, F. E. Spada, F. T. Parker, A. Hutten, and G. Thomas, *Phys. Rev. Lett.*, Vol. 68, p. 3745, (1992).
56. R. D. Shull, E. D. Siegel, 'NIST Activities in Nanotechnology in R&D Status and Trends', (1998).
57. M. El-Hilo, K. O. Grady and R. W. Chantrell, *J. Appl. Phys.*, Vol. 76, p. 6811, (1994).
58. R. D. Shull, R. D. McMichael and J. J. Ritter, *Nanostructured Mater.*, Vol. 2, p. 205, (1993).
59. R. B. Schwarz and E. D. Siegel, 'Storage of Hydrogen Powders with Nanosized Crystalline Domains', In *R&D Status and Trends*, (1998).
60. G. Beranger, F. Duffaut, J. Morlet and J. F. Tiers, 'The Iron-Nickel Alloys' Lavoisier Publishing, New York, (1996).

61. A. H. M. Vander Berg, A. A. M. Flaman and J. F. Tiers, 'The Iron-Nickel Alloys', Lavoisier Publishing, p. 335, New York, (1996).
62. U. Erb, C. Cheung, M. R. Baghbanan and G. Palumbo, Proceedings of the 1st Nano-Micro-Interface Conference (NaMiX), Germany, (2003).
63. G. Palumbo, U. Erb, J. L. Merea, G. D. Hibbard, I. Brooks, F. Gonzalez and K. Panagiotopoulos, 'Electrodeposited Nanocrystalline Coatings for Hard-Facing Applications', p. 204, Chicago, (2002).
64. M. Moniruzzaman and A. S. M. A. Haseeb, 'Electrodeposition of Zn-Ni Alloy Coatings and Study of their Microhardness in Relation to Composition, Structure and Plating Parameters', Proceedings 2nd Annual Paper Meet of Mech. Engg. Div. (IEB), pp. 113-121, Rajshahi, Bangladesh, Sept., (1995).
65. A. Brenner, 'Electrodeposition of Alloys' Vol. 1, (1963).
66. M. M. Abu-Krishna, A. M. Zaky and A. A. Toghian, 'Morphology, Composition and Corrosion Properties of Electrodeposited Zn-Ni Alloys from Sulphate Electrolytes', *J. Corr. Sci. and Egg.*, Vol. 7, (2005).
67. A. Brenner, 'Electrodeposition of Alloys, Principle and Practice', Academic Press, vol. 2, Chap. 31, p. 239, New York, (1963).
68. A. Brenner, 'Electrodeposition of Alloys', Academic Press, Vol. 1, London, (1963).
69. M. Matloz, *J. Electrochem. Soc.*, Vol. 140, p. 2272, (1993).
70. H. Deligianni and L. T. Romankiw, 'Insitu Surface pH Measurement During Electrolysis Using a Rotating pH Electrode', *J. Res. Develop.*, Vol. 37, pp. 85-95, (1993)
71. J. Matulis and R. Slizys, *Electrochem. Acta.*, Vol. 9, p. 1177, (1964).
72. B. N. Popov, K. M. Yin and R. E. White, *J. Electrochem. Soc.*, Vol. 140, p. 1321, (1993).
73. D. L. Grimmitt, M. Schwartz and K. Nobe, *J. Electrochem. Soc.*, Vol. 137, p. 3414, (1990).
74. D. F. Susan, K. Barnak and A. R. Marder, 'Electrodeposited Ni-Al Particle Composite Coatings Thin Solid Films', Vol. 307, pp. 133-140, (1997).

75. K. Barmak, S. W. Banovic, C. M. Petronis, D. F. Susan and A. R. Marder, 'Structure of Electrodeposited Graded Composite Coatings of Ni-Al-Al₂O₃', *J. of Microscopy*, Vol. 185, pp. 265-274, (1997).
76. K. Sieradzki, *JECS*, Vol. 140, p. 2868, (1993).
77. L. F. De Senna, S. L. Diaz, L. Sathler, 'Hardness Analysis and Morphological Characterization of Copper-Zinc Alloys Produced in Pyrophosphate-Based Electrolytes', *J. Mat. Research*, Vol. 8, pp. 275-279, (2005).
78. L. Sathler and K. Barmak, 'Hardness Analysis of Fe-Ni Alloy Produced from Sulphate Electrolytes', *J. Materials Research*, Vol. 6, pp. 299-302, (2005).
79. N. V. Myung, D. Y. Park, D. E. Urgiles and T. George, *Electrochim. Acta.*, Vol. 49, p. 4397, (2004).
80. J. L. McCreary, K. T. Aust, G. Palumbo and U. Erb, *Mater. Res. Soc. Symp. Proc.*, Vol. 581, p. 461, (2000).
81. A. R. Marder and A. M. Flaman 'Characterization of Copper-Zinc Alloys Produced in Sulphate Electrolytes', *J. Materials Research*, Vol. 8, pp. 285-299, (2004).
82. F. Ebrahimi and H. Q. Li, 'Structure and Properties of Electrodeposited Nanocrystalline FCC Ni-Fe Alloys', *J. Rev. Adv. Mater. Sci.*, Vol. 5, pp. 134-138, (2003).
83. Y. H. Hsin and Y. Chao-Chen, 'Electrodeposition and Corrosion Resistance of Zn-Pd Alloy from the ZnCl₂-EMIC', Vol. 58, pp. 1055-1062, (2003).
84. S. Luciana, A. Sanches, H. Sergio, A. D. Ademir and H. Mascaro Lucia, 'Electrodeposition of Ni-Mo and Fe-Mo Alloys from Sulfate-Citrate Acid Solutions' *J. Braz. Chem. Soc.*, Vol. 14, pp. 556-563, (2003).
85. J. K. Kwang, L. Sukmoek, G. K. Jung and H. H. Kyung, 'Magnetic Properties of with Nitrogen Added Fe-Ni Invar Films', *J. of Korean Phys. Soc.*, Vol. 45, pp. 1032-1036, (2004).
86. N. X. Sun and S. X. Wang 'Soft High Saturation Magnetization (Fe_{0.7}Co_{0.3})_{1-x}N_x Thin Films for Inductive Write Heads', Vol. 36, p. 2506, (2000).

87. M. Bedir, O. F. Bakkaloglu, I. H. Kkarahan and M. Oztas 'A Study on Electrodeposited Ni_xFe_{1-x} Alloy Films', *J. of phys., Indian Academy of Sciences*, Vol. 66, p. 1093, (2006)
88. M. S. Flores, G. Ciapetti, J. L. Gonzalez-Carrasco, M. A. Montealegre, M. Multigner, S. Pagani and G. Rivero, 'Evaluation of Magnetic Behaviour and in Vitro Biocompatibility of Ferritic PM2000 Alloy', *J. of Mat. Sci.*, Vol. 15, pp. 559-565, (2004).
89. G. Herzer, *J. Appl. Phys.*, Vol. 26, p. 1397, (1990).
90. H. Akihiko and Y. Shimada, *J. Appl. Phys.*, Vol. 67, p. 6981, (1990).
91. B. D. Cullity, 'Introduction to Magnetic Materials', Wesley, (1972).
92. M. Takahashi, Y. Takahashi, H. Shoji, 'Magneto-crystalline Anisotropy for α' -Fe-C and α' -Fe-N Films', *J. of IEEE Transactions*, Vol. 37, pp. 2179-2181, USA, (2002).

List of Publications/Presentations (As of May, 2008)

Proceedings publications

1. M. A. Islam and M. Moniruzzaman, 'Properties of the Electrodeposited Fe-Ni Alloy Coating on Cu Substrate', Proceedings, 12th Annual Paper Meet of Mech. Engg. Div. (IEB), Dhaka, Bangladesh, Feb. 8-9, (2008), p.1-8.
2. S. K. Das, M. A. Islam, M. Moniruzzaman and K. M. Shorowordi, 'Effect of Bath Composition and Plating Parameters on the Morphology of Electrodeposited Fe-Ni Alloy Coatings', Proceedings, 11th Annual Paper Meet of Mech. Engg. Div. (IEB), Dhaka, Bangladesh, Dec 25-26, (2006), p. 86-91.

